Surface Potential Measurements of Micropatterned Self-Assembled Monolayers (SAMs) on n-Si(111) via Kelvin Probe Force Microscopy

GARCIA MARIA CARMELA TAN

2022

Surface Potential Measurements of Micropatterned Self-Assembled Monolayers (SAMs) on n-Si(111) via Kelvin Probe Force Microscopy

By

GARCIA MARIA CARMELA TAN

A DISSERTATION

Submitted to

GRADUATE SCHOOL OF ENGINEERING,
KYOTO UNIVERSITY

in partial fulfilment of the requirements for the degree of

DOCTOR OF PHILOSOPHY

2022

Table of Contents

Abstract ………………………………………………………………………. **1**

Chapter 1 : Introduction ….…………………………………………………………. **3**

1.1. Self-assembled monolayers (SAMs) ………………………………………. **3**

1.1.1. Definition of SAMs …………………………………………….. 3

1.1.2. SAMs on Silicon ……………………………………………….. 4

1.1.2.1. Organosilane SAMs on Si/SiO_2 substrate ……………….. 5

1.1.2.2. *SAMs covalently bonded on Si substrate* ……………….. 6

1.2. Work Function and Surface Potential ……………………………………. **7**

1.2.1. Definition of work function and surface potential ……………….. 7

1.2.2. SAMs and surface dipoles……………….…………………………….. 9

1.2.3. Using SAMs to control surface potential or work function ……… 10

1.3. Contact Potential Difference and Kelvin Probe Force Microscopy ……. **14**

1.3.1. Contact Potential Difference …………………………………….. 14

1.3.2. Kelvin Probe Force Microscopy …………………..………….. 15

1.4. Micropatterning SAMs via VUV Photolithography ……………………. **19**

1.4.1. VUV Light ………………………………………….………….. 19

1.4.2. VUV Photolithography ………………………………………….. 20

1.5. Objectives ….…………………………………………….……………………. **21**

1.6. Outlines ….………………………………………….…………………………. **21**

References ….……………………………………………..…………...………. **24**

Chapter 2 : Formation of Micropatterned SAMs ..……………………………………. **36**

2.1. Introduction ..…………………………….………………………………………. **36**

2.2. Experimental Methods ..……………………………...…………………. **38**

2.2.1. SAM preparation ………………………………….………………….. 38

2.2.2. VUV Photolithography of the SAM ……………………………….. 40

2.2.3. Optimization of etching conditions after VUV irradiation ……….. 42

2.3. Results and Discussion ..……………………………..…………………. **43**

2.3.1. Formation of HD SAM …………………………….……….. 43

2.3.2. Optimization of VUV irradiation conditions for micropatterning of HD SAM ………………………….………………….……….. 45

2.3.2. Optimization of the etching condition required for micropatterned SAMs 51

2.4. Conclusions 58

References 59

Chapter 3: Influence of the interface dipole on the surface potentials of SAMs on n-Si (111) grafted via Si-C, Si-O and Si-S bonds 65

3.1. Introduction 65

3.2. Experimental methods 69

3.2.1. Preparation of Hydrogen-terminated Silicon 69

3.2.2. SAM Formation 69

3.2.3. Formation of Micropatterned SAMs 70

3.2.4. Characterization 72

3.3. Results and discussion 72

3.3.1. Properties of HD, HDO and HDT SAMs 72

3.3.2. Surface Potential Measurements via KPFM 74

3.4. Conclusions 86

References 87

Chapter 4: Effects of Chain Length on the Surface Potentials of 1-Alkene Self-Assembled Monolayers on n-Si (111) 94

4.1 Introduction 94

4.2. Experimental methods 96

4.2.1 Materials 96

4.2.2 Sample preparation 98

4.2.3 Characterization 99

4.3. Results and Discussion 99

4.4. Conclusions 111

References 112

Chapter 5: Investigation on the effects of Si-C and Si-O interface bonds on the surface potential and conductivity of aromatic SAMs on n-Si (111) 121

5.1. Introduction 121

5.2. Experimental Methods 123

5.2.1. Materials ….…………………………………………..…….…….….. 123
5.2.3. Sample Preparation ...……………………………..………..…….. 124
5.2.3. Characterization ...……………………………..….…….…..…….. 127
5.3. Results and Discussion ..……………………………..…………………. 128
5.3.1. Formation of aromatic SAMs ...………………………..…….. 128
5.3.2. KPFM Measurements for Surface Potential ...……………..…….. 133
5.3.4. CAFM Measurements for conductivity ..…………………..……..140
5.4. Conclusions …..……………………………………….…………………… 143
References ….…………..…………………………………….………………… 144

Chapter 6 : Summary and Conclusions ….…………………………………………… 152

Acknowledgements ……………………..………………………………………… 154

Achievements ……..……………………..………………………………………… 158

Curriculum Vitae ……………………..………………………………….……….. 160

Abstract

The performance of molecular electronics is governed by energy barriers at material interfaces. For optimum device performance, charge injection barriers at interfaces should be minimized. This can be attained through selection of materials with appropriate work functions. One approach to increase or decrease the work function of materials is through the adsorption of different molecules to form self-assembled monolayers (SAMs). The formation of SAMs introduces a dipole at the surface which may result in a change in the surface potential and a shift in the vacuum level at the interface, thereby modifying the work function of the surface. Ideally, by careful manipulation of the magnitude and orientation of the dipole at the surface through the use of different molecules, the surface potential or work function can be tailored for specific applications. By studying how the surface potential of a substrate can be controlled using different molecules, scientists can have a better understanding of how to improve the charge carrier efficiency of electronic devices.

In this research, we observe changes in surface potential of SAMs on n-Si (111) via Kelvin Probe Force Microscopy (KPFM). Micropatterned SAMs were used for KPFM analysis to provide a reference during measurements. Micropatterning was conducted via VUV photolithography at $\lambda = 172$ nm. Irradiation of SAMs at this wavelength initiate the photodegradation of the molecule at the surface. When irradiated through a photomask, regions of one SAM can be removed and a second SAM can be grafted, allowing two SAMs to be attached to the same substrate. The photolithography process was optimized to ensure that the surface potential of the first SAM is reproducible and can thus serve as a reference to observe changes in the surface potential of the second SAM. HD SAM [HD : $CH_3(CH_2)_{13}CH=CH_2$] was used as reference in this study to monitor changes in the surface potential of n-Si (111) due to the adsorption of other molecules

SAMs formed from straight CH_2 chains and molecules with aromatic groups having different molecular lengths or binding chemistry to silicon were chosen for this study. While many previous studies have succeeded in modifying the surface potentials of substrates by changing functional groups of the precursor molecules, not much study have been conducted on methods to fine-tune the material's surface potential through the use small structural modifications or the binding chemistry of the molecule to the substrate. For both SAMs formed from straight-chain and aromatic molecules, the interfacial bond with the substrate affected the final surface potential considerably, due to the charge rearrangements that occur in the molecules when the molecule is grafted. Dipole moments of the molecules obtained using Molecular Package (MOPAC) semi-empirical computations gave a reasonable estimate of the surface potential of the SAMs, however other factors also affected the surface potential measurements, such as the molecular packing and quality of the SAM. The packing of the molecules on the substrate have been reported to affect depolarization of the SAM which can cause a deviation from the surface potential expected from dipole computations. The quality of the SAMs was also found to affect the KPFM readings, which is something that should be considered in surface potential studies. Increasing our understanding of how surface potential can be controlled or affected by different parameters can lead to further improvement of the charge carrier efficiency of electronic devices.

Chapter 1 : Introduction

1.1. Self-assembled monolayers (SAMs)

1.1.1. Definition of SAMs

Self-assembled monolayers (SAMs) are highly ordered molecular thin films that are formed on the surface of a solid substrate through the process of spontaneous attachment of a molecular layer on a substrate[1,2]. This self-assembling nature of SAMs occurs via a combination of interactions between the adsorbing molecules with each other, as well as with the substrate. The result is a highly ordered array of molecules forming an ultra-thin layer on the surface.

SAMs are most often formed by immersing a substrate in a solution of precursor molecules that is able to chemically react to the substrate surface[2]. The molecules chemisorb on the surface and are immobilized on the substrate through chemical bonding, which allows them to be more stable mechanically, thermodynamically and chemically compared to Langmuir-Blodgett (LB) films. The thickness of the SAM is dependent on the length of the precursor molecules as well as the tilt angle of the molecules on the substrate. The molecule involved in the formation of SAMs has three parts[2,3] which is shown in Figure 1.1. The three parts are described below:

(a) **Head Group** : this is the end of the molecule which attaches to the surface of the substrate

(b) **Body or Backbone** : the aliphatic or aromatic part of the molecule which provides rigidity and length/thickness to the film. This portion of the molecule is also responsible for the packing and ordering of the molecules.

(c) **Tail or Terminal group** : this portion of the molecule gives the film its functionality. It is responsible for the topography, surface energy and chemistry of the SAM.

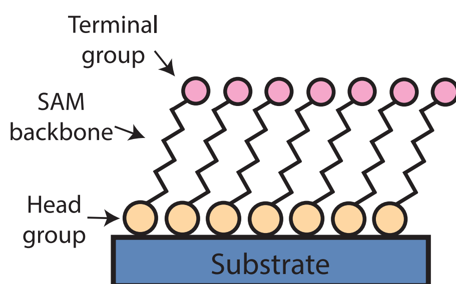

Figure 1.1. Structure of SAMs

SAMs are highly ordered and the surface properties of the substrate can be controlled by choosing the head group of the molecule to be attached. The molecules chosen for SAMs often has one end that has a favorable and specific interaction with the substrate, which allows it to form a stable monolayer film. The configuration and geometry of the molecules in the SAM is a result of its interactions with the surface and nearby molecules. The uniformity and order of SAMs may be affected by the cleanliness and purity of the substrate, the purity of the precursor solution, the length of the molecule, the type of head group, and the amount of time the monolayer is allowed to assemble. SAMs can be formed by immersing substrates in solutions containing precursor molecules, or allowing the film to condense on the substrate surface from a gas phase precursor.

The process of modifying surfaces via SAMs is an important field in bottom-up nanotechnology. The ability to modify and choose the head and tail groups of the precursor molecules allows SAMs to have a wide array of applications[2]. Some common SAMs include organosilane SAMs on silicon, alkanethiol SAMs on metals and alkene SAMs on hydrogen-terminated silicon. Applications of SAMs include surface coatings for the control of wetting, friction[4], corrosion protection[5–8], biotechnology[9], sensing[10,11], and electronics[3,12–14].

1.1.2. SAMs on Silicon

Many studies of SAMs have been done on sulfur-containing molecules (thiols) on coinage metals such as gold[15–21]. However, semiconductor substrates such as silicon offer more versatility in electronic fabrication due to their complex band systems.

Silicon wafers are widely used in modern electronic technology in the past decades. As technology evolves, the size of devices to be put on these silicon wafers continue to shrink to sub-nanometer scale. As the surface-to-volume ratio increases in these small devices, surface characteristics and properties play an increasingly significant role in device operation. As such, many studies on the modification of silicon surfaces using SAMs have been done in the past few years[13]. The modification of silicon surfaces using SAMs combines the advantage of the well-developed silicon technology with the versatility of the properties of different molecules. There are two categories of SAMs on silicon : (a) organosilane SAMs on SiO_2 and (b) SAMs directly bonded to the silicon substrate. The two types are discussed below.

1.1.2.1. Organosilane SAMs on Si/SiO_2 substrate

Several studies have successfully formed SAMs using organosilanes[22–26]. Silanes are molecules consisting of one silicon atom connected to four functional groups (SiX_4). When at least one of these functional groups is replaced with organic functional groups, the molecule is known as organosilane. These molecules are known to react with hydroxyl groups on an oxide surface. As such, organosilane SAMs can be formed on silicon substrates which are covered with its native oxide. However, the native oxide layer of silicon usually contains a high density of traps and thus it is advisable to remove this and grow an ultra-thin layer of thermal oxide for better control over the SAM's properties[13]. A silicon with a clean oxide layer will have a high density of silanol groups (Si-OH) groups on the surface, which is suitable for the grafting of organosilane SAMs.

The formation of organosilane SAMs require the presence of a trace amount of water, which is usually enough from the environment. Organosilane SAMs are grafted on silicon substrates through Si-O-Si bonds[24]. Due to the high vapor pressure of silanes, they are often deposited in vapor phase on the substrate. Depositing organosilane SAMs in vapor phase

also has the advantage of reduced aggregate deposition on the surface, as well as requiring a smaller amount of precursor solution as compared to the liquid-phase deposition[23].

1.1.2.2. SAMs covalently bonded on Si substrate

Although organosilanes form dense and high-quality SAMs, they are formed on top of the native silicon oxide, thus there exists a thin insulating layer between the SAM and the silicon substrate, limiting its applications in electronics. In 1993, Linford and Chidsey discovered a method which allows SAMs to form directly on silicon[27]. The native oxide is removed through etching and the surface passivated with hydrogen atoms to form hydrogen terminated silicon (H-Si). The etching step usually involves HF and NH_4F solutions which have been found to passivate the surface and terminate the silicon dangling bonds with hydrogen[28,29]. Silicon surfaces etched using HF solution only have been found to be atomically rough[30], as opposed to etching using NH_4F solution which produce atomically flat surfaces[31]. For example, etching of Si (111) surfaces with HF were found to produce surfaces with Si atoms terminated by mono- and di-hydrides[30], while etching in NH_4F solution produced a monohydride surface. Si (111)[27,32] and Si (100)[32,33] has been used in past studies as substrates for direct grafting of SAMs on Si. Studies have shown that hydrogen termination of Si (111) leads to atomically flat surface, characterized by clear terrace sites[34], as opposed to Si (100) which has a rougher surface[29].

To graft molecules directly to the silicon substrate, a reaction initiator, such as thermal excitation or photo irradiation is needed. In 2008, Sano et. al tested different methods of grafting 1-hexadecene to Si (111) surface. Hydrosilyation, the process of reaction between the SAM precursor and H-Si, was initiated using thermal, UV and visible light activation[35]. Under the right conditions, the Si-H bond on the surface undergoes homolytic cleavage which yields a dangling silicon bond on the surface. This dangling bond is free to react with the double bond of the alkenes in the precursor solution, which leads to the

attachment of the alkene molecule to the substrate. This reaction results in the formation of another radical which abstracts a hydrogen atom from the nearby site, and the cycle continues. Multiple studies have shown that 1-alkene precursors can successfully form well-ordered SAMs directly on silicon[4,36–38], with a 50% coverage of the surface with the molecule. The rest of the area of the substrate will have the Si-H group remaining[39] due to steric hindrance[27]. This SAM coverage was also verified computationally by several studies[39].

Aside from alkenes, other molecules have been successfully grafted directly to silicon without an oxide layer, such as thiols[36,40,41] and alcohols[4,37,38,40]. However it was found that alcohol SAMs on silicon displayed lower orientational order and chemical durability than alkene SAM[38]. Test on alkanethiol SAMs on silicon showed even lower molecular density and chemical durability than alcohol SAMs[41].

Whether it is for silicon or other substrates, one application of SAMs in the field of material science is the modification of electrode work functions of easier charge injection[42–44], which is the focus of this dissertation.

1.2. Work Function and Surface Potential

1.2.1. Definition of work function and surface potential

For any semiconductors, parameters such as Fermi energy (E_F), vacuum level position (V_L), energy gap (E_{GAP}), work function (WF) electron affinity (EA) and ionization energy (IE) are of great importance because they define and dictate the electronic structure and behavior of the material at the surface or interface. They are also largely responsible for the charge transport between two materials with an interface. A diagram depicting these parameters for a semiconductor is shown in Figure 1.2.

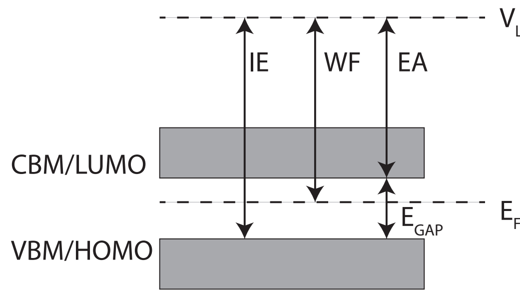

Figure 1.2. Energy band diagram of a semiconductor depicting IE (ionization energy), WF (work function), EA (electron affinity), E_{GAP} (energy band gap), V_L (vacuum level) and E_F (Fermi level)

For metals, E_F is the energy level that separates the occupied and unoccupied states and thus IE, EA and WF are all equal to each other. For semiconductors, these values differ due to the more complex band structure. These parameters can vary greatly between samples of the same material due to differences in their purity, crystallographic orientation, surface roughness, surface composition and even the cleanliness of the surface.

Of the parameters mentioned, much research has been dedicated to the study of the work function of materials. The work function can be imagined the energy barrier which electrons at the Fermi level need to overcome to be able to escape the solid. This property can also provide insight on the quality or state of the material's surface, since the presence of adsorbates or contaminants is known to alter its value. By definition, work function is the minimum energy needed to remove an electron from a solid to a point just outside the surface[45]. In terms of the energy levels in the band diagram, it is equal to the energy difference between the vacuum level and the Fermi level. The vacuum level is defined as the energy level of an electron just outside the solid and it is highly dependent on the nature of the surface. Electrons are typically bound to a solid material, and cannot easily escape to the vacuum due to an energy barrier. From the diagram, we can see that WF depends directly on the position of E_{vac} and E_F.

The work function is often thought of to be the combination of two components – a

bulk component and a surface component[46]. The bulk component is affected by the electron density and density of states in the material. The surface component can be thought of as an additional potential step due to a dipole on the surface. The presence of this surface dipole may result to a potential step (positive or negative) at the surface, known as surface potential, which can change the work function by changing the vacuum level at the surface (Figure 1.3). For metal-organic interfaces, this shift in the vacuum level due to the presence of a dipole would result to a shift upwards or downwards of the energy bands of the organic material. In Figure 1.3 the effect of a dipole layer on the energy bands of a metal-organic interface is depicted. The presence of the dipole made the organic side more positive, making it more attractive for electrons. As such, this dipole between the metal electrode and organic film results to a downward shift of vacuum level for the organic material[47].

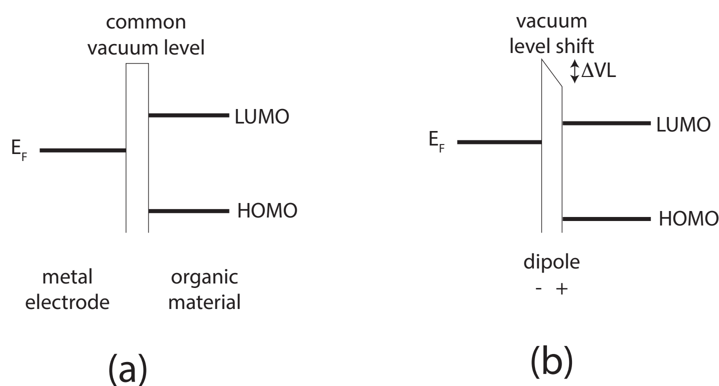

Figure 1.3. Shift in vacuum level due to presence of a dipole at the interface

1.2.2. SAMs and surface dipoles

Studies have found that SAMs introduce a dipole layer on a substrate surface, changing its surface potential and shifting the vacuum level at the interface[47,48]. The orientation and strength of this dipole layer determines the direction and magnitude of the vacuum level shift[47]. In the field of material science, there is much interest in tailoring the surface potential or work function of a substrate through the adsorption of various molecules.

By studying how the surface potential of a substrate can be controlled using different dipole moments due to various molecules, scientists can have a better understanding of how to improve the charge carrier efficiency of electronic devices.

A schematic illustration of how vacuum level shift can increase or decrease the energy barrier in metal-organic systems is depicted in Figure 1.4. Without the dipole layer, the energy difference between the Fermi energy of the electrode and the HOMO level of the organic material is quite large and results to a substantial energy barrier (E_h) which charge carriers (in this case, holes) need to overcome to cross the interface. By inserting an oriented dipole layer between the electrode and the organic material, the energy barrier can be increased or decreased, depending on the direction of the dipole

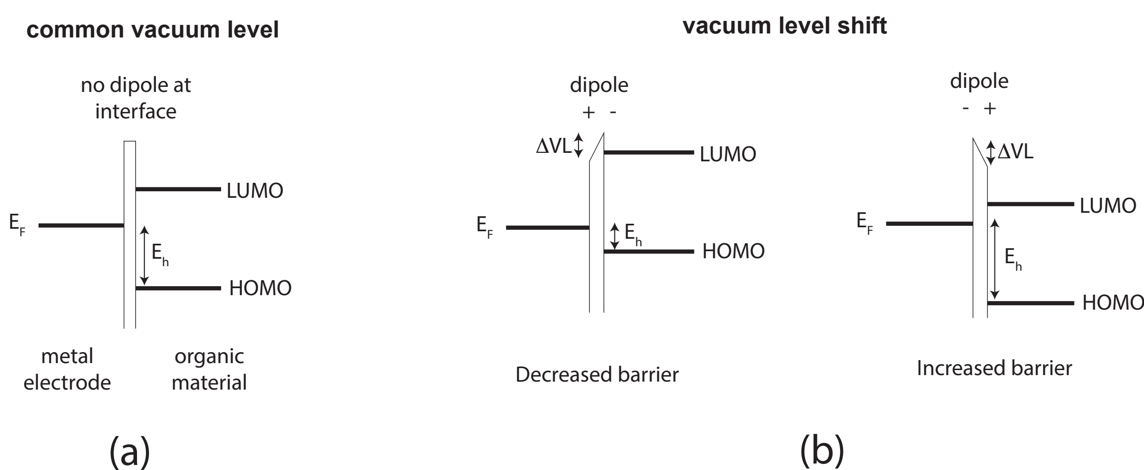

Figure. 1.4. Schematic illustration of shifting vacuum levels at the interface of metal electrodes and organic materials due to the existence of a dipole layer

1.2.3. Using SAMs to control surface potential or work function

Due to the versatility of SAMs and its ability to add a dipole layer to the surface of an electrode which can modify the work function or surface potential, numerous studies have investigated the extend of how this dipole can be optimized to produce desired changes in work function.

A study by Campbell et. al demonstrated control over charge injection between copper (Cu) metal and organic material using SAMs of conjugated thiols[49]. In their study, adsorbates that would shift the energy barriers in opposite directions to demonstrate the control SAMs can offer were chosen. Kelvin probe force microscopy analysis was used to measure the changes in surface potentials of the metal electrodes. Their results demonstrated that SAMs can significantly affect how easily charge carriers can cross through the interface and are an effective way to control charge injection in organic devices.

Hlavalthy et al studied the adsorption of alkanes and alkenes on platinum at temperatures between 323 to 573 K[50]. Their results showed that the work function always decreases when there is hydrocarbon adsorption, with alkenes causing a larger work function change than alkanes. In both cases, SAMs formed from longer molecules induced greater work function changes. The study concluded that the difference in H:C ratio for these precursor molecules were responsible for the difference in their dipole moments. Higher temperatures used during SAM fabrication were also found to increase the change in work function possibly due to the increase in surface concentration which would lead to a greater dipole present on the surface of the Pt.

Evans and Ulman have demonstrated that surface potential of alkylthiol SAMs on gold was affected by the hydrocarbon chain length[20]. Their experiments showed that the surface potential of the SAM covered substrate varied linearly with the chain length, with an average increase of 9.2 mV per additional methyl unit. Later, Lu et. al conducted similar experiments and confirmed that the surface potential increased with longer chain lengths[51]. Other researchers have also observed changes in the work function of gold using different chain length alkylthiols due to the presence of dipoles on the surface[52].

Other studies focused on making slight modifications to the molecular precursors to control the surface dipole. Hayashi et al. demonstrated that modifying the tail end substituent of the molecules from methyl, fluoromethyl and amino groups significantly affect the dipole

moment of the SAMs, leading to differences in surface potential[53]. Egger et al. studied how they can control the dipole of SAMs on Au(111) surfaces by distributing a series of dipoles along the molecular backbone[54]. Instead of SAMs made of molecules with non-polar backbones (oligophenylthiols) containing either an acceptor or donor headgroup to introduce a dipole layer, they chose molecules composed of dipolar pyrimidine moieties linked head-to-tail. By changing the orientation of the nitrogen in the pyrimidine group with respect to the metal substrate, they were able to fabricate SAMs with dipoles either pointing up or pointing down, thus modifying the work function of the gold substrate.

Most of the studies mentioned above used metal substrates, such as Au or Pt since the self-assembly of thiols on metals have been widely established, however researchers have recently been investigating the effect of SAMs on certain semiconductors as well. Unlike metals, semiconductors have a much more complex band structure which gives more versatility when studying parameters such as work function or surface potentials.

Cohen et. al used SAMs of dicarboxylic acid on CdTe to modify the band bending and electron affinity[55]. By using different molecules with different dipole moments they found that there is a linear correlation between the dipole moment of the SAM and the change in the electron affinity of the substrate. In their research, dipole moment was varied by substituting different functional groups in their precursor molecules. By controlling the magnitude and direction of the dipole they were able to increase or decrease the electron affinity or work function of their substrates. Their work demonstrated the ability of SAMs to tune semiconductor macroscopic properties through small modifications in the molecular structure.

Szwajca et. al studied the effect of alkylthiol SAMs on InAs [56]. Using alkylthiols of different chain lengths, they obtained the SAM dipole moments through Kelvin Probe Force Microscopy measurements. Through application of computational methods they were able to estimate the packing densities of the SAMs on the InAs substrates.

Among the many semiconductors, research in silicon has been attracting attention due to its use in present day electronics. In 2001 Sugimura et. al used organosilane (alkylsilane and fluoroalkylsilane) SAMs on silicon to introduce dipole moments to the silicon substrate[57]. Through experiment and ab initio computations, they were able to verify that the magnitude and direction of the precursor molecule dipole moment modified the surface potential of silicon. The surface potential of the fluoroalkylsilane SAM was much lower than that of the alkylsilane SAM due to the electronegativity of the fluorine atoms. Saito et. al also conducted a similar study on silicon and their findings showed that the dipole moment of the precursor molecule can be used to predict the surface potential of the SAM given the proper approximation of the area occupied by the molecule[58].

When using SAMs to vary the surface potential of the substrate, the equation below can be used.

$$V_{SAM} = \frac{\mu}{A\epsilon_0\epsilon_{SAM}} \quad \text{Equation 1.1}$$

The equation shows that surface potential is inversely proportional to the area occupied by the molecule (A), the dielectric constant of the SAM (ϵ_{SAM}) and proportional to the dipole moment of the SAM perpendicular to the substrate (μ). The surface dipole of the SAM may be affected by the gas phase dipole moment of individual molecules as well as the dipole formed due to covalent-bond formation when the molecule attaches to the substrate[54,59,60]. The gas phase dipole moment of the molecule refer to the dipole moment of the molecule while it is not grafted to the substrate. Once the molecule is grafted to the substrate, interfacial charge rearrangements often occur as a result of the molecular grafting, and a small interfacial dipole will occur on top of the gas phase dipole moment. While the gas phase dipole can be used to predict the net dipole moment of the SAM, particularly in cases when the covalent bond between molecule and substrate is constant, depolarization effects due to electrostatic interactions between molecules has also been shown to strongly

influence net dipole[59]. In a previous study, the effect of the length of a weakly polarizable hydrocarbon spacer of alkanethiol SAMs on the work function of Au (111) was observed[59]. The researchers found that although alkanethiol molecules carry permanent dipole moments in gas phase, upon formation of the monolayer, the position of the tail group changes slightly due to mutual interactions, resulting to a slight deviation of the dipole moment from the gas phase[59]. Thus, the net dipole moment of the SAM and the gas phase dipole may be quite different due to the presence of the interface dipole and depolarization effects which must be carefully considered.

These days, different methods are available to study the surface dipole or work function of materials. Some methods can measure work function directly, such photoemission spectroscopy methods such as UPS. Another approach is to measure the contact potential difference of the surface and comparing it to that of a reference sample with a known work function, which is the basis of the Kelvin Probe Force Microscopy (KPFM).

1.3. Contact Potential Difference and Kelvin Probe Force Microscopy

1.3.1. Contact Potential Difference

Contact potential difference (CPD) is the potential difference which is present when two materials of different work functions are electrically connected. Prior to Kelvin Probe Force Microscopy (KPFM), the Kelvin Probe Method was used to measure CPD between materials. This technique uses two conductors placed in a parallel plate capacitor configuration with very little space in between them. When two metals which have different work functions are electrically connected, electrons from the metal with the lower work function will flow to the metal which has the higher work function[45]. This transfer of electrons continues until the Fermi levels of the metals reach equilibrium and coincide. As a result of the charge transfer, the metals are left with a net surface charge or surface potential (Figure 1.5). This slight surface charge results to a potential drop from one metal to another,

which is called the contact potential difference (CPD)[51,61]. CPDs are dependent on the materials and are related to its work function as well as surface dipole moments[61]. CPD measurements are very sensitive and may be affected by humidity, contamination and local reorientation of dipoles[62].

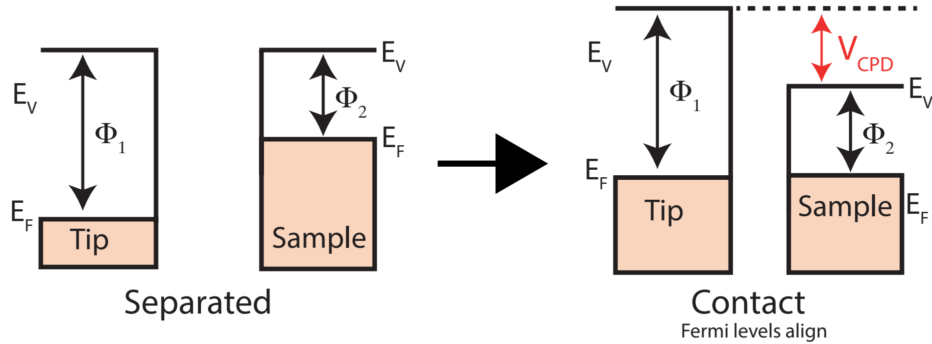

Figure 1.5. Presence of contact potential difference (CPD) between two materials with different work functions when in electrical contact

In the Kelvin Probe method, a counter potential is applied to the system to neutralize the CPD between the two materials. This counter potential is equivalent to -CPD. The Kelvin probe method can give an accurate reading of the CPD, however the measured value is the average of the whole surface area and does not provide a good representation of the local changes of the CPD of the surface. In 1991, Nonnenmacher et. al modified an ac scanning force microscope to obtain a high lateral resolution CPD measurement of a surface[62]. They conducted measurements on gold, platinum and palladium gratings on a gold substrate and found clear CPD variations along the surface. Their system was also able to successfully measure topography and contact potential difference and lead to the development of the Kelvin Probe Force Microscope.

1.3.2. Kelvin Probe Force Microscopy

The technique developed by Nonnemacher et al. is an important step in the field of material science because it successfully measured topography and contact potential

difference of samples simultaneously with very high resolution[62]. This allows researchers to take a closer look at the source of CPD variations and deepen their understanding of the factors that affect it.

During KPFM measurement, the difference in the work function of the cantilever tip and the sample results in a CPD between them (Figure 1.6). KPFM measurements have the advantage of not being restricted to conductive samples because the mechanism behind it relies on electrostatic force rather than current passing through the sample[51]. KPFM is a useful tool that can measure the local changes in the contact potential difference between an atomic force microscope (AFM) tip and a sample.

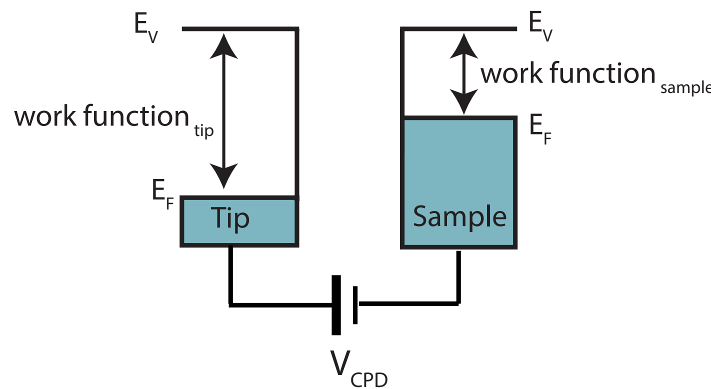

Figure 1.6. CPD is nullified by applying an equivalent voltage in the opposite polarity during KPFM measurement

All KPFM systems use the following components – an alternating (ac) voltage, an adjustable direct current (dc) offset, a conducting AFM tip, a lock-in amplifier, and a feedback circuit to control the dc tip potential to compensate for the CPD[63]. Selection of the proper tip and parameters used in KPFM measurements will determine if the images will be of high resolution and stable. Many researchers have then used worked on ways to develop and improve the KPFM to obtain better and clearer resolutions[51,57,61,64,65].

Two modes of KPFM analysis are can be used during analysis - single-pass scan or a double-pass lift-up scan[45]. During single-pass scan mode, the topographical and surface potential signals are detected simultaneously by using two different tip oscillation frequencies. Using single-pass scan mode results in a higher spatial resolution and more accurate topographical images can be obtained due to the minimization of electrostatic forces in this mode. However, one disadvantage of using single-pass scan mode is the risk of cross talk from the two signals[66]. Dual-pass scans on the other hand uses separate signals for topography and surface potential, however a longer scan time is required because the tip is scanned across the surface twice. During the first scan, details of the surface topography is measured and stored. This information is then used in the second scan to ensure constant tip height during the measurement of the surface potential. Although single-pass KPFM is faster and can provide better spatial resolution, several studies have used dual-pass KPFM with good and precise results[56,63,67].

The changes in the CPD detected during KPFM measurement gives insight to the surface potential and work function of the sample. Because an AFM tip is used, KPFM provides very high spatial resolution. In 1999, a study conducted by Lu et al. showed that KPFM is capable of measuring topography and CPD with a topographic and CPD resolution of 0.05nm and 3 meV respectively[51]. Their CPD measurements were able to distinguish regions in the monolayer film comprising of chemically different terminal head groups. Using KPFM they were also able to confirm a previous study conducted by Evans and Ulman which showed that surface potential is dependent on alkyl chain length[20]. Evans did their study using Kelvin Probe method, which integrates of the entire surface of the film, while Lu's study used KPFM.

During KPFM measurement, tip selection is very important and can affect the resolution and quality of the images. Jacobs et. al reported that tip geometry is one of the most crucial parameters to consider when trying to improve the resolution and accuracy of

KPFM images[63]. In another research, Vatel et al. found that the tip-to-sample distance and tip features, such as the radius and shape are most crucial in obtaining accurate measurements[68]. In their experiments they found that the tip-to-sample distance must be kept small and a sharp tip must be used in order to obtain KFM images and topographic images with high spatial resolutions. By keeping these parameter optimized, they were able to detect surface potentials less than 5 mV and observe monolayer-height steps in the topographic image of their GaAs samples. Tip scan rate is also something to consider when conducting KPFM measurements. Sugimura et. al found that using a very slow scan rate (0.1 Hz) clearly showed the distinction in surface potential between alkylsilane and fluoroalkylsilane SAM, but using a faster scan rate (1 Hz) did not produce an accurate image.

KPFM measurement is not constrained to ultrahigh vacuum conditions and can be performed under ambient pressure[51]. However, environmental conditions, particularly humidity should also be closely monitored during KPFM analysis because some studies have found that an adsorbed water layer on the surface of the sample can cause shielding and lead to a degradation in the surface potential contrast[69,70]. As such, the surface hydrophobicity of the sample can also affect the measurements. More hydrophobic samples had greater potential contrasts.

One thing to note is that KPFM is a relative measurement technique and requires the use of a reference material. One reference material often used is Highly Ordered Pyrolytic Graphite (HOPG)[71] due to its chemical inertness and established work function. However, other reference materials may also be used for comparison provided that it is consistent and reliable. In this study we used SAM formed from 1-hexadecene (HD) precursor as reference material during KPFM measurements. The reference HD SAM and the SAM being analyzed were grafted to the same silicon substrate via VUV micropatterning.

1.4. Micropatterning SAMs via VUV Photolithography

Several methods for micropatterning of SAMs have been reported in literature, such as photolithography[72,73], micro-contact printing[74,75] and AFM lithography[76–78]. Of these, photolithography offers the most versatility because it allows patterning of a large area with a photomask during a single illumination period. It has been reported that vacuum ultraviolet (VUV) photolithography has been successful in producing micropatterned SAMs. This method has been used to pattern organosilane SAMs[53,76,79,80] and alkene SAMs on silicon[72,81].

1.4.1. VUV Light

Light with a wavelength below 400 nm is categorized as ultraviolet light (UV) and falls on the right side of the spectrum (Figure 1.7). UV light is further categorized into four spectral ranges, which are UV-A (315-400 nm), UV-B (280 - 315 nm), UV-C (200 - 280 nm) and vacuum ultraviolet (VUV) (<200 nm). For the VUV light range, this light is easily absorbed by the oxygen in the atmosphere and thus often requires a vacuum environment. Sources of VUV light are excimer lamps, where "excimer" is the abbreviated form of "excited dimer".

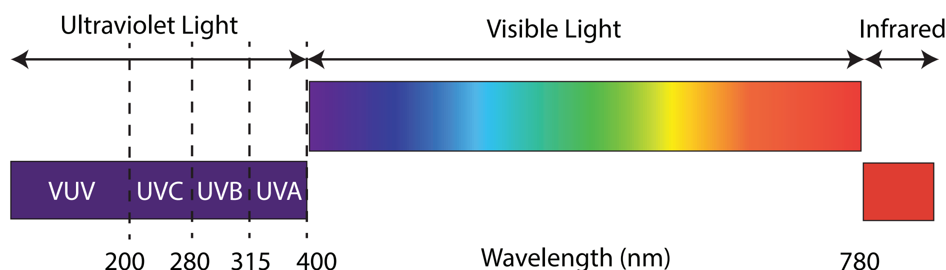

Figure 1.7. Light spectrum including ultraviolet light, visible light and infrared

VUV light been used for cleaning[82], etching[83] or surface modification[84,85]. VUV light has also been known to dissociate chemical bonds such as C-C, C-H and C-Si, and thus can be used to degrade/remove SAMs on a substrate[72]. With the use of a photomask during VUV

light irradiation, some parts of the SAM sample can remain intact while the irradiated regions will be removed. This is the basis of VUV photolithography.

1.4.2. VUV Photolithography

During VUV irradiation, the oxygen in the atmosphere absorbs the VUV light and is converted to atomic oxygen, given by the following reaction[80].

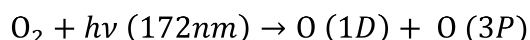

$$O_2 + h\nu\ (172nm) \rightarrow O\ (1D) +\ O\ (3P)$$

These atomic oxygen species have strong oxidative reactivity and can aid in the removal of organic materials[82]. VUV light can dissociate the C-C and C-H bonds in SAMs and converts them to radicals. The chemical reaction of these radicals to the oxygen and water molecules in the atmosphere results to the formation of hydrophilic groups such as hydroxyl and carboxyl[76]. When SAMs are irradiated using VUV light, photodegradation occurs which begins at the terminal group of the molecule and approaches the headgroup during the process[80]. When irradiated through a photomask, only the irradiated region would be degraded while the masked region would remain intact. Through VUV photolithography, two kinds of SAM could be grafted to the same surface. A first SAM is formed on the substrate before undergoing VUV irradiation with the use of a photomask and a second SAM can be grafted in the regions where the VUV light had removed the first SAM. Previous studies have shown that VUV photolithography was successful in micropatterning organosilane SAMs[53,76,79,80,86] and alkene SAMs[72,81] on silicon.

SAMs have shown to have good potential to be used as a photoresist during VUV photolithography due to their uniformity and strong molecular order. Particularly SAMs covalently bonded onto silicon are promising since they display higher chemical resistivities to HF[38,87]. HF is often in the etching process to remove the oxide layer left behind by VUV irradiation, allowing a second SAM to be grafted to the substrate. Due to their strong Si-C covalent bond to silicon and chemical resistivity to HF, 1-alkene SAMs are very good

candidates as photoresists in preparing micropatterned SAMs[87]. In our study we used 1-hexadecene SAM (HD SAM) as our photoresist to fabricate our micropatterned SAMs for KPFM measurements.

1.5 Objectives

The objective of this research is to measure changes in the surface potential of n-Si (111) via Kelvin Probe Force Microscopy (KPFM) due to the adsorption of different molecules. To ensure that our KPFM measurements are not affected by changes in the cantilever tip, measurements were conducted using micropatterned SAMs prepared via VUV photolithography using a photomask. Many studies have modified the surface potential of SAMs by changing the functional groups of the molecules,[42,58] but few studies have been done on how to further fine tune the surface potential of substrates by using small structural modifications or by altering the binding chemistry of the molecule to the substrate. By understanding the relationship of various parameters between the surface potential we can deeper our understanding on how we can utilize different molecules in the optimization of silicon's work function and improve its charge injection capabilities in electronic applications.

1.6 Outlines

Chapter 1 covers a review of relevant literature concerning self-assembled monolayers (SAMs) and their role in the field of molecular electronics. Focus is given to SAMs directly grafted to silicon via covalent bonds, being that silicon is one of the widely used semiconductor in the field of present-day electronics and understanding how to optimize it will be beneficial to the advancement of technology. The importance of SAMs in improving device performance through minimizing energy loss of charge carriers as they cross between material interfaces are highlighted in this chapter. A thin molecular layer at a

substrate surface introduces a dipole layer which cause a change in the surface potential and shifts the vacuum level energy at the interface. This shift can be controlled to increase or decrease the work function of the substrate. Past studies which have demonstrated how different molecules are able to control the dipole layer on the material surface are reviewed in this chapter.

Chapter 2 In this chapter we optimized the parameters for the formation of micropatterned SAMs via VUV photolithography of 1-hexadecene SAM (HD SAM). Micropatterning of SAMs have numerous applications, one of which is to provide a stable reference material during KPFM measurements. Having a reference material is necessary because surface potential measurements using KPFM method may be affected by the electrodes/probe used during characterization. We conducted a series of test with varying VUV irradiation time and chamber pressure to determine the best combination required to complete the photodegradation of HD SAM on n-Si (111). Using Kelvin Probe Force Microscopy (KPFM), we observed the micropatterns formed on HD SAM using the different VUV irradiation times. Etching conditions during the photolithography process was also optimized to ensure that only minimal damage to the reference HD SAM. Atomic Force Microscopy (AFM) was observe the effects of different etching conditions to the HD SAM layer. Based on the results, determined the optimum etching conditions necessary to remove the oxide layer that is formed as a result of VUV photoirradiation, while minimizing the damage on the HD SAM layer.

Chapter 3 In this chapter, we concentrated on the effects of different interface dipoles on the material's surface potential. Three molecules which possess the same hydrocarbon chain (n = 16) but differ in the interfacial bonds formed with the silicon substrate (Si-C, Si-S and Si-O) have been selected for this study. SAMs using 1-hexadecene (HD SAM), 1-hexadecanethiol (HDT SAM) and 1-hexadecanol (HDO SAM) on hydrogen terminated Si (111) substrate were prepared. Using HD SAM as a photoresist and the

optimized conditions we found in Chapter 2, we formed micropatterned HD-HD, HD-HDT and HD-HDO SAMs. We obtained the surface potential difference and topographic contrasts of the micropatterned SAMs via Kelvin Probe Force Microscope (KPFM). The dipole moments of the precursor molecules and the SAMs were computed for using Molecular Package (MOPAC) semi empirical computations and compared with the KPFM measurements.

Chapter 4 This chapter aimed to understand the surface potential variations of silicon due to the SAM formed using 1-alkene precursors of different lengths. Previous studies on the surface potential of alkylthiol SAMs on Au have reported a linear dependence on the chain length of the molecules, however it is uncertain if the same can be observed for semiconductor surfaces, which is the objective of this experiment. SAMs on n-Si (111) using 1-alkene precursors with hydrocarbon chain lengths equal to n = 10, 12, 14, 16, 18 and 20 were prepared in this chapter. Even-chained molecules were chosen to avoid any odd-even effects that have been known to occur due to the geometry of the molecules with respect to the substrate. The surface potential differences and topographic contrasts were measured using KPFM with HD SAM (n = 16) as the reference. Other tests measured other properties such as ellipsometric thickness, atomic compositions, water contact angles and morphologies to determine the qualities of the individual SAMs.

Chapter 5 This chapter measured the surface potentials of Si-C and Si-O bound aromatic SAMs on n-Si (111). Aromatic molecules have a smaller HOMO-LUMO gap than alkenes which allows charge to be transported more easily, possibly providing the sample with increased conductivity. We prepared aromatic SAMs using styrene ($C_6H_5CH=CH_2$), benzyl alcohol ($C_6H_5CH_2$-OH), 4-phenyl-1-butene ($C_6H_5(CH_2)_2CH=CH_2$), and 3-phenyl-1-propanol ($C_6H_5(CH_2)_3$-OH). Micropatterned SAMs were prepared using the aromatic SAMs with HD SAM as reference. The surface potential difference and topographic contrast using KPFM. The variations in surface potential due to the nature of the covalent bond of the

SAMs to the silicon substrate were discussed. Conductive AFM (CAFM) was also performed to observe the electrical properties of the SAMs.

Chapter 6 summarizes the results and findings of this thesis

References

(1) Gooding, J. J.; Mearns, F.; Yang, W.; Liu, J. Self-Assembled Monolayers into the 21st Century: Recent Advances and Applications. *Electroanalysis* **2003**, *15* (2), 81–96. https://doi.org/10.1002/elan.200390017.

(2) Ulman, A. Formation and Structure of Self-Assembled Monolayers. *Chem. Rev.* **1996**, *96*, 1533–1554.

(3) Casalini, S.; Bortolotti, C. A.; Leonardi, F.; Biscarini, F. Self-Assembled Monolayers in Organic Electronics. *Chem. Soc. Rev.* **2017**, *46*, 40–71. https://doi.org/10.1039/c6cs00509h.

(4) Nakano, M.; Ishida, T.; Sano, H.; Sugimura, H.; Miyake, K.; Ando, Y.; Sasaki, S. Tribological Properties of Self-Assembled Monolayers Covalently Bonded to Si. *Appl. Surf. Sci.* **2008**, *255*, 3040–3045. https://doi.org/10.1016/j.apsusc.2008.08.073.

(5) Behpour, M.; Mohammadi, N. Investigation of Inhibition Properties of Aromatic Thiol Self-Assembled Monolayer for Corrosion Protection. *Corros. Sci.* **2012**, *65*, 331–339. https://doi.org/10.1016/j.corsci.2012.08.036.

(6) Zhang, J.; Liu, Z.; Han, G. C.; Chen, S. L.; Chen, Z. Inhibition of Copper Corrosion by the Formation of Schiff Base Self-Assembled Monolayers. *Appl. Surf. Sci.* **2016**. https://doi.org/10.1016/j.apsusc.2016.07.116.

(7) Appa Rao, B. V.; Yakub Iqbal, M.; Sreedhar, B. Self-Assembled Monolayer of 2-(Octadecylthio)Benzothiazole for Corrosion Protection of Copper. *Corros. Sci.* **2009**, *51*, 1441–1452. https://doi.org/10.1016/j.corsci.2009.03.034.

(8) Appa Rao, B. V.; Narsihma Reddy, M. Formation, Characterization and Corrosion

Protection Efficiency of Self-Assembled 1-Octadecyl-1H-Imidazole Films on Copper for Corrosion Protection. *Arab. J. Chem.* **2017**. https://doi.org/10.1016/j.arabjc.2013.12.026.

(9) Chaki, N. K.; Vijayamohanan, K. Self-Assembled Monolayers as a Tunable Platform for Biosensor Applications. *Biosensors and Bioelectronics*. 2002. https://doi.org/10.1016/S0956-5663(01)00277-9.

(10) Flink, S.; Van Veggel, F. C. J. M.; Reinhoudt, D. N. Sensor Functionalities in Self-Assembled Monolayers. *Adv. Mater.* **2000**. https://doi.org/10.1002/1521-4095(200009)12:18<1315::AID-ADMA1315>3.0.CO;2-K.

(11) Tanaka, T.; Yajima, T.; Uchida, K. Impact of Defects in Self-Assembled Monolayer on Humidity Sensing by Molecular Functionalized Transistors. *Jpn. J. Appl. Phys.* **2020**, *59* (SI). https://doi.org/10.35848/1347-4065/ab80dc.

(12) Rampi, M. A.; Schueller, O. J. A.; Whitesides, G. M. Alkanethiol Self-Assembled Monolayers as the Dielectric of Capacitors with Nanoscale Thickness. *Appl. Phys. Lett.* **1998**, *72*, 1781–1783.

(13) Aswal, D. K.; Lenfant, S.; Guerin, D.; Yakhmi, J. V.; Vuillaume, D. Self Assembled Monolayers on Silicon for Molecular Electronics. *Anal. Chim. Acta* **2006**, *568*, 84–108. https://doi.org/10.1016/j.aca.2005.10.027.

(14) Whitesides, G. M.; Kriebel, J. K.; Love, J. C. Molecular Engineering of Surfaces Using Self-Assembled Monolayers. *Sci. Prog.* **2005**, *88* (Pt 1), 17–48. https://doi.org/10.3184/003685005783238462.

(15) Mark H. Schoenfisch and Jeanne E. Pemberton. Air Stability of Alkanethiol Self-Assembled Monolayers on Silver and Gold Surfaces. *J. Am. Chem. Soc.* **1998**, *120*, 4502–4513.

(16) Howell, S.; Kuila, D.; Kasibhatla, B.; Kubiak, C. P.; Janes, D.; Reifenberger, R. Molecular Electrostatics of Conjugated Self-Assembled Monolayers on Au(111)

Using Electrostatic Force Microscopy. *Langmuir* **2002**, *18* (13), 5120–5125. https://doi.org/10.1021/la0157014.

(17) Weiss, E. A.; Kriebel, J. K.; Rampi, M. A.; Whitesides, G. M. The Study of Charge Transport through Organic Thin Films: Mechanism, Tools and Applications. *Philos. Trans. R. Soc. A Math. Phys. Eng. Sci.* **2007**, *365* (1855), 1509–1537. https://doi.org/10.1098/rsta.2007.2029.

(18) Folkers, J. P.; Laibinis, P. E.; Whitesides, G. M. Self-Assembled Monolayers of Alkanethiols on Gold: The Adsorption and Wetting Properties of Monolayers Derived from Two Components with Alkane Chains of Different Lengths. *J. Adhes. Sci. Technol.* **1992**. https://doi.org/10.1163/156856192X00700.

(19) Laxman Kankate, Andrey Turchanin, and A. G. On the Release of Hydrogen from the S-H Groups in the Formation of Self-Assembled Monolayers of Thiols. *Langmuir* **2009**, *25* (18), 10435–10438.

(20) Evans, S. D.; Ulman, A. Surface Potential Studies of Alkyl-Thiol Monolayers Adsorbed on Gold. *Chem. Phys. Lett.* **1990**, *170*, 462–466. https://doi.org/10.1016/S0009-2614(90)87085-6.

(21) Lee, N.; Kang, H.; Ito, E.; Hara, M.; Noh, J. Effects of Solvent on the Structure of Octanethiol Self-Assembled Monolayers on Au(111) at a High Solution Temperature. *Bull. Korean Chem. Soc.* **2010**, *31* (8), 2137–2138.

(22) Desbief, S.; Patrone, L.; Goguenheim, D.; Gue, D.; Vuillaume, D. Impact of Chain Length , Temperature , and Humidity on the Growth of Long Alkyltrichlorosilane Self-Assembled Monolayers W. *Phys. Chem. Chem. Phys.* **2011**, *13*, 2870–2879. https://doi.org/10.1039/c0cp01382j.

(23) Sugimura, H.; Hozumi, A.; Kameyama, T.; Takai, O. Organosilane Self-Assembled Monolayers Formed at the Vapour/Solid Interface. In *Surface and Interface Analysis*; 2002. https://doi.org/10.1002/sia.1358.

(24) Haensch, C.; Hoeppener, S.; Schubert, U. S. Chemical Modification of Self-Assembled Silane Based Monolayers by Surface Reactions. *Chem. Soc. Rev.* **2010**, *39* (6), 2323. https://doi.org/10.1039/b920491a.

(25) Dulcey, C. S.; Georger, J. H.; Chen, M. S.; McElvany, S. W.; O'Ferrall, C. E.; Benezra, V. I.; Calvert, J. M. Photochemistry and Patterning of Self-Assembled Monolayer Films Containing Aromatic Hydrocarbon Functional Groups. *Langmuir* **1996**, *12* (6), 1638–1650. https://doi.org/10.1021/la9509514.

(26) Sagiv, J. Organized Monolayers by Adsorption. 1. Formation and Structure of Oleophobic Mixed Monolayers on Solid Surfaces. *J. Am. Chem. Soc.* **1980**, *102* (1), 92–98. https://doi.org/10.1021/ja00521a016.

(27) Linford, M. R.; Chidsey, C. E. D.; Fenter, P.; Eisenberger, P. M. Alkyl Monolayers on Silicon Prepared from 1-Alkenes and Hydrogen-Terminated Silicon. *J. Am. Chem. Soc.* **1995**, *117* (11), 3145–3155. https://doi.org/10.1021/ja00116a019.

(28) Higashi, G. S.; Chabal, Y. J.; Trucks, G. W.; Raghavachari, K. Ideal Hydrogen Termination of the Si (111) Surface. *Appl. Phys. Lett.* **1990**, *56* (7), 656–658. https://doi.org/10.1063/1.102728.

(29) Dumas, P.; Chabal, Y. J.; Jakob, P. Morphology of Hydrogen-Terminated Si(111) and Si(100) Surfaces upon Etching in HF and Buffered-HF Solutions. *Surf. Sci.* **1992**, *269–270* (C), 867–878. https://doi.org/10.1016/0039-6028(92)91363-G.

(30) Burrows, V. A.; Chabal, Y. J.; Higashi, G. S.; Raghavachari, K.; Christman, S. B. Infrared Spectroscopy of Si(111) Surfaces after HF Treatment: Hydrogen Termination and Surface Morphology. *Appl. Phys. Lett.* **1988**, *53* (11), 998–1000. https://doi.org/10.1063/1.100053.

(31) Higashi, G. S.; Becker, R. S.; Chabal, Y. J.; Becker, A. J. Comparison of Si(111) Surfaces Prepared Using Aqueous Solutions of NH4F versus HF. *Appl. Phys. Lett.* **1991**, *58* (15), 1656–1658. https://doi.org/10.1063/1.105155.

(32) Sieval, B. A. B.; Linke, R.; Zuilhof, H.; Sudhölter, E. J. R. High-Quality Alkyl Monolayers on Silicon Surfaces. *Adv. Mater.* **2000**, *12* (9), 1457–1460.

(33) Sieval, A. B.; Demirel, A. L.; Nissink, J. W. M.; Linford, M. R.; Van Der Maas, J. H.; De Jeu, W. H.; Zuilhof, H.; Sudhölter, E. J. R. Highly Stable Si-C Linked Functionalized Monolayers on the Silicon (100) Surface. *Langmuir* **1998**, *14* (7), 1759–1768. https://doi.org/10.1021/la971139z.

(34) Gao, F.; Teplyakov, A. V. Challenges and Opportunities in Chemical Functionalization of Semiconductor Surfaces. *Appl. Surf. Sci.* **2017**, *399*, 375–386. https://doi.org/10.1016/j.apsusc.2016.12.083.

(35) Sano, H.; Maeda, H.; Matsuoka, S.; Lee, K. H.; Murase, K.; Sugimura, H. Self-Assembled Monolayers Directly Attached to Silicon Substrates Formed from 1-Hexadecene by Thermal, Ultraviolet, and Visible Light Activation Methods. *Jpn. J. Appl. Phys.* **2008**, *47*, 5659–5664. https://doi.org/10.1143/JJAP.47.5659.

(36) Huang, Y.; Chen, C.; Chen, C.; Hung, W. Fabrication of Octadecyl and Octadecanethiolate Self-Assembled Monolayers on Oxide-Free Si(111) with a One-Cell Process. *Appl. Mater. interfaces* **2013**, *5*, 5771–5776. https://doi.org/10.1021/am401270z.

(37) Wallart, X.; De Villeneuve, C. H.; Allongue, P. Truly Quantitative XPS Characterization of Organic Monolayers on Silicon: Study of Alkyl and Alkoxy Monolayers on H-Si(111). *J. Am. Chem. Soc.* **2005**, *127* (21), 7871–7878. https://doi.org/10.1021/ja0430797.

(38) Sano, H.; Maeda, H.; Ichii, T.; Murase, K.; Noda, K.; Matsushige, K.; Sugimura, H. Alkyl and Alkoxyl Monolayers Directly Attached to Silicon: Chemical Durability in Aqueous Solutions. *Langmuir* **2009**, *25* (10), 5516–5525.

(39) Sieval, A. B.; Van den Hout, B.; Zuilhof, H.; Lee, M. V.; Sudhölter, E. J. R. Molecular Modeling of Alkyl Monolayers on the Si(111) Surface. *Langmuir* **2000**, *16* (7), 2987–

2990. https://doi.org/10.1021/la048894e.

(40) Garcia, M. C. T.; Utsunomiya, T.; Ichii, T.; Sugimura, H. Surface Potential Contrasts between 1-Alkene, 1-Thiol and 1-Alcohol Self-Assembled Monolayers on Silicon (111) Substrate. *Jpn. J. Appl. Phys.* **2020**, *59* (SD), SDDC06. https://doi.org/10.7567/1347-4065/ab5925.

(41) Sano, H.; Ohno, K.; Ichii, T.; Murase, K.; Sugimura, H. Alkanethiol Self-Assembled Monolayers Formed on Silicon Substrates. *Jpn. J. Appl. Phys.* **2010**. https://doi.org/10.1143/JJAP.49.01AE09.

(42) Campbell, I. H.; Kress, J. D.; Martin, R. L.; Smith, D. L.; Barashkov, N. N.; Ferraris, J. P. Controlling Charge Injection in Organic Electronic Devices Using Self-Assembled Monolayers. *Appl. Phys. Lett.* **1997**, *71* (24), 3528–3530. https://doi.org/10.1063/1.120381.

(43) Ganzorig, C.; Kwak, K. J.; Yagi, K.; Fujihira, M. Fine Tuning Work Function of Indium Tin Oxide by Surface Molecular Design: Enhanced Hole Injection in Organic Electroluminescent Devices. *Appl. Phys. Lett.* **2001**, *79* (2), 272–274. https://doi.org/10.1063/1.1384896.

(44) Kress, J. D.; Martin, R. L.; Barashkov, N.; Ferraris, J. P. Controlling Charge Injection in Organic Electronic Devices Using Self-Assembled Monolayers. *Phys. Rev. B - Condens. Matter Mater. Phys.* **1996**, *54* (20), 14321–14324. https://doi.org/10.1063/1.120381.

(45) Palermo, V.; Palma, M.; Samori, P. Electronic Characterization of Organic Thin Films by Kelvin Probe Force Microscopy. *Advanced Materials*. January 19, 2006, pp 145–164. https://doi.org/10.1002/adma.200501394.

(46) Kahn, A. Fermi Level, Work Function and Vacuum Level. *Mater. Horizons* **2016**, *3* (1), 7–10. https://doi.org/10.1039/c5mh00160a.

(47) Ishii, H.; Sugiyama, K.; Ito, E.; Seki, K. Energy Level Alignment and Interfacial

Electronic Structures at Organic/Metal and Organic/Organic Interfaces. *Adv. Mater.* **1999**, *11* (8), 605–625.

(48) Heimel, G.; Romaner, L.; Zojer, E.; Bredas, J. The Interface Energetics of Self-Assembled Monolayers on Metals. *Acc. Chem. Res.* **2008**, *41* (6), 721–729.

(49) Campbell, I.; Rubin, S.; Zawodzinski, T.; Kress, J.; Martin, R.; Smith, D.; Barashkov, N.; Ferraris, J. Controlling Schottky Energy Barriers in Organic Electronic Devices Using Self-Assembled Monolayers. *Phys. Rev. B - Condens. Matter Mater. Phys.* **1996**, *54* (20), 14321–14324. https://doi.org/10.1103/PhysRevB.54.R14321.

(50) Hlavathy, Z.; Tétényi, P.; Paal, Z. Adsorption of Alkanes and Alkenes on Pt as Studied by Work Function Changes. *J. CHEM. SOC. FARADAY TRANS* **1992**, *88* (14), 2059–2064. https://doi.org/10.1016/S0039-6028(98)00290-8.

(51) Lu, J.; Delamarche, E.; Eng, L.; Bennewitz, R.; Meyer, E.; Gu, H. Kelvin Probe Force Microscopy on Surfaces : Investigation of the Surface Potential of Self-Assembled Monolayers On. *Langmuir* **1999**, *15*, 8184–8188. https://doi.org/10.1021/la9904861.

(52) Alloway, D. M.; Hofmann, M.; Smith, D. L.; Gruhn, N. E.; Graham, A. L.; Colorado, R.; Wysocki, V. H.; Lee, T. R.; Lee, P. A.; Armstrong, N. R. Interface Dipoles Arising from Self-Assembled Monolayers on Gold: UV-Photoemission Studies of Alkanethiols and Partially Fluorinated Alkanethiols. *J. Phys. Chem. B* **2003**, *107* (42), 11690–11699. https://doi.org/10.1021/jp034665+.

(53) Hayashi, K.; Saito, N.; Sugimura, H.; Takai, O.; Nakagiri, N. Surface Potential Contrasts between Silicon Surfaces Covered and Uncovered with an Organosilane Self-Assembled Monolayer. *Ultramicroscopy* **2002**, *91* (1–4), 151–156. https://doi.org/10.1016/S0304-3991(02)00094-3.

(54) Egger, D. A.; Rissner, F.; Gerold, R. M.; Hofmann, O. T.; Wittwer, L.; Heimel, G.; Zojer, E. Self-Assembled Monolayers of Polar Molecules on Au(111) Surfaces: Distributing the Dipoles. *Phys. Chem. Chem. Phys.* **2010**, *12* (17), 4291–4294.

https://doi.org/10.1039/c004746p.

(55) Cohen, R.; Bastide, S.; Cahen, D.; Libman, J.; Shanzer, A.; Rosenwaks, Y. Controlling Surfaces and Interfaces of Semiconductors Using Organic Molecules. *Opt. Mater. (Amst).* **1998**, *9* (1–4), 394–400. https://doi.org/10.1016/S0925-3467(97)00065-7.

(56) Szwajca, A.; Wei, J.; Schukfeh, M. I.; Tornow, M. Self-Assembled Monolayers of Alkyl-Thiols on InAs: A Kelvin Probe Force Microscopy Study. *Surf. Sci.* **2015**, *633*, 53–59. https://doi.org/10.1016/j.susc.2014.11.023.

(57) Sugimura, H.; Hayashi, K.; Saito, N. Kelvin Probe Force Microscopy Images of Microstructured Organosilane Self-Assembled Monolayers. *Jpn. J. Appl. Phys.* **2001**, *40*, 4373.

(58) Saito, N.; Hayashi, K.; Sugimura, H.; Takai, O.; Nakagiri, N. Surface Potential Images of Self-Assembled Monolayers Patterned by Organosilanes: Ab Initio Molecular Orbital Calculations. *Surf. Interface Anal.* **2002**, *34* (1), 601–605. https://doi.org/10.1002/sia.1369.

(59) Sushko, B. M. L.; Shluger, A. L. Intramolecular Dipole Coupling and Depolarization in Self-Assembled Monolayers **. *Adv. Funct. Mater.* **2008**, *18*, 2228–2236. https://doi.org/10.1002/adfm.200701305.

(60) Sushko, M. L.; Shluger, A. L. Dipole-Dipole Interactions and the Structure of Self-Assembled Monolayers. *J. Phys. Chem. B* **2007**, *111*, 4019–4025. https://doi.org/10.1021/jp0688557.

(61) Lü, J.; Eng, L.; Bennewitz, R.; Meyer, E.; Güntherodt, H. J.; Delamarche, E.; Scandella, L. Surface Potential Studies of Self-Assembling Monolayers Using Kelvin Probe Force Microscopy. *Surf. Interface Anal.* **1999**. https://doi.org/10.1002/(SICI)1096-9918(199905/06)27:5/6<368::AID-SIA530>3.0.CO;2-W.

(62) Nonnenmacher, M.; O'Boyle, M. P.; Wickramasinghe, H. K. Kelvin Probe Force Microscopy. *Appl. Phys. Lett.* **1991**, *58* (25), 2921–2923. https://doi.org/10.1063/1.105227.

(63) Jacobs, H. O.; Knapp, H. F.; Stemmer, A. Practical Aspects of Kelvin Probe Force Microscopy. *Rev. Sci. Instrum.* **1999**, *70* (3), 1756–1760. https://doi.org/10.1063/1.1149664.

(64) Yasutake, M.; Aoki, D.; Fujihira, M. Surface Potential Measurements Using the Kelvin Probe Force Microscope. *Thin Solid Films* **1996**. https://doi.org/10.1016/0040-6090(95)06772-8.

(65) Rosenwaks, Y.; Shikler, R.; Glatzel, T.; Sadewasser, S. Kelvin Probe Force Microscopy of Semiconductor Surface Defects. *Phys. Rev. B - Condens. Matter Mater. Phys.* **2004**, *70* (8), 1–7. https://doi.org/10.1103/PhysRevB.70.085320.

(66) Li, G.; Mao, B.; Lan, F.; Liu, L. Practical Aspects of Single-Pass Scan Kelvin Probe Force Microscopy. *Rev. Sci. Instrum.* **2012**, *83* (11), 113701.1-8. https://doi.org/10.1063/1.4761922.

(67) Park, J.; Bang, D.; Jang, K.; Haam, S.; Yang, J.; Na, S. The Work Function of Doped Polyaniline Nanoparticles Observed by Kelvin Probe Force Microscopy. *Nanotechnology* **2012**, *23* (36), 1–7. https://doi.org/10.1088/0957-4484/23/36/365705.

(68) Vatel, O.; Tanimoto, M. Kelvin Probe Force Microscopy for Potential Distribution Measurement of Semiconductor Devices. *J. Appl. Phys.* **1995**, *77* (6), 2358–2362. https://doi.org/10.1063/1.358758.

(69) Nakagiri, N.; Sugimura, H.; Ishida, Y.; Hayashi, K.; Takai, O. Effects of an Adsorbed Water Layer and Self-Assembled Organosilane Monolayers on Scanning Probe Microscopy of Silicon Pn Structures. *Surf. Sci.* **2003**, *532–535*, 999–1003. https://doi.org/10.1016/S0039-6028(03)00456-4.

(70) Sugimura, H.; Ishida, Y.; Hayashi, K.; Takai, O.; Nakagiri, N. Potential Shielding by the Surface Water Layer in Kelvin Probe Force Microscopy. *Appl. Phys. Lett.* **2002**, *80* (8), 1459–1461. https://doi.org/10.1063/1.1455145.

(71) Hansen, W. N.; Hansen, G. J. Standard Reference Surfaces for Work Function Measurements in Air. *Surf. Sci.* **2001**, *481* (1–3), 172–184. https://doi.org/10.1016/S0039-6028(01)01036-6.

(72) Khatri, O. P.; Sano, H.; Murase, K.; Sugimura, H. Regulation of Pattern Dimension as a Function of Vacuum Pressure: Alkyl Monolayer Lithography. *Langmuir* **2008**, *24* (20), 12077–12084. https://doi.org/10.1021/la8021613.

(73) Takakusagi, S.; Uosaki, K. Photopatterning of an Organic Monolayer Formed on a Si Single Crystal Surface via Si-C Covalent Bond by UV Irradiation in an Inert Atmosphere. *Japanese J. Appl. Physics, Part 1 Regul. Pap. Short Notes Rev. Pap.* **2006**, *45* (11), 8961–8966. https://doi.org/10.1143/JJAP.45.8961.

(74) Xia, Y.; Whitesides, G. M. Use of Controlled Reactive Spreading of Liquid Alkanethiol on the Surface of Gold to Modify the Size of Features Produced by Microcontact Printing. *J. Am. Chem. Soc.* **1995**, *117*, 3274–3275.

(75) Wilbur, J. L.; Kumar, A.; Biebuyck, H. A.; Kim, E.; Whitesides, G. M. Microcontact Printing of Self-Assembled Monolayers: Applications in Microfabrication. *Nanotechnology* **1996**, *7* (4), 452–457. https://doi.org/10.1088/0957-4484/7/4/028.

(76) Sugimura, H.; Nakagiri, N. Force Microscopy Imaging of Photopatterned Organosilane Monolayers: Application to Probe Alignment in AFMpatterning Following Photolithography. *Appl. Phys. A Mater. Sci. Process.* **1998**. https://doi.org/10.1007/s003390051176.

(77) Liu, G. Y.; Xu, S.; Qian, Y. Nanofabrication of Self-Assembled Monolayers Using Scanning Probe Lithography. *Acc. Chem. Res.* **2000**, *33* (7), 457–466. https://doi.org/10.1021/ar980081s.

(78) Zhang, Y.; Balaur, E.; Maupai, S.; Djenizian, T.; Boukherroub, R.; Schmuki, P. Nanopatterning of Si(1 1 1) Surfaces by Atomic Force Microscope Scratching of an Organic Monolayer. *Electrochem. commun.* **2003**, *5* (4), 337–340. https://doi.org/10.1016/S1388-2481(03)00052-3.

(79) Hong, L.; Hayashi, K.; Sugimura, H.; Takai, O.; Nakagiri, N.; Okada, M. Micropatterning of Organosilane Self-Assembled Monolayers Using Vacuum Ultraviolet Light at 172 Nm: Resolution Evaluation by Kelvin-Probe Force Microscopy. *Surf. Coatings Technol.* **2003**. https://doi.org/10.1016/S0257-8972(03)00077-X.

(80) Sugimura, H.; Saito, N.; Maeda, N.; Ikeda, I.; Ishida, Y.; Hayashi, K.; Hong, L.; Takai, O. Surface Potential Microscopy for Chemistry of Organic Self-Assembled Monolayers in Small Domains. *Nanotechnology* **2004**, *15*, S69–S75. https://doi.org/10.1088/0957-4484/15/2/015.

(81) Soliman, A. I. A.; Tu, Y.; Utsunomiya, T.; Ichii, T.; Sugimura, H. Low Damage Reductive Patterning of Oxidized Alkyl Self-Assembled Monolayers through Vacuum Ultraviolet Light Irradiation in an Evacuated Environment. *Langmuir* **2017**. https://doi.org/10.1021/acs.langmuir.7b02739.

(82) Falkenstein, Z. Surface Cleaning Mechanisms Utilizing VUV Radiation in Oxygen-Containing Gaseous Environments. In *Lithographic and Micromachining Techniques for Optical Component Fabrication*; Kley, E.-B., Herzig, H. P., Eds.; 2001; Vol. 4440, pp 246–255. https://doi.org/10.1117/12.448055.

(83) Tu, Y.; Utsunomiya, T.; Ichii, T.; Sugimura, H. Vacuum-Ultraviolet Promoted Oxidative Micro Photoetching of Graphene Oxide. *ACS Appl. Mater. Interfaces* **2016**, *8* (16), 10627–10635. https://doi.org/10.1021/acsami.6b00994.

(84) Soliman, A. I. A.; Utsunomiya, T.; Ichii, T.; Sugimura, H. Vacuum Ultraviolet Treatment of Acid- and Ester-Terminated Self-Assembled Monolayers: Chemical

Conversions and Friction Reduction. *Langmuir* **2018**. https://doi.org/10.1021/acs.langmuir.7b04327.

(85) Tu, Y.; Utsunomiya, T.; Ichii, T.; Sugimura, H. Enhancing the Electrical Conductivity of Vacuum-Ultraviolet-Reduced Graphene Oxide by Multilayered Stacking. *J. Vac. Sci. Technol. B, Nanotechnol. Microelectron. Mater. Process. Meas. Phenom.* **2017**, *35* (3), 03D110. https://doi.org/10.1116/1.4982722.

(86) Hong, L.; Hayashi, K.; Sugimura, H.; Takai, O.; Nakagiri, N. Micropatterning of Organosilane Self-Assembled Monolayers Using Vacuum Ultraviolet Light at 172 Nm : Resolution Evaluation by Kelvin-Probe Force Microscopy. **2003**, *170*, 211–214.

(87) Sugimura, H.; Sano, H.; Lee, K.-H.; Murase, K. Organic Monolayers Covalently Bonded to Si as Ultra Thin Photoresist Films in Vacuum UV Lithography. *Jpn. J. Appl. Phys.* **2006**, *45* (6B), 5456–5460. https://doi.org/10.1143/JJAP.45.5456.

Chapter 2: Formation of Micropatterned SAMs

2.1. Introduction

The fabrication of patterned molecular layers at the nanometer resolution has been of much interest due to its wide range of potential applications in fields such as molecular electronics[1,2] and bio devices[3–5]. Several methods of micropatterning include microcontact printing[6,7], electron beam lithography[8,9], scanning probe microscopy-based patterning[10–12] and photolithography[13,14]. Of these methods, photolithography is advantageous because it is capable of transferring an entire photomask pattern to a substrate with a single irradiation, allowing it to be used in large scale operations. Several studies have been done on the micropatterning of self-assembled monolayers (SAMs) on silicon[13,15–17].

In this chapter we aim to fabricate micropatterned SAMs on silicon as a means to observe and compare changes in the surface potential difference of different SAMs using one SAM as a reference. The surface potential or work function of a substrate can be measured using Kelvin Probe Force Microscopy (KPFM)[18–22]. The KPFM system is a modification of the conventional atomic force microscope (AFM) setup which enables it to map changes in the surface potential simultaneously with the topography of the sample[23–25]. Typically in KPFM measurements, calibration to a standardized material such as HOPG[26,27] is done to determine the absolute work function or surface potential of the sample being measured. However, an alternative method is to use a stable reference material as a basis for comparison. Having a reference material is necessary because surface potential measurements using KPFM method may be affected by the electrodes/probe used during characterization[28]. To ensure a more reliable data, surface potential measurements against a stable reference material is recommended. Measurements involving micropatterned SAMs with one SAM to be used as a reference material is a suitable method for this[18–21].

In **Chapters 3, 4 and 5**, micropatterned SAMs formed via vacuum ultraviolet (VUV) photolithography will be used for observing changes in the surface potential of a silicon substrate due to the adsorption of several molecules. To ensure the reliability and quality of the micropatterned SAMs, the conditions for photolithography must be verified and optimized. KPFM measurements are very sensitive to the quality of the SAM[25], thus it is necessary to verify if the SAM formed during the photolithography process will be of the same quality as SAM formed on a fresh silicon substrate. This is because the substrate undergoes irradiation and etching during photolithography thus we should check if the quality will be the same.

In the fabrication of micropatterned SAM via VUV photolithography, photoresists with uniform thickness and properties, as well as high chemical resistivity to withstand etching should be chosen. SAMs formed from 1-alkenes have been successfully patterned in past studies using vacuum UV photolithography with a wavelength of 172nm[13,29,30]. To obtain a clear and accurate pattern, certain factors such as the wavelength of the UV light, distance between the lamp and sample, quality of the sample and vacuum pressure inside the irradiation chamber should be considered since these may affect the spatial resolution of the final sample[13].

Aside from its uniformity, another advantage of using 1-alkene SAMs as a photoresist is that these SAMs have a strong covalent attachment to the Si substrate. This bond results to a higher chemical resistivity to HF compared to SAMs that are formed on oxide-covered Si[31,32]. In the formation of the micropatterned SAMs in this study, where two SAMs are grafted to the same silicon substrate, the original or photoresist SAM is subjected to HF and NH_4F etching after VUV irradiation. Conditions need to be optimized to minimize the damage done to the photoresist SAM during this step. It is also necessary to determine if the surface potential is affected by this damage and determine if this change is reproducible and thus will be reliable reference material for other SAMs during KPFM measurements.

The main objectives of this chapter is to determine the optimum parameters for the formation of micropatterned SAMs via VUV lithography of 1-hexadecene SAM (HD SAM). The irradiation time and pressure in the chamber during VUV photolithography is varied to establish the most favorable combination to obtain the clearest micropattern. A series of etching tests were also conducted to determine the conditions required for the HD SAM to experience minimal damage and ensure that it will be a reliable reference for surface potential comparison with other SAMs. The specific objectives of this study are as follows:

(1) To find the ideal VUV irradiation time and pressure inside the chamber needed to photodegrade the 1-hexadecene (HD SAM) on silicon,

(2) To use Kelvin Probe Force Microscope (KPFM) to observe the micropatterns formed on HD SAM using the different VUV irradiation times,

(3) To use Atomic Force Microscopy (AFM) to determine the optimum etching conditions necessary to remove the oxide layer that is formed as a result of VUV photoirradiation, while minimizing the damage on the HD SAM layer, and

(4) To compare the quality of the new SAM formed on the VUV-irradiated and etched substrate with that formed on a fresh silicon substrate.

2.2. Experimental Methods

2.2.1. SAM preparation

Polished n-doped silicon (111) wafers from Electronics and Materials Corp. (phosphorus-doped, resistivity range of 1–10 Ω cm) was ultrasonically cleaned with ethanol (Nacalai Tesque, 99.5%) and ultrapure water (UPW) for 20 minutes each to remove impurities present on the surface. Photochemical cleaning of the wafer was conducted via VUV light irradiation (UER 20-172V, Ushio) for 20 minutes in an ambient atmosphere to remove any organic impurities present on the surface. To remove the native oxide on the

silicon substrate, it must undergo a series of etching steps, which are depicted in Figure 2.1. The cleaned silicon substrate was first immersed in 5% hydrofluoric acid solution (Morita Chemical) for 5 minutes in the dark to remove the oxide layer from the surface. The substrate was washed twice in UPW then immersed immediately in a 40% ammonium fluoride solution (Morita Chemical) for 1 minute to terminate the substrate with hydrogen. The ammonium fluoride (NH_4F) was heated to 80 degrees prior to substrate immersion to remove any dissolved oxygen which can interfere with the hydrogen-termination process. To form SAMs covalently attached to silicon, this preparation of hydrogen terminated silicon (H-Si) is necessary.

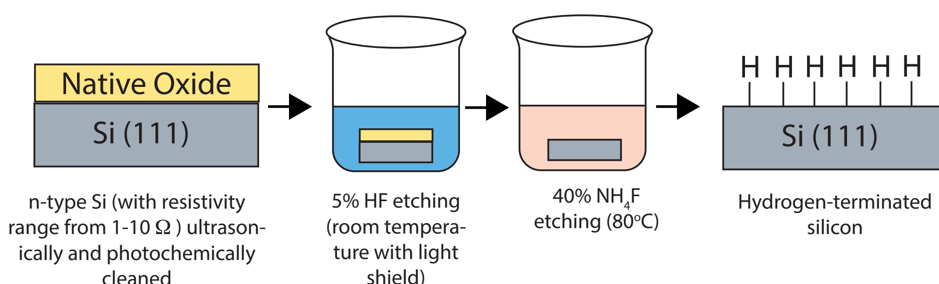

Figure 2.1. Procedure for preparing hydrogen terminated silicon from n-Si(111)

To form the SAM, the H-Si substrate was placed together with the 1-hexadecene (Tokyo Chemical Industry, >99%) precursor in a quartz cylindrical vessel with two glass tubes and a rubber stopper at the end of the cylinder (Figure 2.2). The glass tubes were used to purge the precursor solution with N_2 gas and ensure that the silicon substrate does not oxidize during the grafting process. The wafer was then irradiated with UV light (REX-250, Asahi spectra) for one hour while immersed in the solution to initiate the SAM formation. The substrate was collected from the vessel after irradiation and was ultrasonically cleaned with ethanol and ultrapure water for 10 minutes each to remove any adsorbed particles on

the surface. The SAM that remains grafted on the silicon wafer will be referred to as HD SAM.

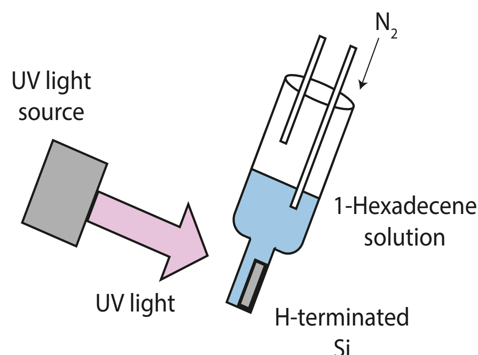

Figure 2.2. Setup used to form the SAM using UV irradiation

2.2.2. VUV Photolithography of the SAM

To form micropatterned SAMs, VUV light was used to remove HD SAM from certain regions on the silicon substrate and a new SAM will be grafted in its place. However, before this step, it is necessary to determine the optimum conditions for this process.

To observe how successfully the HD SAM will be removed from the silicon substrate using VUV light, the sample was irradiated with a Xe-excimer lamp (Ushio, UER20-172V) with a wavelength of 172 nm at an irradiation distance of 5 mm (Figure 2.3). The pressure inside the chamber was kept at either 1000 Pa or atmospheric pressure during the irradiation process to observe the effects of air pressure on the degradation of the SAM. The irradiation time was varied from 10 to 60 minutes. The irradiated SAMs were characterized with XPS and a water contact angle goniometer to determine which condition was the best for removal of the HD SAM.

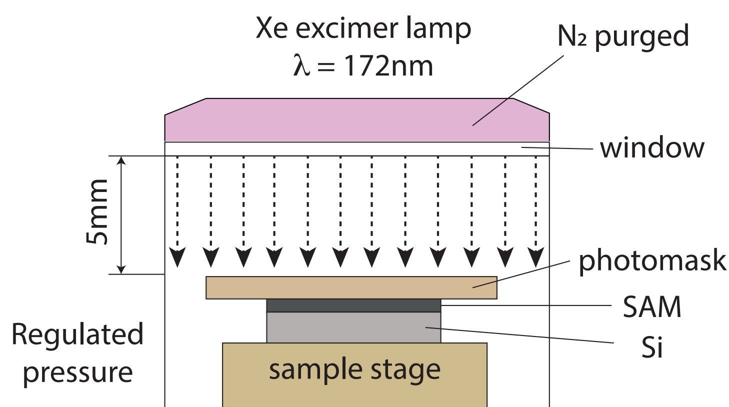

Figure 2.3. VUV irradiation setup for micropatterning of HD SAM

To determine how well the micropatterns will transfer to the silicon substrate during the photolithography process, samples covered with a photomask were also irradiated with VUV light. The photomasks consisted of a 100 nm thick chromium pattern attached to a 2 mm quartz plate, whose transparency at λ=172 nm is 93%. A circle and square photomask were used in these experiments. The circle photomask shields a majority of the sample from the VUV light and only irradiates the small circular regions. On the other hand, the square photomask shields the small square regions and allows majority of the surface to be irradiated (Figure 2.4). The irradiation time was varied from 10 to 30 minutes and the quality of the KPFM images were used to determine the optimum conditions needed for micropatterning.

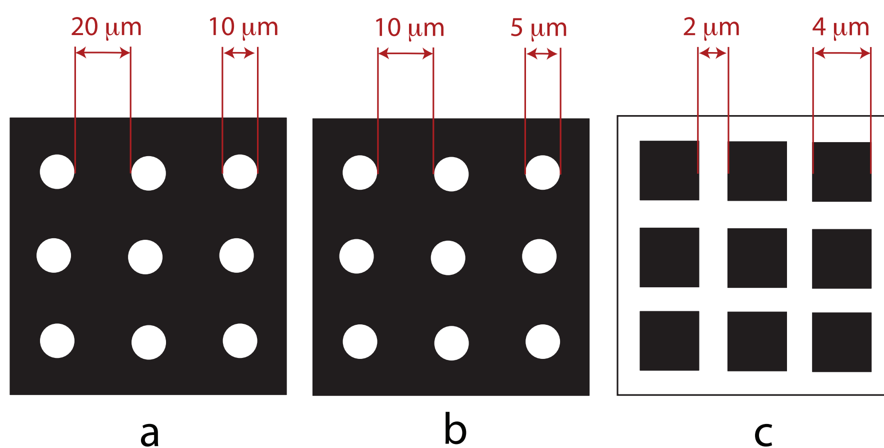

Figure 2.4. Diagram of the (a,b) circle and (c) square photomasks used in the irradiation tests. Dark regions correspond to masked areas and light regions correspond to areas which allow VUV light to pass through.

2.2.3. Optimization of etching conditions after VUV irradiation

After VUV irradiation, the HD monolayer will be removed from the exposed region and an oxide layer would have taken its place. In order to graft a new SAM into this region, the oxide layer must first be removed and terminated with hydrogen, similar to the steps described in sections 2.2.1. However, since part of the substrate still contains the original HD monolayer, etching conditions must be adjusted to ensure that the H-Si will form on the irradiated regions while minimizing the damage experienced by the remaining HD SAM. Thus, a series of etching conditions were studied. The immersion time in HF was varied from 3 to 5 minutes, and the immersion time in NH_4F was varied from 30 to 60 seconds. The condition and quality of the HD SAM was monitored to obtain the optimum etching condition needed to form a good H-Si on the irradiated region while minimizing the damage to the masked HD SAM regions.

2.3. Results and Discussion

2.3.1. Formation of HD SAM

The water contact angle (WCA) and atomic concentrations of H-Si and HD SAM are shown in Table 2.1. The WCA of H-Si was measured to be around 87 degrees, which is consistent with previous studies[31,33]. This value increased significantly upon the formation of HD SAM due to the presence of a dense hydrophobic methyl-terminated layer at the surface once the SAM has formed. The WCA value of the our HD SAM is in good agreement with previous studies that fabricated methyl-terminated SAMs[29,33,34].

Figure 2.5 shows the XPS scan of H-Si and HD SAM. Prior to SAM formation, The Si 2p scan of H-Si substrate shows no peak at 103 eV, indicating that the native silicon oxide was removed during the etching process. The presence of carbon on the H-Si sample is most likely due to contaminants in the atmosphere. After formation of HD SAM, there is a great increase in the C 1s peak and atomic % concentration, indicating that the SAM molecules were properly attached to the silicon substrate. Although the amount of oxygen increased from 2.91 to 5.21, the absence of a peak at 103 eV for the HD SAM once again shows that the underlying silicon substrate is not oxidized and that the SAM has passivated the surface. Figure 2.6 shows the AFM topographic image of H-Si and HD SAM. The characteristic terrace steps can be observed for the H-Si sample. After grafting of the HD SAM, the terraces can still be clearly seen which indicates a uniform monolayer has formed.

Table 2.1. Properties of H-Si and HD SAM

	WCA	Atomic % Concentration		
		C 1s	O 1s	Si 2p
H-Si	87.60 ± 1.2	4.69	2.91	92.40
HD SAM	105.90 ± 0.7	32.75	5.21	62.04

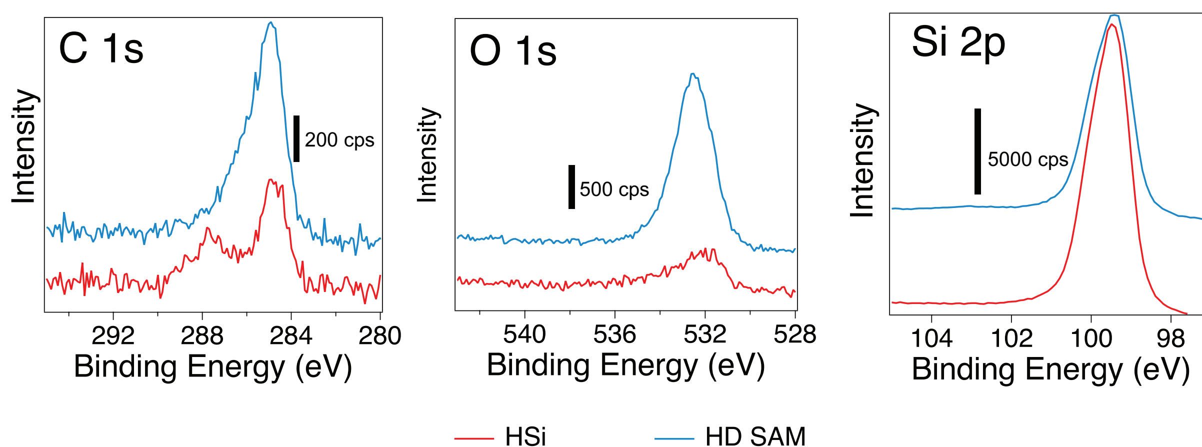

Figure 2.5. XPS peaks of the H-Si and HD SAM

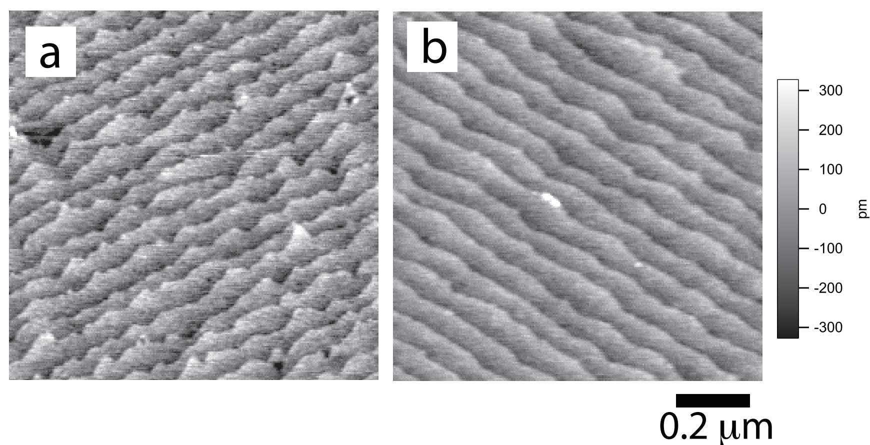

Figure 2.6. AFM topographic image of the (a) H-Si and (b) HD SAM samples

The characterization of HD SAM shows that it is well formed and of good quality, thus is a good candidate to be used a photoresist in VUV photolithography due to the strong nature of the Si-C covalent bond and strong chemical resistivity. However, surface potential

measurements using KPFM are very sensitive to the quality of the surface and even slight damage to the monolayer is enough to alter the readings. Thus, we must optimize and determine the extent the micropatterning process has on the HD photoresist in order to be able to use it as a reliable reference for our future SAMs.

2.3.2. Optimization of VUV irradiation conditions for micropatterning of HD SAM

HD SAM was irradiated with VUV light at a distance of 5 mm at two pressure conditions (1 x 10^3 Pa and 1 x 10^5 Pa) to determine the optimum time needed to remove the HD monolayer from the silicon substrate. The atomic percent concentrations of C 1s and water contact angles of the substrate after irradiation are summarized in Table 2.2.

Table 2.2. C 1s atomic percent concentration and WCA of HD SAM sample after VUV irradiation at different times at 10^3 Pa and 10^5 Pa

Irradiation time (mins)	10^3 Pa		10^5 Pa	
	C 1s (% concentration)	WCA	C 1s (% concentration)	WCA
10	6.15	6.5	7.53	6.9
20	5.53	5.1	5.85	5.5
30	4.92	2.6	5.72	2.7
60	4.98	2.9	4.42	2.8

For both pressure conditions, it is clear that even after a short irradiation time of 10 minutes after VUV light, the C 1s concentration of HD SAM dropped significantly from its original value of 33% to about 6-8%. Increasing the irradiation time further decreases this value, until it eventually settles to 4-5%. This amount is comparable to the carbon concentration present on a fresh H-Si substrate without any SAM present on the sample (Table 2.1). The presence of this small amount of carbon on the H-Si is possibly due to unavoidable contamination from the atmosphere as the samples are loaded into the XPS machine. For the VUV-irradiated samples, this trace carbon amount may be a combination of the contamination from the environment as well as the presence of oxygen-containing

carbon functional groups that remain on the sample after irradiation. However, with the value this low, it is safe to conclude that the hydrocarbon monolayer has been degraded**.** The presence of the oxygen-containing groups on the substrate is confirmed by the sudden decrease in the sample's water contact angle. Prior to VUV irradiation, the sample had a high water contact angle of 105.9º, which implies that it is densely terminated with methyl ($-CH_3$) groups due to the SAM formation. After irradiation, the water contact angle dropped significantly, which can be attributed to the degradation of the HD monolayer, as well as the transformation of the monolayer to oxygen-containing groups which are hydrophilic in nature. The degradation of the C-C bonds of the HD monolayer and the formation of oxygen groups can also be corroborated by the Si 2p peak (Figure 2.7). Prior to irradiation, the sample had a single peak at 99.5 eV. After irradiation, a distinct peak appears at 103 eV, which originates from the oxides present on the Si substrate.

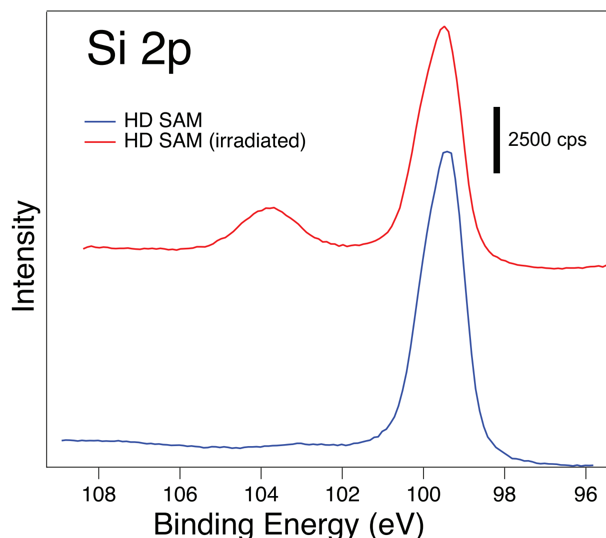

Figure 2.7. Si 2p peak before and after VUV irradiation for 30 mins

The mechanism of VUV degradation of the SAM at λ=172 has been reported to be dependent on the presence of oxygen during the process. VUV light itself does not contain sufficient energy to break the hydrocarbon bonds and decompose the HD monolayer.

However, VUV light at this wavelength results to oxygen excitation and converts the atmospheric oxygen to the single and triplet states (O(1D) and O(3P)). O(1D) in particular has a very strong oxidative reactivity which triggers photodegradation which initiates from the terminal -CH_3 groups and approaches the headgroup. During this process, the terminal -CH_3 groups are transformed to oxygen-containing functional groups. These functional groups are hydrophilic, which is responsible for the sudden decrease in water contact angle of the sample (Table 2.1). Unlike the -CH_3 functional group, these groups are also prone to decomposition by VUV-excitation, which results to the removal of the SAM monolayer from the substrate[13,29].

Although the presence of oxygen is during the VUV irradiation process is crucial to the degradation of the SAM monolayer, and it seems logical to choose a higher pressure during irradiation to have the maximum amount of oxygen, considerations must be made in choosing how much oxygen is present during the process. Table 2.2 shows that the HD monolayer appeared to be equally decomposed at irradiation at 10^3 and 10^5 Pa beyond 20 minutes of irradiation. However, a previous study has found that the increase in active oxygen species may lead to diffusion under the masked areas, making the pattern broader than expected.[13] With a lower vacuum pressure, there is less active oxygen species, decreasing the possibility of diffusion under the masked areas. Therefore, the photoetching of the HD monolayer is more limited to only the irradiated areas. For these reasons, 10^3 Pa was chosen as the pressure at which VUV irradiation will be done. To determine the optimum time needed to transfer the photomask micropattern to the sample, irradiation tests with a photomask was done at 10^3 Pa.

Figure 2.8 shows KFM images of the micropatterns on an HD SAM sample after irradiation at 10^3 Pa. The schematic diagram of the photomasks can be seen in Figure 2.4. The micropatterns formed after irradiation times of 10 (Figures 2.8a, 2.8d, 2.8g), 20 (Figures 2.8b, 2.8e, 2.8h), and 30 (Figures 2.8c, 2.8f, 2.8i) minutes were observed. In the images, the

darker regions correspond to the areas irradiated by VUV light where the HD monolayer has been removed and the lighter regions correspond to masked areas where the HD SAM still remains intact. The KPFM images show that although the XPS results showed that 10 minutes was enough to degrade the HD SAM sample, the patterns that is transferred from the photomask are hazy and unclear, especially for the smaller regions (Figures 2.8d and 2.8g). A longer irradiation time of 20 minutes greatly improved the results and a clearer pattern can be seen(Figures 2.8b, 2.8e and 2.8h). Further increasing the irradiation time to 30 minutes showed even better results with the micropatterns clearly distinguishable, even for the smaller patterns (Figures 2.8c, 2.8f, 2.8i).

The diameters of the circle patterns and length of the square patterns were measured using ImageJ and the results are summarized in Table 2.3. The measured values were compared with the expected values based on the actual diameters of the circles and length of the squares in the photomask used (shown in Figure 2.4). Measurement of the circle patterns in the KPFM images show that irradiation at 10 and 20 minutes resulted in a smaller diameter compared to that of the photomask. Increasing the irradiation time to 30 minutes produced circle patterns that have diameters slightly greater than that of the photomask. This is most probably due to the seeping of the oxygen species under the photomask during the longer irradiation, leading to a slight broadening of the pattern. The same phenomenon can be observed for the square patterns, but in the opposite sense since the photomask pattern is inverted. The length of the squares were greater than that of the actual photomask for irradiation times of 10 and 20 minutes. Irradiating for 30 minutes resulted in a square pattern that is slightly smaller than that of the photomasks due to the broadening of the irradiation regions (the regions in between the squares). As such, irradiation for 60 minutes was not performed because it is clear that 30 minutes irradiation is more than enough to degrade the HD SAM in the irradiated region.

The amount of broadening experienced by each pattern was computed for in terms

of percentage for the samples irradiated for 30 minutes (Table 2.3). It is clear that using larger patterns (Figure 2.8c) resulted in a much smaller % broadening compared to that of the smaller patterns (Figure 2.8f, 2.8i). The large circle pattern experienced only 2% broadening as opposed to the smaller circle and square patterns which experienced 8% and 10% respectively.

From the results of the KPFM measurements, the optimum time for irradiation is determined to be 30 minutes. Shorter irradiation times such as 10 minutes and 20 minutes did not result in clear micropatterns. However, it is recommended to use photomasks with larger patterns rather than smaller ones to minimize the effect of broadening during VUV irradiation.

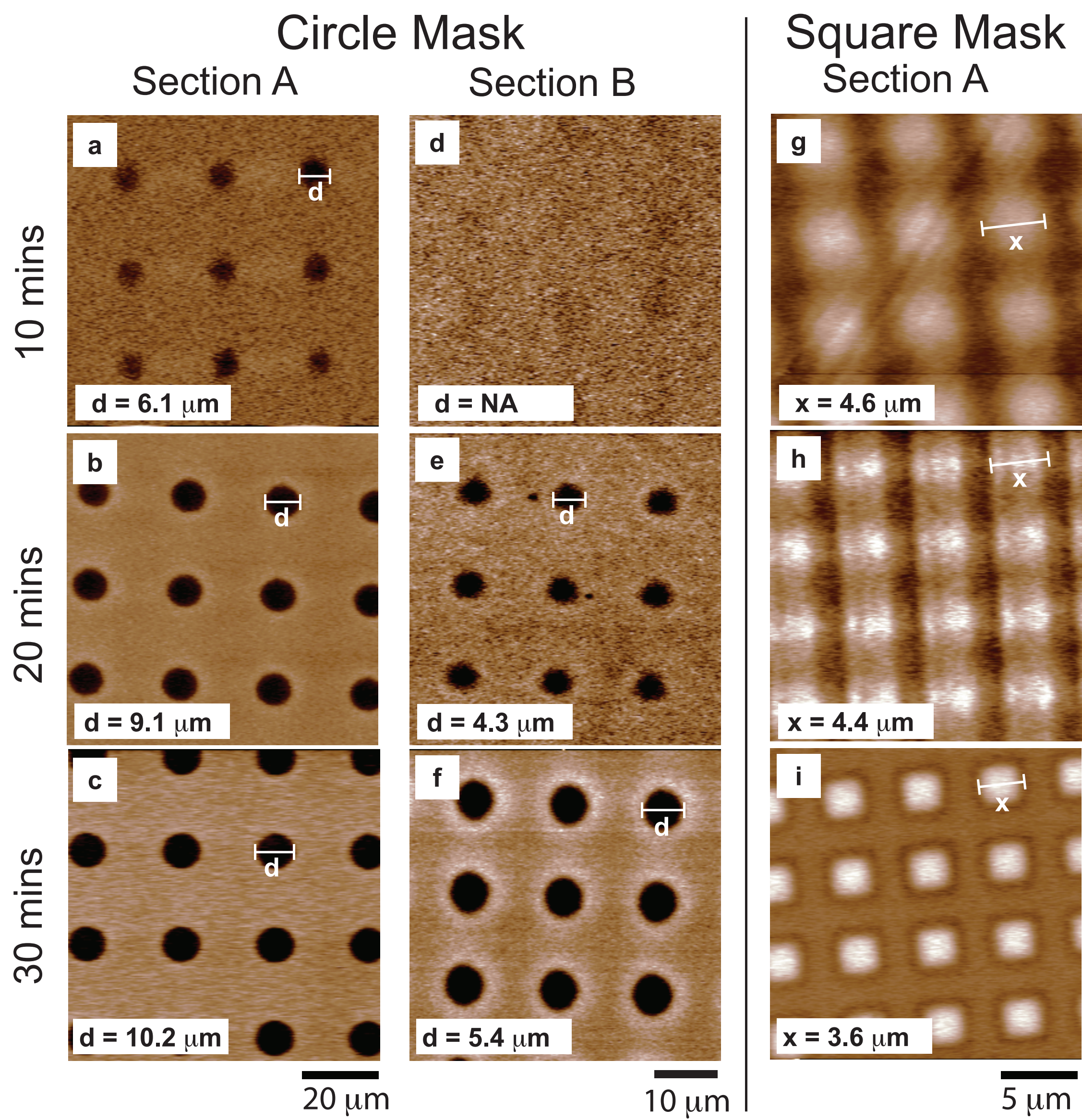

Figure 2.8. Effect of irradiation time on photomask transfer

Table 2.3. Photomask pattern size measurements from the KPFM images

	Actual size of circle/square in photomask (nm)	Measured from KPFM (nm)			% broadening (for 30 m irradiation)
		10 m	20 m	30 m	
Circle (Section A)	10	6.1 ± 0.9	9.1 ± 0.4	10.2 ± 0.4	2 %
Circle (Section B)	5	NA	4.3 ± 0.2	5.4 ± 0.2	8 %
Square	4	4.6 ± 0.3	4.4 ± 0.1	3.6 ± 0.1	10 %

2.3.3. Optimization of the etching condition required for micropatterned SAMs

To form micropatterned SAMs where two different SAMs of a μm scale are formed on the same substrate, the irradiated region must undergo etching once more in order to form H-Si again and prepare it for the grafting of a new SAM. During the preparation of our HD SAM, the etching condition of 5-minute immersion in 5% HF solution followed by 1-minute immersion in 40% NH_4F solution was used. This method was very successful in removing any oxide present on the silicon wafer and forming atomically flat H-Si, as discussed in section 2.3.1. However, this condition causes damage to the HD SAM photoresist that remains on the substrate after irradiation, as seen in Figures 2.9a and 2.9b. Although the terrace step structure of the HD SAM maintains its feature, many large etch pits can be observed on the AFM images when etched with this condition.

In an attempt to determine the cause of damage, samples were etched with HF only for 5 minutes (Figures 2.9c-d) and NH_4F only for 1 minute (Figures 12.9e-f). AFM images show almost no damage for the sample etched with only HF, however considerable damage can be observed for sample etched only in 1 min of NH_4F. It is clear therefore that the cause of the damage to the HD SAM is due to the NH_4F etching and not the HF. This agrees with previous studies which have shown that HD SAM has been found to be resistant to HF etching even up to 30 minutes[31]. However, the NH_4F etching is necessary in forming atomically flat H-Si and thus cannot be removed from the process. Figure 2.10 shows the AFM images of HD SAM samples formed on silicon substrate that was etched with HF solution only (Figure 2.10a) NH_4F solution only (Figure 2.10b). The images clearly show that only the sample etched with NH_4F solution displayed a terrace step structure. Reference shows that although HF etching is successful at removing silicon oxide from the silicon surface, it produces a microscopically rough surface[35]. In order to produce atomically flat and cleaned surface on Si (111), NH_4F immersion is necessary[36]. Studies have shown that HF etching of silicon leads to atomically rough surfaces[37], as opposed to NH_4F etching which

is capable of producing atomically flat surfaces[36]. A previous study found that HF etching of Si (111) surfaces produced Si atoms terminated by mono- and di-hydrides[37], while NH_4F etching resulted in monohydride surfaces.

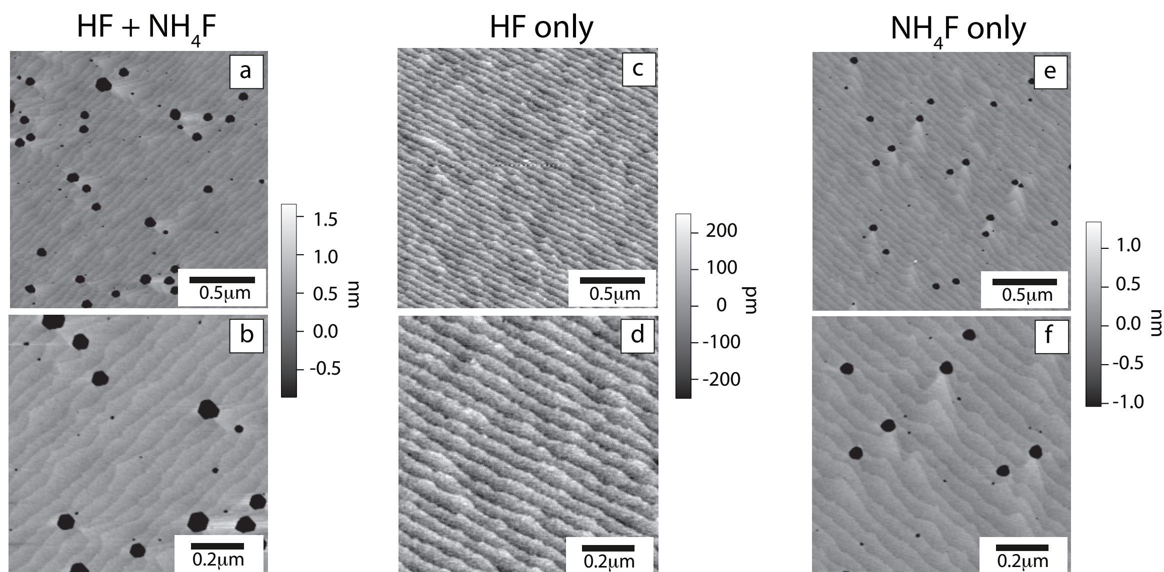

Figure 2.9. HD SAM sample etched in (a,b) HF and NH_4F solution, (c,d) HF solution only, and (e,f) NH_4F solution only

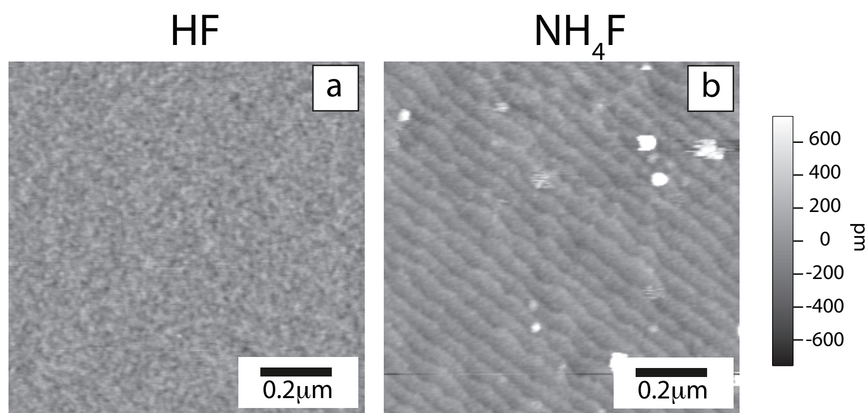

Figure 2.10. HD SAM formed on H-Si substrate prepared by etching in (a) 5% HF only, and (b) 40% NH_4F only

To determine an etching condition which can be used to remove the oxide that forms on the irradiated regions while maintaining the integrity of the HD SAM photoresist, a series of etching tests on HD SAM was conducted. Since it was established earlier that the damage is mostly due to immersion in NH_4F, the etching time for it was shortened. Figure 2.11 shows the topography of the HD SAM sample after etching in 5% HF solution for 5 minutes with varying immersion time in NH_4F. An etching time of 30, 45 and 60 seconds in NH_4F was observed. The images clearly show that the size and number of the etch pits formed on the sample becomes larger with increasing NH_4F immersion time.

In an attempt to further reduce the damage, etching time in HF was also shortened to see if this would give better results. The immersion time in HF was reduced to 3 minutes and the immersion time in NH_4F was once again varied from 30 to 60 seconds (Figure 2.12). The AFM images show that the etch pits are much smaller compared to Figure 2.11 as a result of the shortened HF and NH_4F etching.

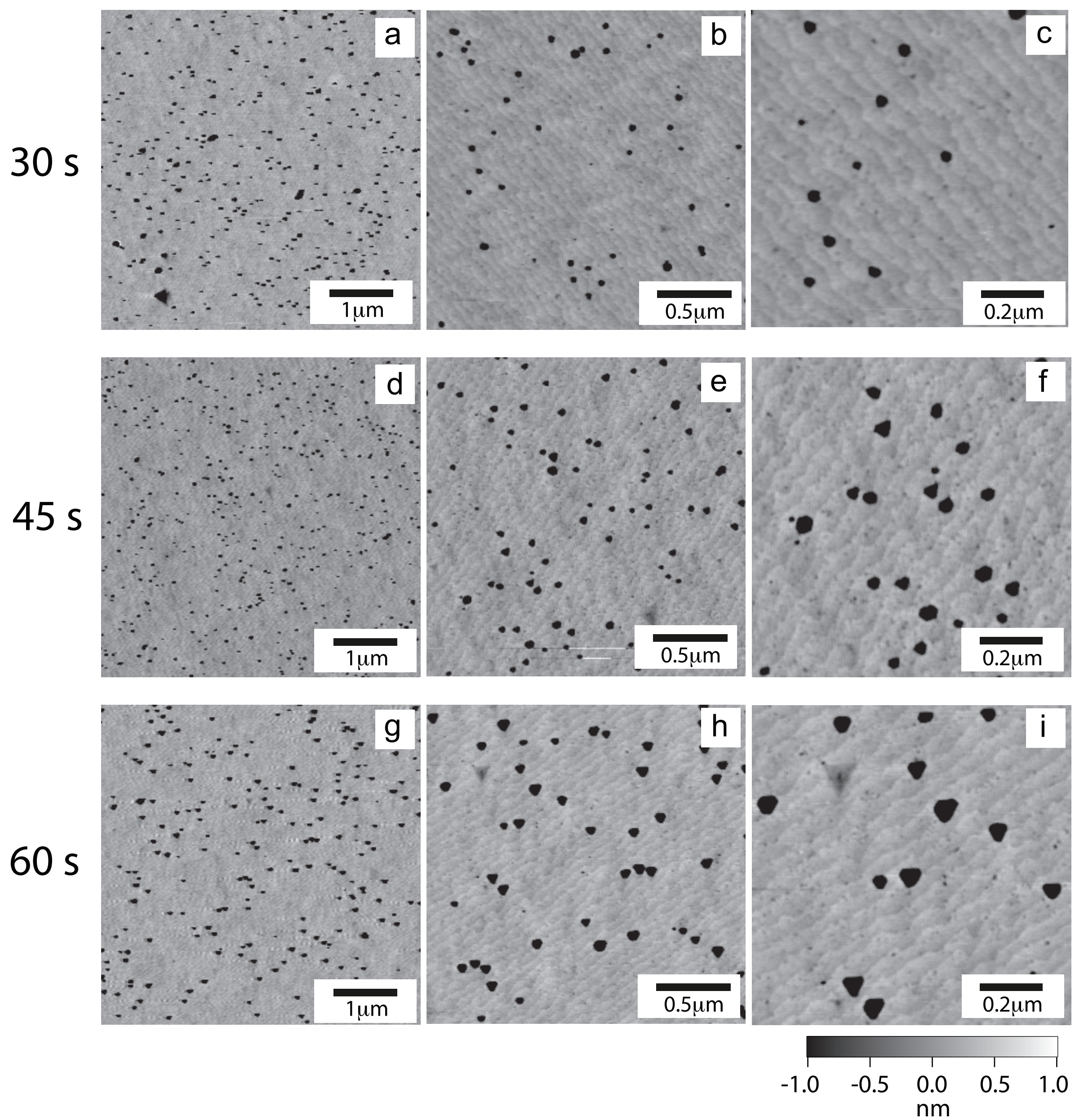

Figure 2.11. Damage on HD SAM caused by 5m immersion in 5% HF and (a-c) 30s, (d-f) 45s, (g-i) 60s immersion in 40% NH_4F

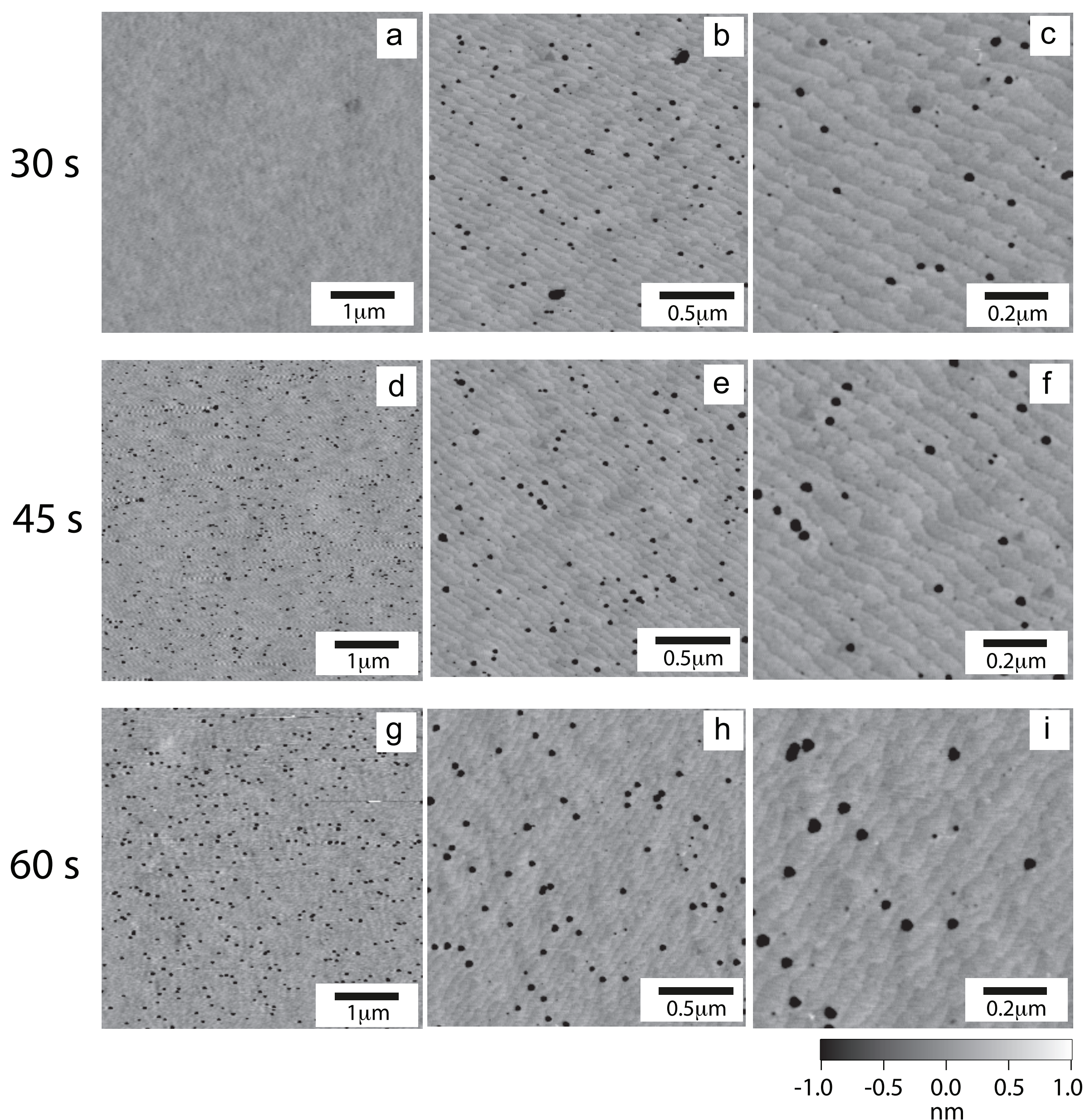

Figure 2.12. Damage on HD SAM caused by 3m immersion in 5% HF and (a-c) 30s, (d-f) 45s, (g-i) 60s immersion in 40% NH_4F

Figure 2.11 and Figure 2.12 shows that decreasing the HF immersion time from 5 minutes to 3 minutes decreases the damage on the HD SAM. For NH_4F etching, immersion for 30 seconds showed the least damage. However, upon checking if these new shortened etching conditions is enough to still form good HD SAM (Figure 2.13), we found that 30 seconds immersion in NH_4F was too short and results to rough terrace steps in the AFM

scan. On the other hand, 45 seconds immersion in NH_4F was enough to form clear and smooth terrace steps. Comparison of the damage sustained for the 30 s and 45 s etch in Figure 12.12 shows that the difference is not significantly greater for 45 s. This result, combined with the better terrace steps formed for the 45 s etching time suggests that this etching condition is better for preparing the irradiated regions to graft a new SAM while minimizing the damage on the HD SAM photoresist.

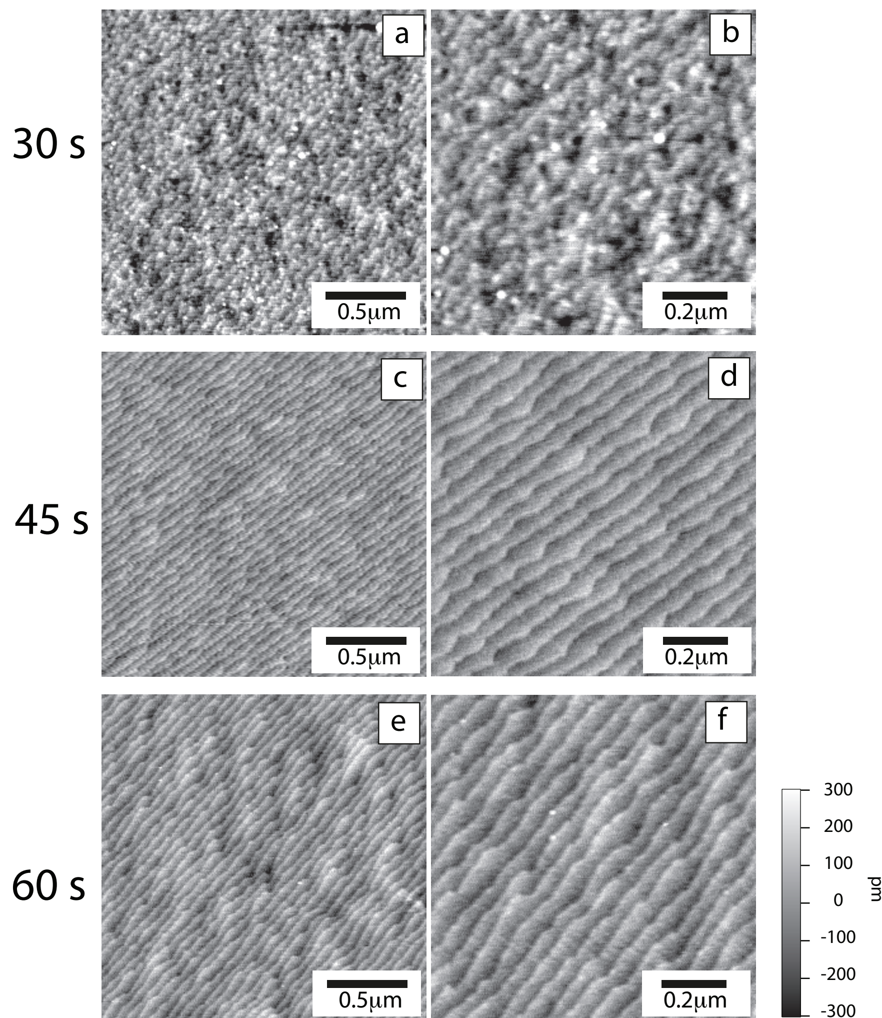

Figure 2.13. HD SAM samples formed on H-Si prepared by 3m etch in 5% HF and (a-b) 30 s, (c-d) 45 s and (e-f) 60 s etch in 40% NH_4F

To verify whether the new SAM that will form on the irradiated region of the substrate, an HD SAM sample was irradiated and etched using the conditions we have determined to be optimum. After irradiation and etching, a new HD SAM was grafted to the substrate. Figure 2.14 shows that the new HD SAM displayed clear terrace steps in the AFM scan. XPS analysis show the transformation of the C 1s, O 1s and Si 2p peaks of the original HD SAM during each stage of the experiment (Figures 2.15). After VUV irradiation, a decrease in the C 1s peak and increase in the O 1s peak is observed, due to the decomposition of the carbon chain and formation of oxygen containing functionalities. A small peak at 103 eV can also be found on the Si 2p scan, indicating the substrate has been oxidized. After the irradiated sample is etched using the new parameters, the peak at 103 eV in the Si 2p scan disappears, as well as the O 1s peak, indicating that the oxide layer has been removed. Finally, after formation of a new HD SAM layer, an increase in the C 1s peak can be observed, indicating that the new HD monolayer has successfully been grafted. Table 2.4 summarizes the properties of the original HD SAM and the new HD SAM formed after VUV irradiation and etching. The WCA, atomic percent concentrations and ellipsometric thickness of the original and the new HD SAM suggests that the two HD SAM are very similar in terms of quality and characteristics. Thus, the irradiation and etching conditions optimized in this experiment is suitable for preparing micropatterned SAMs with minimal damage on the HD SAM photoresist.

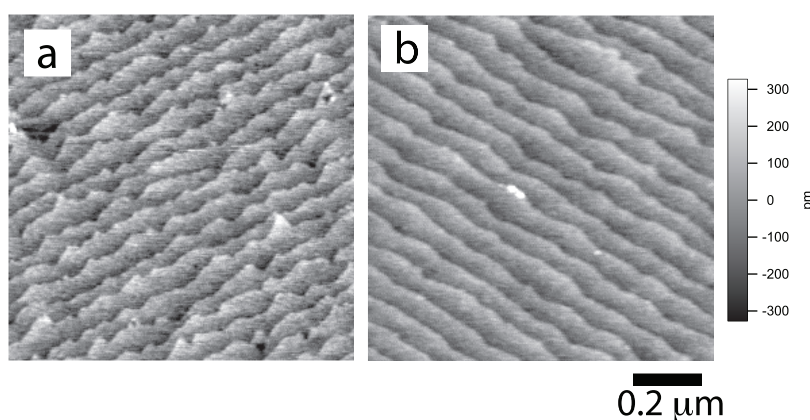

Figure 2.14. Terrace steps of new HD SAM on irradiated + etched surface

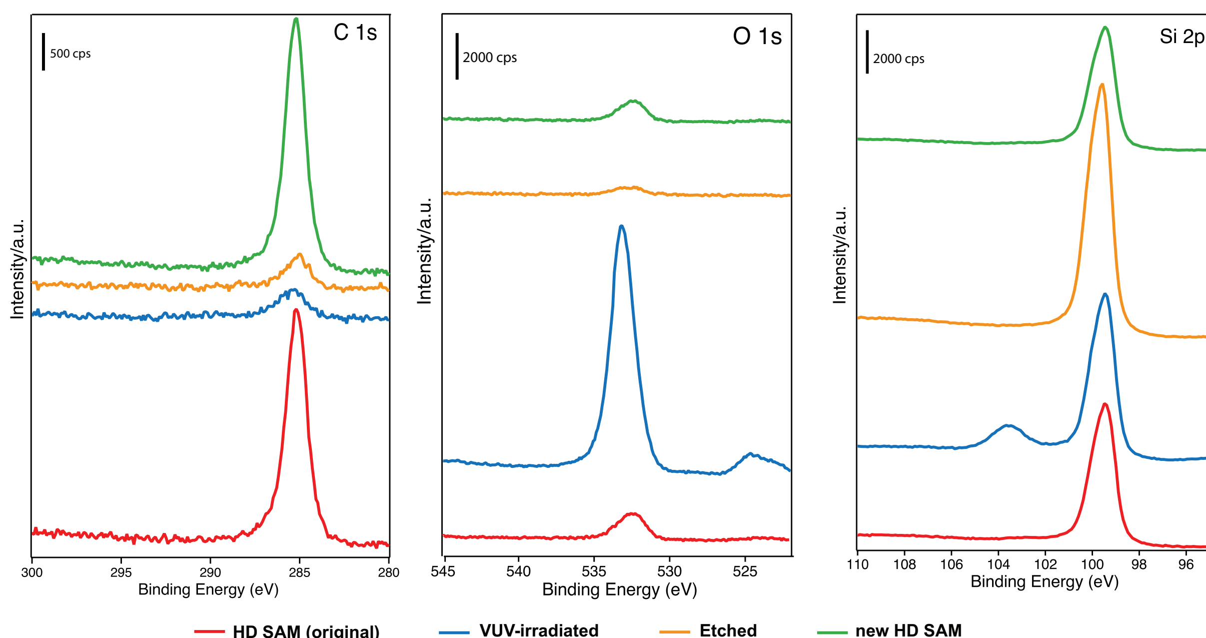

Figure 2.15. XPS peaks observed during irradiation, etching and formation of new HD SAM

Table 2.4. Properties of original and new HD SAM

		HD SAM (original)	New HD SAM
Atomic % Concentration	O 1s	4.35	4.03
	C 1s	32.47	31.13
	Si 2p	63.18	64.84
WCA		105.3 ± 1.0	104.7 ± 0.7

2.4. Conclusions

In this chapter we discussed the aspects of VUV photolithography which must be taken into consideration when preparing our micropatterned SAM for KPFM measurements. We determined the optimum irradiation time, pressure as well as the best etching condition to produce a micropatterned SAM which has minimal damage on the photoresist HD SAM. We found that the best irradiation time was 30 minutes in 1 x 10^3 Pa. This condition was able to properly remove the HD SAM while limiting the risk of pattern broadening that might occur due to too much oxygen. XPS results and KPFM show that 30 mins provides low C

1s concentration and a clear KPFM image. Etching tests show that the best condition to use is 3 minute immersion in in HF followed by 45 seconds immersion in in NH_4F. This produces minimal damage on the HD SAM photoresist, but is still able to remove the oxide layer left behind by VUV irradiation and form atomically flat H-Si that will result in a SAM with clear terrace steps and properties almost identical to one that is prepared on a fresh silicon substrate. The optimized conditions for VUV irradiation determined in this study will be used in **Chapters 3, 4 and 5** to prepare our micropatterned SAMs for KPFM measurements. The shortened etching time discussed here will be used for **Chapters 4 and 5**. *Note: The etching times in HF and NH_4F used in Chapter 3 is slightly shorter compared to that discussed here due to the chemicals being from a different manufacturer, resulting in a slightly different outcome. However, similar etching tests were conducted to ensure that the quality of the reference HD SAM is preserved.*

References

(1) Briseno, A. L.; Aizenberg, J.; Han, Y.; Penkala, R. A.; Moon, H.; Lovinger, A. J.; Kloc, C.; Bao, Z. Patterned Growth of Large Oriented Organic Semiconductor Single Crystals on Self-Assembled Monolayer Templates Scheme 1. Schematic Illustration of the Experimental Procedure for the SAM-Induced Growth of Organic Semiconductor Crystals from an Oligoacene/T. *J. Am. Chem. Soc* **2005**, *127* (001), 12164–12165.

(2) Ellsworth, A. A.; Borner, K.; Yang, J.; Walker, A. V. Towards Molecular Electronics: Using Solution-Based Methods to Deposit Nanowires. *ECS Trans.* **2014**, *58* (43), 1–10. https://doi.org/10.1149/05843.0001ecst.

(3) Kumar, A.; Abbott, N. L.; Kim, E.; Biebuyck, H. A.; Whitesides, G. M. Patterned Self-Assembled Monolayers and Meso-Scale Phenomena. *Acc. Chem. Res.* **1995**, *28*, 219–226.

(4) Yamauchi, F.; Kato, K.; Iwata, H. Micropatterned, Self-Assembled Monolayers for Fabrication of Transfected Cell Microarrays. *Biochim. Biophys. Acta - Gen. Subj.* **2004**, *1672* (3), 138–147. https://doi.org/10.1016/j.bbagen.2004.03.008.

(5) Lu, L.; Kam, L.; Hasenbein, M.; Nyalakonda, K.; Bizios, R.; Göpferich, A.; Young, J. F.; Mikos, A. G. Retinal Pigment Epithelial Cell Function on Substrates with Chemically Micropatterned Surfaces. *Biomaterials* **1999**, *20* (23–24), 2351–2361. https://doi.org/10.1016/S0142-9612(99)00164-7.

(6) Xia, Y.; Whitesides, G. M. Use of Controlled Reactive Spreading of Liquid Alkanethiol on the Surface of Gold to Modify the Size of Features Produced by Microcontact Printing. *J. Am. Chem. Soc.* **1995**, *117*, 3274–3275.

(7) Wilbur, J. L.; Kumar, A.; Biebuyck, H. A.; Kim, E.; Whitesides, G. M. Microcontact Printing of Self-Assembled Monolayers: Applications in Microfabrication. *Nanotechnology* **1996**, *7* (4), 452–457. https://doi.org/10.1088/0957-4484/7/4/028.

(8) Tiberio, R. C.; Craighead, H. G.; Lercel, M.; Lau, T.; Sheen, C. W.; Allara, D. L. Self-Assembled Monolayer Electron Beam Resist on GaAs. *Appl. Phys. Lett.* **1993**, *62* (5), 476–478. https://doi.org/10.1063/1.108938.

(9) Lercel, M. J.; Tiberio, R. C.; Chapman, P. F.; Craighead, H. G. Self-Assembled Monolayer Electron-Beam Resists on GaAs and SiO2. *J. Vac. Sci. Technol. B Microelectron. Nanom. Struct.* **1993**, *11* (6), 2823. https://doi.org/10.1116/1.586609.

(10) Sugimura, H. Scanning Probe Lithography: Application of Organosilane Self-Assembled Monolayers as Ultra-Thin Resist Films.

(11) Liu, G. Y.; Xu, S.; Qian, Y. Nanofabrication of Self-Assembled Monolayers Using Scanning Probe Lithography. *Acc. Chem. Res.* **2000**, *33* (7), 457–466. https://doi.org/10.1021/ar980081s.

(12) Zhang, Y.; Balaur, E.; Maupai, S.; Djenizian, T.; Boukherroub, R.; Schmuki, P. Nanopatterning of Si(1 1 1) Surfaces by Atomic Force Microscope Scratching of an

Organic Monolayer. *Electrochem. commun.* **2003**, *5* (4), 337–340. https://doi.org/10.1016/S1388-2481(03)00052-3.

(13) Khatri, O. P.; Sano, H.; Murase, K.; Sugimura, H. Regulation of Pattern Dimension as a Function of Vacuum Pressure: Alkyl Monolayer Lithography. *Langmuir* **2008**, *24* (20), 12077–12084. https://doi.org/10.1021/la8021613.

(14) Takakusagi, S.; Uosaki, K. Photopatterning of an Organic Monolayer Formed on a Si Single Crystal Surface via Si-C Covalent Bond by UV Irradiation in an Inert Atmosphere. *Japanese J. Appl. Physics, Part 1 Regul. Pap. Short Notes Rev. Pap.* **2006**, *45* (11), 8961–8966. https://doi.org/10.1143/JJAP.45.8961.

(15) Hong, L.; Hayashi, K.; Sugimura, H.; Takai, O.; Nakagiri, N.; Okada, M. Micropatterning of Organosilane Self-Assembled Monolayers Using Vacuum Ultraviolet Light at 172 Nm: Resolution Evaluation by Kelvin-Probe Force Microscopy. *Surf. Coatings Technol.* **2003**. https://doi.org/10.1016/S0257-8972(03)00077-X.

(16) Chandekar, A.; Sengupta, S. K.; Whitten, J. E. Thermal Stability of Thiol and Silane Monolayers: A Comparative Study. *Appl. Surf. Sci.* **2010**. https://doi.org/10.1016/j.apsusc.2009.11.020.

(17) Yang, K.-Y.; Kim, J.-W.; Hong, S.-H.; Lee, H. Patterning of the Self-Assembled Monolayer Using the Zero Residual Nano-Imprint Lithography. **2007**. https://doi.org/10.4028/www.scientific.net/SSP.124-126.523.

(18) Sugimura, H.; Hayashi, K.; Saito, N. Kelvin Probe Force Microscopy Images of Microstructured Organosilane Self-Assembled Monolayers. *Jpn. J. Appl. Phys.* **2001**, *40*, 4373.

(19) Sugimura, H.; Hayashi, K.; Saito, N.; Nakagiri, N.; Takai, O. Surface Potential Microscopy for Organized Molecular Systems. *Appl. Surf. Sci.* **2002**, *188* (3–4), 403–410. https://doi.org/10.1016/S0169-4332(01)00958-8.

(20) Hayashi, K.; Saito, N.; Sugimura, H.; Takai, O.; Nakagiri, N. Regulation of the Surface Potential of Silicon Substrates in Micrometer Scale with Organosilane Self-Assembled Monolayers. *Langmuir* **2002**, *18* (20), 7469–7472. https://doi.org/10.1021/la011707h.

(21) Sugimura, H.; Saito, N.; Maeda, N.; Ikeda, I.; Ishida, Y.; Hayashi, K.; Hong, L.; Takai, O. Surface Potential Microscopy for Chemistry of Organic Self-Assembled Monolayers in Small Domains. *Nanotechnology* **2004**, *15*, S69–S75. https://doi.org/10.1088/0957-4484/15/2/015.

(22) Ichii, T.; Fukuma, T.; Kobayashi, K.; Yamada, H.; Matsushige, K. Phase-Separated Alkanethiol Self-Assembled Monolayers Investigated by Non-Contact AFM. *Appl. Surf. Sci.* **2003**, *210*, 99–104. https://doi.org/10.1016/S0169-4332(02)01487-3.

(23) Vatel, O.; Tanimoto, M. Kelvin Probe Force Microscopy for Potential Distribution Measurement of Semiconductor Devices. *J. Appl. Phys.* **1995**, *77* (6), 2358–2362. https://doi.org/10.1063/1.358758.

(24) Lu, J.; Delamarche, E.; Eng, L.; Bennewitz, R.; Meyer, E.; Gu, H. Kelvin Probe Force Microscopy on Surfaces : Investigation of the Surface Potential of Self-Assembled Monolayers On. *Langmuir* **1999**, *15*, 8184–8188. https://doi.org/10.1021/la9904861.

(25) Nonnenmacher, M.; O'Boyle, M. P.; Wickramasinghe, H. K. Kelvin Probe Force Microscopy. *Appl. Phys. Lett.* **1991**, *58* (25), 2921–2923. https://doi.org/10.1063/1.105227.

(26) Farias, E. D.; Zoloff Michoff, M. E.; Sueldo Occello, V.; Brunetti, V.; Mario, M. C. G.; Glatzel, T. KPFM and DFT as Tools to Correlate the Charge Distribution and Molecular Orientation of Dendritic Adsorbates on Different Surfaces. *Appl. Surf. Sci.* **2021**, *565* (July). https://doi.org/10.1016/j.apsusc.2021.150552.

(27) Hansen, W. N.; Hansen, G. J. Standard Reference Surfaces for Work Function Measurements in Air. *Surf. Sci.* **2001**, *481* (1–3), 172–184.

https://doi.org/10.1016/S0039-6028(01)01036-6.

(28) Jacobs, H. O.; Knapp, H. F.; Stemmer, A. Practical Aspects of Kelvin Probe Force Microscopy. *Rev. Sci. Instrum.* **1999**, *70* (3), 1756–1760. https://doi.org/10.1063/1.1149664.

(29) Sugimura, H.; Sano, H.; Lee, K.-H.; Murase, K. Organic Monolayers Covalently Bonded to Si as Ultra Thin Photoresist Films in Vacuum UV Lithography. *Jpn. J. Appl. Phys.* **2006**, *45* (6B), 5456–5460. https://doi.org/10.1143/JJAP.45.5456.

(30) Saito, N.; Kadoya, Y.; Hayashi, K.; Sugimura, H.; Takai, O. Micropatterned 1-Alkene Self-Assembled Monolayer on Hydrogen-Terminated Silicon by Vacuum Ultraviolet Lithography. *Japanese J. Appl. Physics, Part 1 Regul. Pap. Short Notes Rev. Pap.* **2003**. https://doi.org/10.1143/JJAP.42.2534.

(31) Saito, N.; Youda, S.; Hayashi, K.; Sugimura, H.; Takai, O. Alkyl Self-Assembled Monolayer Prepared on Hydrogen-Terminated Si(111) through Reduced Pressure Chemical Vapor Deposition : Chemical Resistivities in HF and NH 4 F Solutions . *Chem. Lett.* **2002**, *31* (12), 1194–1195. https://doi.org/10.1246/cl.2002.1194.

(32) Saito, N.; Youda, S.; Hayashi, K.; Sugimura, H.; Takai, O. Chemical Resistivity of Self-Assembled Monolayer Covalently Attached to Silicon Substrate to Hydrofluoric Acid and Ammonium Fluoride. *Surf. Sci.* **2003**, *532–535*, 970–975. https://doi.org/10.1016/S0039-6028(03)00158-4.

(33) Saito, N.; Kadoya, Y.; Hayashi, K.; Sugimura, H.; Takai, O. Micropatterned 1-Alkene Self-Assembled Monolayer on Hydrogen-Terminated Silicon by Vacuum Ultraviolet Lithography. *Japanese J. Appl. Physics, Part 1 Regul. Pap. Short Notes Rev. Pap.* **2003**, *42* (4 B), 2534–2537. https://doi.org/10.1143/JJAP.42.2534.

(34) Sano, H.; Maeda, H.; Matsuoka, S.; Lee, K. H.; Murase, K.; Sugimura, H. Self-Assembled Monolayers Directly Attached to Silicon Substrates Formed from 1-Hexadecene by Thermal, Ultraviolet, and Visible Light Activation Methods. *Jpn. J.*

Appl. Phys. **2008**, *47*, 5659–5664. https://doi.org/10.1143/JJAP.47.5659.

(35) Higashi, G. S.; Chabal, Y. J.; Trucks, G. W.; Raghavachari, K. Ideal Hydrogen Termination of the Si (111) Surface. *Appl. Phys. Lett.* **1990**, *56* (7), 656–658. https://doi.org/10.1063/1.102728.

(36) Higashi, G. S.; Becker, R. S.; Chabal, Y. J.; Becker, A. J. Comparison of Si(111) Surfaces Prepared Using Aqueous Solutions of NH4F versus HF. *Appl. Phys. Lett.* **1991**, *58* (15), 1656–1658. https://doi.org/10.1063/1.105155.

(37) Burrows, V. A.; Chabal, Y. J.; Higashi, G. S.; Raghavachari, K.; Christman, S. B. Infrared Spectroscopy of Si(111) Surfaces after HF Treatment: Hydrogen Termination and Surface Morphology. *Appl. Phys. Lett.* **1988**, *53* (11), 998–1000. https://doi.org/10.1063/1.100053.

Chapter 3: Influence of the interface dipole on the surface potentials of SAMs on n-Si (111) grafted via Si-C, Si-O and Si-S bonds

3.1. Introduction

Organic molecular films have been attracting interest due to their applications in friction control[1,2], corrosion prevention[3,4], biosensing[5,6] and molecular electronics[7–10]. To reduce the operation voltage of devices and improve the performance of molecular electronics, the injection barriers between the electrons/holes and the substrate should be minimized. This is often done by choosing materials with appropriate work functions – lower work function materials are chosen as cathodes for easier electron injection with while higher work function materials are used as anodes for easier hole injection[11]. One disadvantage of this method is that we are limited by the materials we can choose as electrodes based on their work functions. An alternative way is to modify the work function of an electrode to improve charge injection through the use of self-assembled monolayers (SAMs).

Studies have shown that SAMs can introduce a dipole layer on a surface of an electrode and change its surface potential by shifting the vacuum level at the interface[11,12]. This is useful in reducing the charge injection barriers between material interfaces[12]. In Figure 3.1, a schematic illustration of how a shift in vacuum level results in a decrease in the electron energy barrier (E_b) between a metal electrode and an organic material The direction and magnitude of the vacuum level shift can be controlled by changing the orientation and strength of the dipole layer at the interface[12,13].

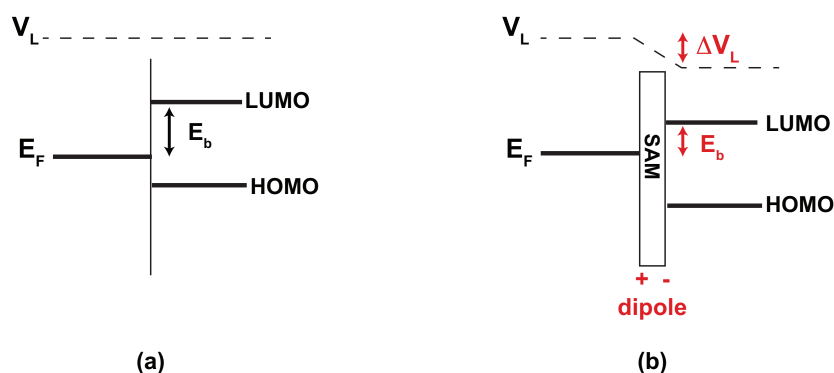

Figure 3.1. Control of electron injection barrier (E_b) through a SAM dipole. (a) shows the interface without a dipole having a common vacuum level and (b) shows the vacuum level shift due to the SAM

A previous study by Evans and Ulman on the surface potential of alkylthiol SAMs on gold envisioned the monolayer as a dipole sheet, with one side having a sheet of negative charges, and a sheet of positive charges on the other side[14]. It was hypothesized that this net dipole was comprised of two smaller dipoles present on the SAM. These are the R^+-S^- dipole (with R = C_nH_{2n+1}), and the Au^+-S^- dipole. This idea suggests that the final surface potential of the SAM on the substrate is affected by the molecular dipole that exists due to the alkyl chain as well as due to the interfacial Au-S bond.

Many other researchers have focused on alkylthiol SAMs on metal substrates[11,13,15–18], however studies involving semiconductors have recently been attracting attention as well[19–21]. Semiconductors, such as silicon, offer a much interesting potential due to their complex band structures and their widespread use in modern-day electronics. Several methods have been reported in which a molecule can be directly grafted onto a silicon substrate using covalent bonds. Studies have been successful in grafting SAMs via Si-C[22–25], Si-O[22,23,26], Si-S[22,27], Si-N[22,26] and Si-Te[27] bonds. By varying the bond between the substrate and the SAM molecule, it is possible to modify the energy levels at interfaces and tailor the surface potential of the substrate. Altering the covalent bond between the SAM

molecule and the silicon substrate can lead to modification of energy levels at the interface which can affect the surface potential of the substrate[12,26,28].

To measure the surface potential in small domains, many researchers have found that using the Kelvin Probe Force Microscopy (KPFM) to be an effective way tool[18,29–32]. This method modifies the conventional atomic force microscope (AFM) setup which allows researchers to map specific surface potential changes across a surface, rather than obtaining the bulk surface potential of the material. Using KPFM also allows simultaneous mapping of the surface potential and topography of the sample which may give further insight to the variations in surface potential[17,33,34]. Measurements obtained via KPFM are very sensitive and is quite dependent on the electrodes/probe used during characterization[35]. It is often recommended to compare surface potential measurements obtained via KPFM to a reference material to avoid potential variations that might occur through the use of different cantilever tips. In this study, we used micropatterned SAMs formed via vacuum ultraviolet (VUV) photolithography, with one molecule acting as reference to be used in in our KPFM measurements.

In Chapter 2 we discussed how micropatterned SAMs may be formed using vacuum ultraviolet (VUV) photolithography using 1-alkene SAM as a photoresist. Previous studies using 1-alkene SAMs have shown that they can be successfully patterned using VUV photolithography with an irradiation wavelength of 172 nm[23,36,37]. These 1-alkene SAMs also show good stability against HF, due to the strong Si-C bond[38,39], which is important since the surfaces will undergo etching to form the micropatterned SAMs. Thus, 1-alkene SAMs are a good choice material to be used as photoresist in VUV photolithography for the formation of micropatterned SAMs. In Chapter 2 we optimized the parameters needed to be able to successfully form micropatterned SAMs using 1-hexadecene SAM as photoresist.

Previous researches have shown that molecules bound to a silicon substrate via the same interfacial bond exhibit difference in their surface potentials in accordance to the

molecule's terminal functional groups[20,29–31,40,41]. Researchers in some of these studies used simplified SAM models in their computations, which only considered the dipole from the molecules' terminal functional groups[30,31,41]. This is founded on the notion that the dipole formed at the interface is consistent for all SAMs because the molecules are attached to the substrate in the same manner, thus any differences in the net apparent dipole moment of the molecules must be due to the terminal groups. In this research, we wish to concentrate on the effects of different interface dipoles on the material's surface potential. Three molecules which possess the same hydrocarbon chain (n = 16) but differ in the interfacial bonds formed with the silicon substrate (Si-C, Si-S and Si-O) have been selected for this study.

The main objective of this chapter is to measure and compare the surface potential contrasts between 1-alkene, 1-thiol and 1-alcohol self-assembled monolayers on a hydrogen-terminated Si (111) substrate. The specific objectives of this study are as follows:

(1) Form SAMs using 1-hexadecene (HD SAM), 1-hexadecanethiol (HDT SAM) and 1-hexadecanol (HDO SAM) on hydrogen terminated Si (111) substrate

(2) Form micropatterned HD-HD, HD-HDT and HD-HDO SAMs on Si (111) substrate

(3) Obtain the surface potential difference and topographic contrasts of the micropatterned SAMs using Kelvin Probe Force Microscope (KPFM)

(4) Compute for the dipole moments for the precursor molecules and the SAM using Molecular Package (MOPAC) semi empirical computations

(5) Discuss the variations in the surface potentials of the SAMs in terms of the dipole moments estimated from the MOPAC computations

3.2. Experimental methods

3.2.1. Preparation of Hydrogen-terminated Silicon

A n-Si (111) wafer (phosphorus-doped, resistivity range of 1-10 Ω cm was cut into 1 × 1 cm^2 squares and cleaned ultrasonically using ethanol (Nacalaitesque, 99.5%) and ultrapure water (UPW) for 20 minutes each. To eliminate organic contaminants on the substrate surface, photochemical cleaning was performed via vacuum ultraviolet (VUV) irradiation from a Xe-excimer lamp (Ushio, UER 20-172V) in an ambient environment for 20 minutes. This was followed by substrate etching in a 5% hydrofluoric acid (HF, Stella Chemifa) solution for 5 minutes under dark conditions. The substrate was washed twice in UPW and immersed in a 40% ammonium fluoride (NH_4F, Daikin) solution for 30 seconds to produce hydrogen-terminated silicon (H-Si). The NH_4F solution was heated to 80°C prior to substrate immersion to eliminate dissolved oxygen which can produce etch pits on the substrate surface. The prepared H-Si substrate was thoroughly rinsed in UPW after chemical etching. *Note: The etching times in HF and NH_4F used in this chapter is slightly different compared to that discussed in Chapter 2 due to the different chemical manufacturer. However, similar etching tests to Chapter 2 were conducted to ensure that the quality of the HD SAM is preserved.*

3.2.2. SAM Formation

The SAM formation on the substrate was initiated using UV light irradiation. This was conducted using a custom-made quartz vessel which consisted of a rectangular cell of 5 mm thickness attached to one end of a cylindrical tube with a volume of about 100 cm^3. To graft the molecules to the substrate and form the SAM, the H-Si substrate was placed in the quartz vessel with the precursor solution and irradiated for one hour using UV light (REX-250, Asahi spectra). The quartz vessel was placed between 8 to 10 cm away from the UV light source to attain an intensity between 95 to 100 $mWcm^{-2}$. During the process, two glass

tubes connected to a rubber stopper at the end of the cylinder were used to purge the setup with N_2 gas to ensure that the silicon substrate oxidation is kept to a minimum. The SAM precursors in this study were 1-hexadecene (Tokyo Chemical Industry, >99.5%), 1-hexadecanethiol (Tokyo Chemical Industry, >97%) and 1-hexadecanol (Tokyo Chemical Industry, >98%) to form HD, HDT and HDO SAMs respectively (Figure 3.2). Neat 1-hexadecene was used as the HD SAM precursor, while 0.5 M solution in mesitylene (Nacalai Tesque, 98%) was used for both HDT and HDO SAMs. After the UV irradiation, the samples were cleaned ultrasonically for 10 minutes each in mesitylene (for HDT and HDO), ethanol and UPW to remove any physisorbed material on the surface.

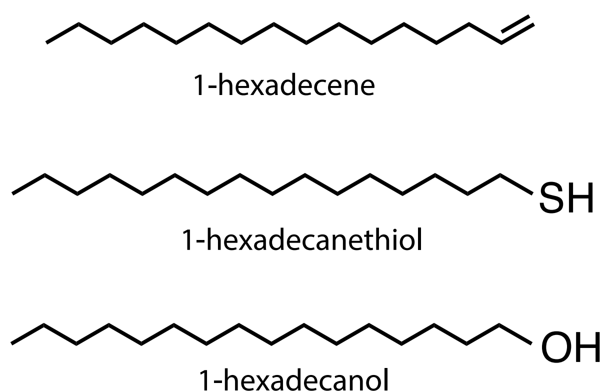

Figure 3.2. Chemical structure of precursors used in SAM formation

3.2.3. Formation of Micropatterned SAMs

To form the micropatterned SAMs, HD SAM was irradiated with a Xe-excimer lamp (Ushio, UER20-172V) with a wavelength of 172 nm and intensity of 10 mWcm^{-2} in a vacuum chamber. During irradiation, distance from the lamp window to the substrate was kept constant at 5 mm and the pressure inside the chamber was regulated to 10^3 Pa. The substrate was irradiated through a photomask with 10 μm lines and spaces. The photomask consisted of a 100 nm thick chromium pattern attached to a 2 mm thick quartz plate whose

transparency at λ = 172 nm was 93% (Figure 3.3). The samples were irradiated under the photomask for 30 minutes. These parameters were tested and optimized in **Chapter 2**. After VUV irradiation, the sample was once again etched to form H-Si on the irradiated regions and a new SAM was grafted on the new H-Si regions (Figure 3.4).

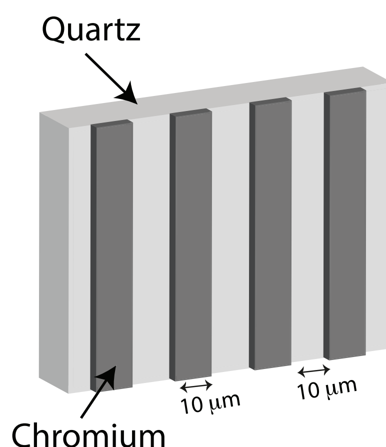

Figure 3.3. Schematic illustration of line photomask used

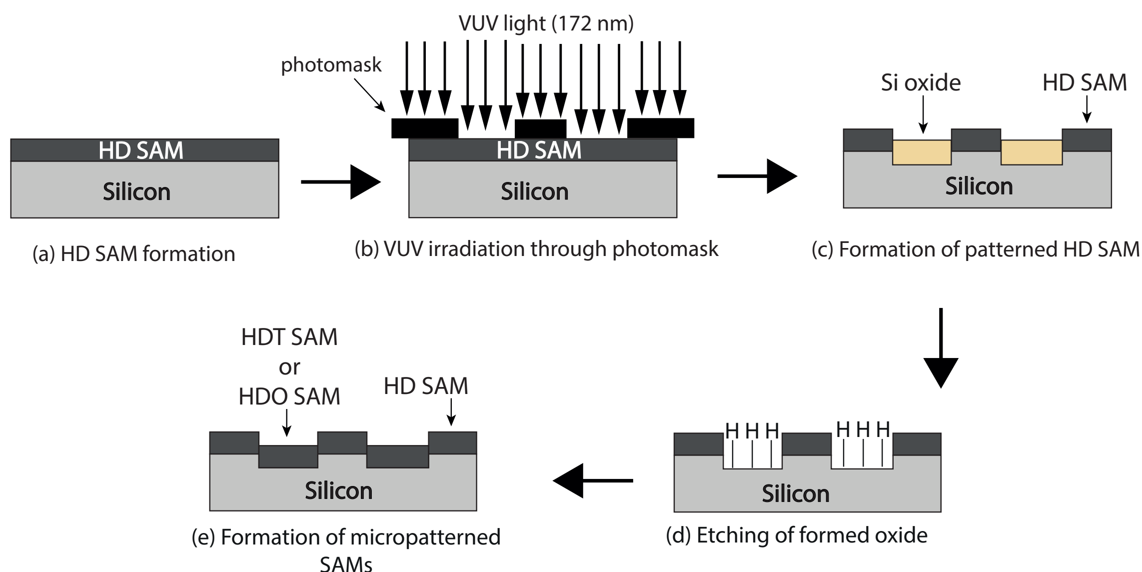

Figure 3.4. Schematic diagram of VUV photolithography and micropatterning process

3.2.4. Characterization

The HD, HDT and HDO SAMs were characterized using X-ray photoelectron spectroscopy (ESCA-3400 Kratos Analytical), static contact angle meter (DM 500, Kyowa Interface Science CA-X Co.), atomic force microscopy, and ellipsometry (FE-5000, Otsuka Electronics).

The surface potentials and topography of the micropatterns were observed using a Kelvin Probe Force Microscope based on amplitude modulation AFM (Asylum Research MFP-3D). The topography and surface potentials are obtained using a two-pass procedure, with the topographic line is acquired first in tapping mode and the surface potential is acquired second in lift mode. KPFM measurements were conducted in ambient air with Rh-coated silicon cantilever tips (SI-DF-3R, Hitachi Hitech). The resonance frequency of the Si cantilever was approximately 27 kHz and the amplitude was 1.0 V. KPFM images of the samples were acquired at a probe scan rate ranging from 0.5 to 0.8 Hz.

The geometrical structures of HD, HDT and HDO SAMs were optimized using MOPAC semi empirical computations and their dipole moments were predicted using molecular orbital computations utilizing the PM7 theory.

3.3. Results and discussion

3.3.1. Properties of HD, HDO and HDT SAMs

The individual properties of the SAMs are summarized in Table 2.1. The water contact angles (WCA) of all the samples indicated a methyl terminated surface and is in good agreement with previous studies[39,42]. The XPS scans (Figure 3.5) show that no peak is present at 103 eV for all three SAMs suggesting that the silicon surface was successfully passivated. The increase in atomic % concentration of the C 1s peak indicates that the precursor molecules were successfully grafted to the surface. For the HDT scan the small peak in the S 2s scan shows the presence of sulfur which exists due to the thiol end group.

The AFM images of the SAMs (Figure 3.6) show clear terraces indicating that a uniform monolayer was formed on H-Si. These results indicate that the SAMs were in formed with good order and packing density.

Table 3.1. Properties of HD, HDT and HDO SAMs

	WCA	Atomic % Concentration			
		C 1s	O 1s	Si 2p	S 2s
HD SAM	104.9 ± 1.3	33.9 ± 2.1	5.1 ± 0.9	61.1 ± 3.0	-
HDT SAM	100.8 ± 1.7	24.2 ± 2.2	5.5 ± 0.7	69.9 ± 1.7	0.5 ± 0.2
HDO SAM	102.1 ± 1.6	26.0 ± 1.4	7.3 ± 2.5	66.7 ± 3.9	-

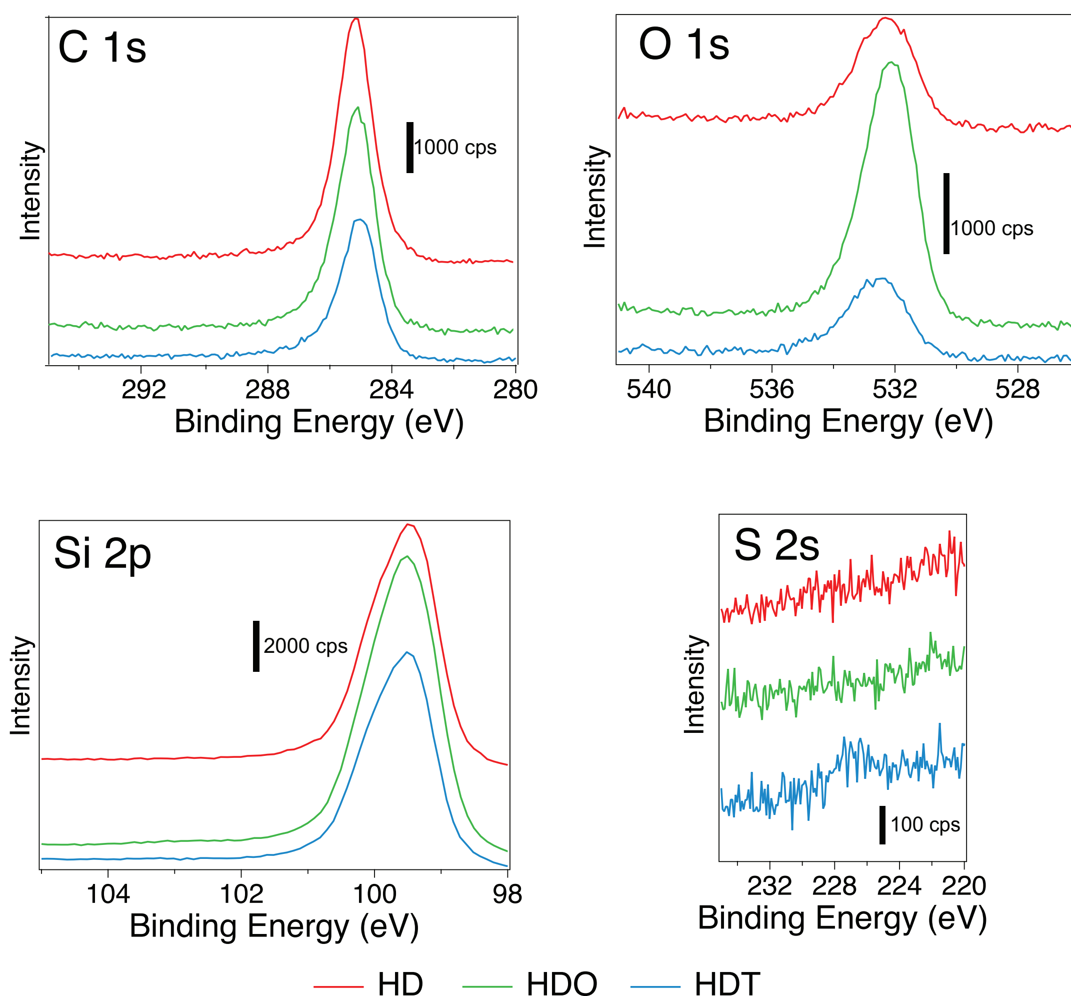

Figure 3.5. XPS peaks of the HD, HDO and HDT SAMs

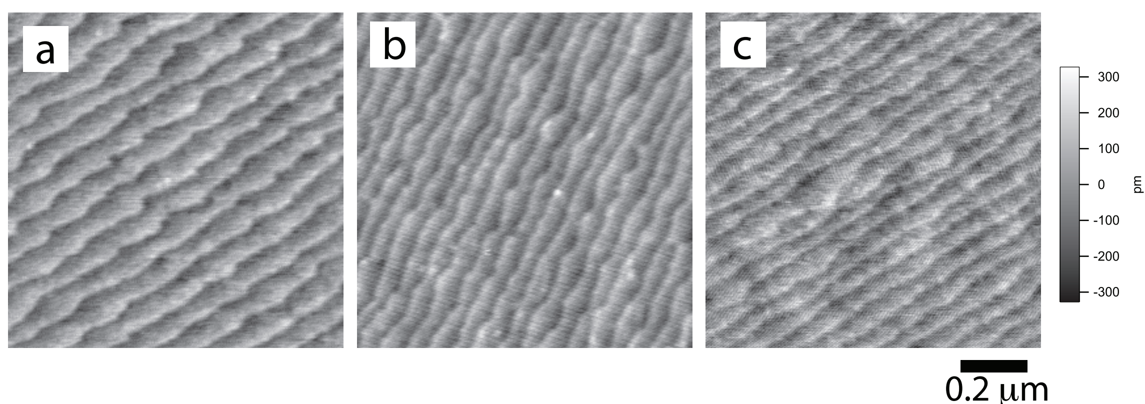

Figure 3.6. AFM of (a) HD, (b) HDO, and (c) HDT SAM

3.3.2. Surface Potential Measurements via KPFM

In Chapter 2 we discussed that HD SAM can be used as a reliable reference material for surface potential measurements. Using the optimized parameters we can observe the corresponding topography and surface potential images for HD SAM after VUV irradiation at 1000 Pa for 30 minutes through a line photomask in Figure 3.7(a) and (b). The line patterns from the photomask are clearly visible in both the topography and KPFM image. For both the topography and surface potential scans, the lighter regions correspond to the mask areas (containing the original HD reference SAM) and the darker regions correspond to the VUV-irradiated sections of the same (containing the oxidized silicon). In the AFM scan, the lower topography of the irradiated region is explained by the degradation of the C-C molecules on the surface which occurs during VUV irradiation. Previous studies have discussed how VUV irradiation of HD SAM leads to the degradation of the alkyl chains and formation of silicon oxide[23]. This was also discussed in Chapter 2 of this dissertation where we demonstrated the appearance of an XPS peak at 103 eV after irradiation due to the existence of silicon oxide. The water contact angle of the irradiated region was also found to decrease due to the oxygen containing polar functional groups. As such, the irradiated region is expected to have lower topography since the masked regions still contain the HD molecules.

A schematic of the photomask used in this experiment can be seen in Figure 3.3. The mask consisted of alternating bands measured to be 10 μm in width. In both the AFM and KPFM scans of the samples in this experiment, it can be observed that the irradiated regions appear slightly wider than the masked regions. In previous literature it was found that diffusion of oxidants under microscopic regions under the photomask during VUV irradiation can cause a broadening of the irradiated region. When the oxidants diffuse under the mask, the HD monolayer there undergoes slight photodegradation as well[37].

The KPFM image in Figure 3.7 (b) shows that the surface potential of the VUV irradiated region is much lower than that compared to the reference HD SAM. From the XPS results of VUV irradiated HD SAM in Chapter 2, we know that these regions contain silicon oxide, and the unirradiated region contains the original HD monolayer. The KPFM measurements shows a difference of -75 mV between the irradiated and unirradiated regions. The AFM images also show a difference in height between the irradiated and unirradiated region. Measurement of the height difference gives us about 0.85 nm, which is less than the length (and estimated thickness) of the HD SAM, which is around 2 nm[37]. Although the HD monolayer is known to have been photodegraded from the VUV irradiation, the height of the irradiated region is higher than that of the original silicon substrate. During SAM formation, the HD monolayer is grafted directly to oxide-free silicon during SAM formation. However, when the monolayer is irradiated, the monolayer is degraded and replaced with silicon oxide, thus the height of the silicon substrate is raised due to the formation of silicon oxide[36].

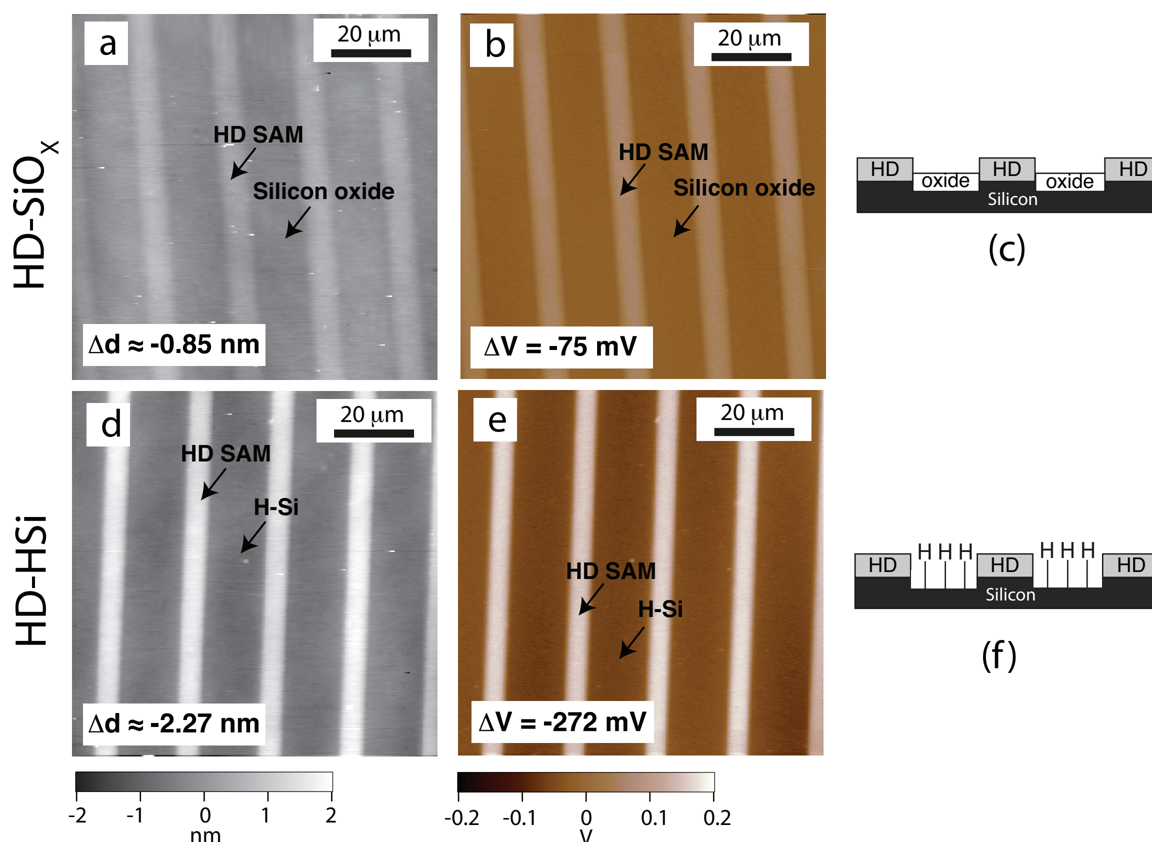

Figure 3.7. Surface potential and topographic images of micropatterned samples. (a) AFM, (b) KFM, and (c) schematic images of HD SAM – silicon oxide samples. (d) AFM, (e) KFM and (f) schematic images of HD SAM – H-Si samples.

Once the old HD SAM is removed from the silicon through VUV irradiation, a new SAM can be grafted in its place. However, the substrate must once again undergo hydrogen termination via HF and NH_4F etching to remove the silicon oxide that formed during the photolithography process. The details of the etching are discussed in Chapter 2 where the process to optimize the etching conditions to have the least amount of damage on the original HD monolayer while still being able to form good H-Si was discussed.

KPFM images of the irradiated and etched micropatterned sample shows a -272 mV contrast between the reference HD SAM and the H-terminated silicon regions (Figure 3.7). The height difference between the two regions also increased from 0.85 nm to 2.27 nm. Both KPFM and AFM images suggests that the silicon oxide layer that formed through VUV

irradiation was removed successfully after the HF and NH_4F etch. The new height difference between the HD region and H-Si region (2.27 nm) is larger than the molecular length and expected thickness of the HD SAM (~2 nm). In Figure 3.4 (c) we can see that during VUV irradiation, the silicon oxide layer that forms in the irradiated regions extend below the original surface of the silicon substrate[23]. Upon etching, this silicon oxide layer is removed and the height of the silicon substrate is lowered, resulting to a larger height difference compared to the thickness of the original SAM In Figure 3.4 (e).

Following Evan's and Ulman's work[14], the HD monolayer on silicon can be envisioned as a dipole sheet on the surface. The net dipole moment can be obtained by obtaining the vector sum of the interface dipole formed between the molecule-substrate bond, and the gas phase dipole of the precursor molecule (Figure 3.8). For our HD SAM samples on H-Si, we can infer that the net dipole points downwards, resulting to a layer of negative charges near the Si substrate and a layer of positive charges close to the monolayer-air interface. We can deduce the orientation of this dipole based on the higher surface potential of the HD SAM compared to both the silicon oxide and hydrogen-terminated silicon regions.

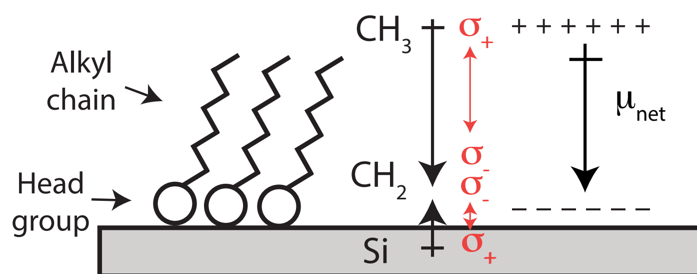

Figure 3.8. Schematic diagram of dipole formed by SAM on a Si substrate

After removal of the silicon oxide through etching, HD SAM was once again deposited on the H-Si regions to see if there are any differences between the reference HD SAM that was used as a photoresist during VUV photolithography and the fresh HD SAM on the irradiated substrate. The results are shown in Figure 3.9. A topographic difference of

-1.48 nm between the new and reference HD regions were measured in the AFM scans. As discussed earlier, this is due to the lowering of the silicon substrate during VUV irradiation and etching step. The new HD SAM is grafted to this lowered region resulting to the lower height, as shown in Figure 3.10.

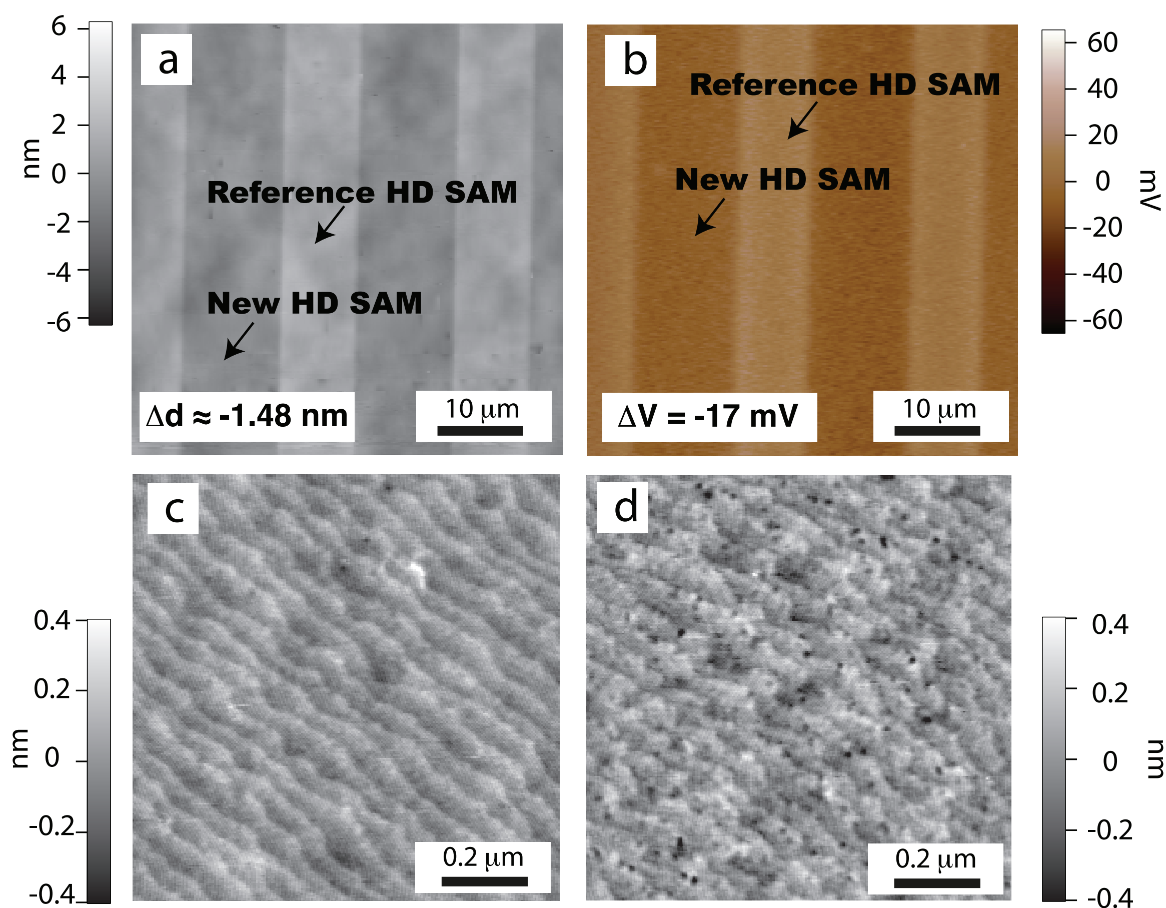

Figure 3.9. Topography and surface potential of micropatterned HD-HD sample. (a) AFM and (b) KFM of micropatterned region. Terrace-step microstructure of the HD SAM surface in the (c) new and (d) reference regions.

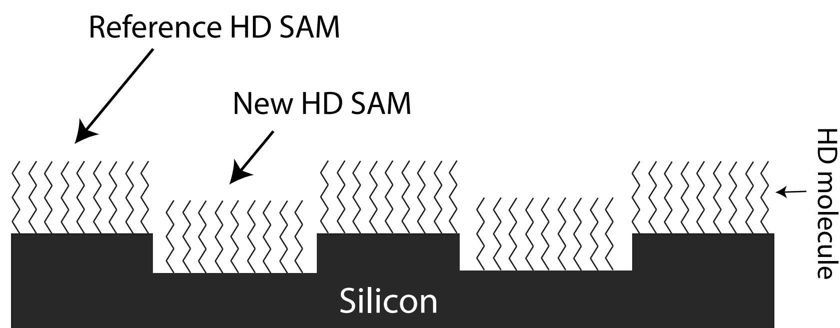

Figure 3.10. Schematic of micropatterned HD-HD SAM surface

If we consider that both the new and reference HD SAM regions contain the same molecule on the same silicon substrate, hypothetically they should have the same surface potential. However, KPFM measurements show a difference of about -17 mV between the two regions. The negative value indicates that the new HD SAM has a lower surface potential than the reference HD SAM. A more in-depth look of the surface of the two regions shows that although both regions display the characteristic terrace step structure of monohydride-terminated Si (111), a closer look at the reference HD SAM region shows the presence of etch pits on the surface. This was due to the damage the monolayer sustained during the etching step in the VUV photolithography process (as discussed in Chapter 2). Because KPFM measurements are very sensitive to the quality of the surface, the minimal damage on the reference region possibly increased its surface potential slightly, resulting to the difference in surface potential between the two HD regions.

The surface potential of a SAM on a substrate is given by Equation 3.1[29–31]. The terms ϕ_{Si} and ϕ_{tip} correspond to the work functions of the silicon substrate and the tip, respectively, and e is the electric charge[43]. In the second term derives from the Helmholtz equation[44–46] and corresponds to the dipole moment of the organic thin film. The net dipole moment of the gas-phase molecule that is normal to the substrate is denoted by μ, while A is the area occupied by the molecule. The permittivity of free space and relative permittivity

of the SAM are denoted by ϵ_0 and ϵ_{SAM}, respectively.

$$V_{SAM} = -\frac{\phi_{Si} - \phi_{tip}}{e} + \frac{\mu}{A\epsilon_0\epsilon_{SAM}} \quad \text{Equation 3.1}$$

In this experiment, the two SAMs are formed on the same same silicon substrate and are measured using the same KPFM probe tip, thus the first terms cancel out and we are left with Equation 3.2.

$$V_{SAM1} - V_{SAM2} = \frac{\mu_{SAM1}}{A_{SAM1}\epsilon_0\epsilon_{SAM1}} - \frac{\mu_{SAM2}}{A_{SAM2}\epsilon_0\epsilon_{SAM2}} \quad \text{Equation 3.2}$$

In the sample where both the reference and new SAM regions contain HD SAM, we can assume μ_{SAM} to be equal since they are formed using the same molecule. The fact that there is a surface potential difference between the two regions suggests that a difference in A_{SAM} or ϵ_{SAM} exists for these two regions. Differences in the value of A_{SAM} suggests that the molecular packing, and thus the area occupied by each molecule, is different for the reference and new HD region. Comparison of the water contact angle (WCA) of the two regions was conducted to determine if there was a significant difference in molecular packing between them. The results, shown in Table 2.2, compare freshly formed HD SAM to that of an HD SAM sample that underwent etching in 5% HF and 40% NH_4F (without irradiation) to simulate the reference HD SAM region in our micropatterned SAMs. The measured WCA show very little difference between the two regions which suggests that the molecular packing is very similar and that the minimal damage experienced by the reference HD SAM region due to the etching process did not significantly affect the density of the grafted SAM. Surface potential measurements are known to be very sensitive to the surface quality of the material, and as we have seen in the AFM images, there is a slight damage to the reference

HD region. Changes in surface potential of a sample can be affected by humidity, oxidation and even possible contaminants on the surface. It is possible that the damage on the reference HD SAM has made it more prone to oxidation or hastened the aging of the material. Not much research has been dedicated to the effects of oxidation and aging on dielectric properties of alkyl SAMs, however studies on ceramics and silicon wafers have found that oxidation and aging has been found to alter the dielectric properties of these materials.[47–49] If a similar case exists for alkyl SAMs on silicon then it can account for the discrepancy between the reference and new HD SAM regions. Nevertheless, multiple measurements and test have shown that the surface potential difference of -17 mV between the new and reference HD SAM are experimentally reproducible and thus it makes HD SAM a reliable reference material for our surface potential measurements in our micropatterned SAMs.

Table 2.2. Water contact angles of reference and new HD SAM regions

	HD SAM (etched)	**HD SAM on irradiated substrate**
WCA	104.70 ± 1.05	104.80 ± 1.15

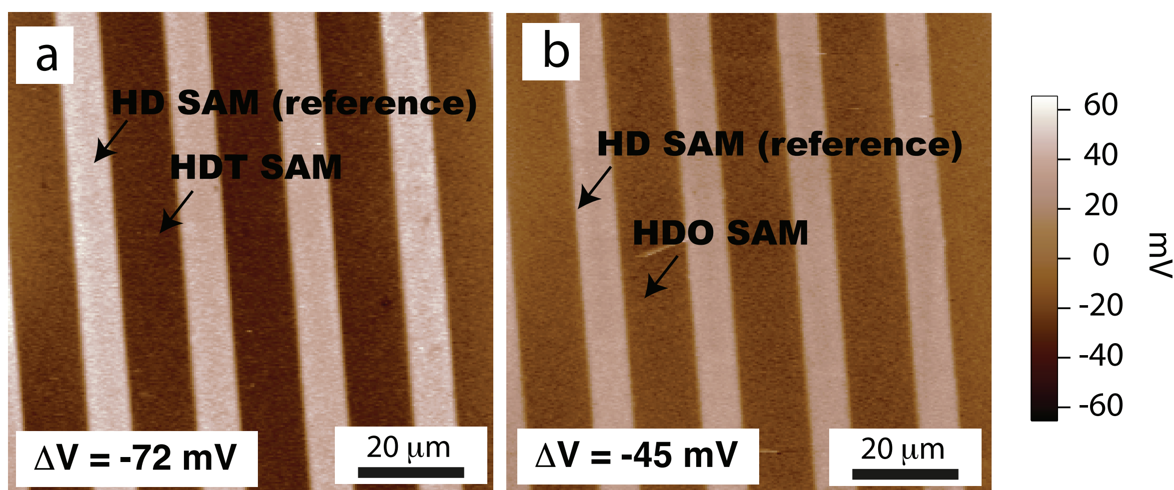

Figure 3.11. KFM images of (a) HD-HDT and (b) HD-HDO SAMs

The KPFM images for the micropatterned HD-HDT and HD-HDO SAMs are shown in Figure 3.11. A difference of -72 mV exists between the reference HD and the HDT region, while a difference of -45 mV is present for the reference HD and the HDO region. Taking the increase in surface potential of the reference HD SAM due to the effect of etching (an increase of 17 mV), the true surface potential contrasts are calculated to be -55 mV and -28 mV for HD-HDT and HD-HDO respectively. For both cases, the HD SAM surface potential is higher, suggesting that the HD monolayer has a higher dipole moment compared to HDT and HDO. The dipole moments of the precursor molecules were computed using the Molecular Orbital PACkage (MOPAC) and are shown in Figure 3.12.

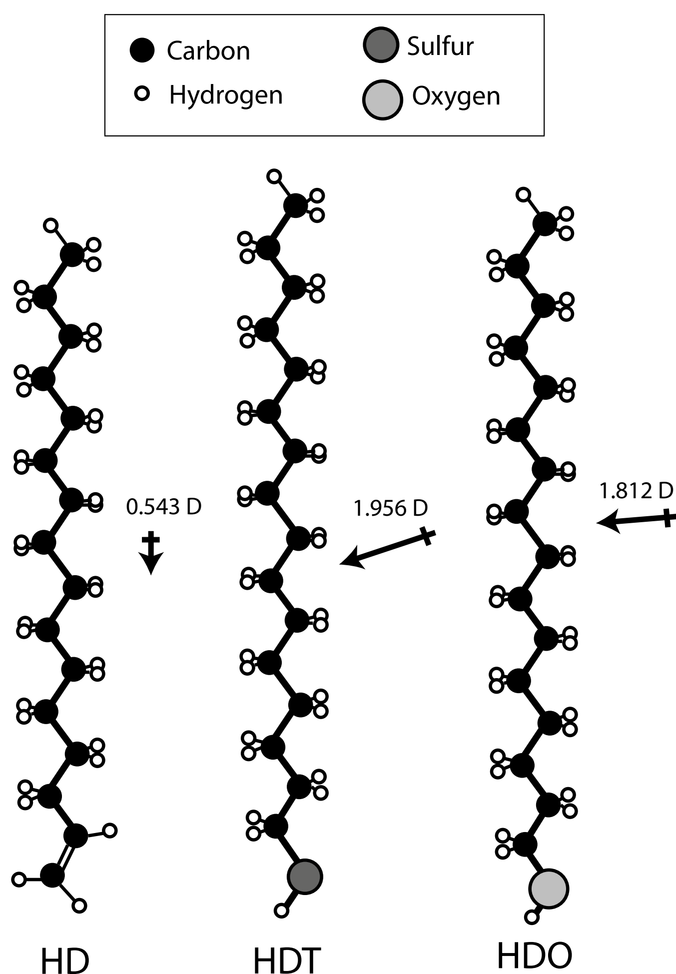

Figure 3.12. Molecular structures and dipole moments of precursors

MOPAC calculations show that the precursors have a dipole moment of 0.543 D, 1.956 D and 1.812 D for HD, HDT and HDO respectively. Working with the assumption that the alkyl chains are aligned perpendicularly to the silicon substrate once they are grafted, we computed the dipole components normal to the surface to be 0.543 D, 0.735 D and 0.231 D for HD, HDT and HDO respectively. In this case, HDO should have the lowest surface potential, followed by HD then HDT, which does not agree with our KPFM results. Going back to Evans and Ulman's idea that the SAM's net dipole is the sum of the dipole moments of the molecule and the bond dipole at the interface[14], we can imagine that the SAM's dipole moment will be slightly different from the dipole of its precursor molecules once the interface dipole is taken into account.

A different study by Zehner et. al on the modification of the work function of gold using thiol SAMs supported the idea that chemisorbed SAMs can be modelled as two dipole sheets with one layer comprising of the effective dipole moment of the adsorbate and the other dipole accounting for the interfacial bond[46]. They proposed that the change in work function (Δϕ) is equal to Equation 3.3, where $\Delta\phi$ is the change in work function, $\frac{1}{A}$ is the density of molecules on the surface and $\frac{\mu_m}{\epsilon_m\epsilon_0}$ is the effective dipole moment of the molecule, and $\frac{\mu_i}{\epsilon_i\epsilon_0}$ is the effective dipole moment at the interface.

$$\Delta\phi = \frac{1}{A}\left[\frac{\mu_m}{\epsilon_m\epsilon_0} + \frac{\mu_i}{\epsilon_i\epsilon_0}\right] \qquad \text{Equation 3.3}$$

Several previous studies on the surface potential changes brought about by organosilane SAMs on silicon focused mostly on the precursor molecular dipole because the interfacial bond was the same for all molecules[20,29–31,40]. Since the molecules were all grafted to the silicon substrate in the same manner, the term corresponding to the effective dipole of the interfacial bond can be ignored under the assumption that it is constant. However, from

the results of our experiment where the molecules are grafted to silicon via different covalent bonds, we can see that the interface dipole plays a big role in the net dipole moment of the SAM. We performed another MOPAC calculation where we incorporated the interface dipole by connecting the precursor molecule to a silicon atom. The results are shown in Figure 3.13.

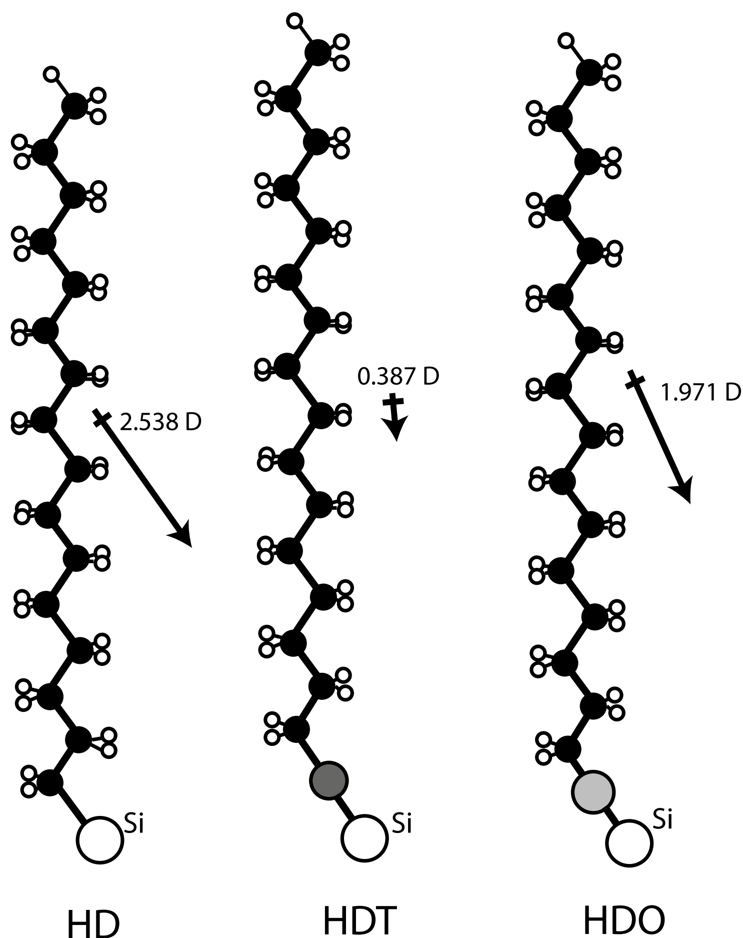

Figure 3.13. Dipole moments of HD, HDT and HDO molecules on Si

The addition of a silicon atom to the precursor molecule changed the outcome of the dipole moment trend significantly. Comparing these to the dipole moments in Figure 3.12, we can observe a large increase in the dipole moment of the HD molecule. By itself, the HD molecule did not have a very large dipole moment due to the fact that it is mostly symmetric, however the formation of the Si-C bond resulted to charge rearrangements along the

backbone resulting to a much larger net dipole moment for HD SAM. Similarly, when the HDT and HDO molecules were grafted to silicon, the net dipole moments were very different from the dipole moment of only the precursor molecule. It is clear that the interfacial covalent bond with silicon lead to the precursor molecules experiencing different polarizations and charge rearrangement in the backbone due to the different electronegativities of the binding atoms of the molecules to silicon. The computed dipole moments of the molecules attached to a single silicon atom we used here are 2.538 D, 0.387 D and 1.971 D for HD, HDT and HDO respectively. Working with the assumption again that the molecules are grafted such that the hydrocarbon chains stand perpendicular to the silicon surface, we computed the components of the dipole moments to be 2.10 D, 0.385 D and 1.827 D for HD, HDT and HDO respectively. These computations agree qualitatively with the KPFM surface potential measurements in our experiment.

The surface potential difference between two SAMs can be computed for using Equation 3.2, which we apply to our systems. In our computations, the area occupied by each molecule was assumed to be 25.5 $Å^2$ for the three SAMs, based on a hypothetical model of a unit cell of Si (111) containing one alkyl chain and one hydroxyl group[50]. The same dielectric constant of 2.76 was also used for all the SAMs[45]. Using these parameters, the calculated surface potential difference between HD and HDT SAM is -918 mV, while HD and HDO would yield a difference of -146 mV. These computed values are much greater than the measured values we obtained during KPFM analysis. Other scientists working with surface potential measurements have also reported greater computed values than those obtained in their experiments due to the approximation during modelling[29,45]. In our computations we used an estimated value of A, however for SAMs with a smaller packing density than expected, the value of A will be much higher and will result to a smaller value of surface potential. Also, we should take into consideration that the dipole moments we used in our computations were obtained for isolated molecules, however, dipole moments of

SAMs may differ from that of the individual molecules due to molecular interactions which can result to screening or depolarization. Our model also utilized a single silicon atom attached to the molecule in observation, however in reality the organic molecule is grafted to a silicon crystal rather than a single silicon atom. Lastly, the estimated dipole moments we obtained were based on MOPAC semi-empirical computations which utilized approximations based on existing experimental data. These semi-empirical computations often give good models and approximations of molecular systems but they are not as complex or extensive as first principles or ab initio computations. It is possible that the simplified model of the molecule attached a single silicon atom, in combination with semi-empirical computations may result in an over-estimation of the dipole moments. In reality, it is possible that the actual dipole moments of SAMs could be much smaller than what we have presented here. However, our estimated dipole moments and computed surface potential qualitatively agree with the experimental results obtained using KPFM analysis of our micropatterned SAMs.

3.4. Conclusions

The surface potentials of micropatterned SAMs of HD, HDT and HDO using HD SAM as reference were studied using KPFM and MOPAC computations. Using a reference SAM in our KPFM measurements ensured that the comparison of the two SAMs were done more accurately than if the measurements were conducted separately, due to the removal of the variations due to the KPFM probe and substrate. The surface potential measurements obtained during KPFM agreed with the MOPAC computed dipole moments of the molecules attached to a silicon atom. This study showed the effect of the interfacial bond between a molecule and the substrate on the dipole moment and resulting surface potential of the material. Simply looking at the dipole moment of the precursor molecule does not completely reflect the true surface potential effect it has on the SAM, especially if they are

grafted through different bonds. The covalent bond between the molecule and substrate polarizes the molecule and yields a second dipole moment at the interface. The net dipole moment of the SAM should consider the sum of the molecular dipole and this interfacial dipole.

Computation for the surface potentials using the estimated dipole moments obtained through MOPAC yielded a higher result than those found in our experiments. This was attributed to the use of a simplified model in our computations as well as the use of semi-empirical approximations rather than first principles computations. However our experimental and computational results qualitatively agree with each other and show that the surface potential of a material is governed not only by the dipole of the molecular precursor but is also affected by the interfacial dipole present due to the covalent bond that is formed between the molecule and substrate.

References

(1) Booth, B. D.; Vilt, S. G.; Lewis, J. Ben; Rivera, J. L.; Buehler, E. A.; McCabe, C.; Jennings, G. K. Tribological Durability of Silane Monolayers on Silicon. *Langmuir* **2011**, *27*, 5909–5917.

(2) Nakano, M.; Ishida, T.; Sano, H.; Sugimura, H.; Miyake, K.; Ando, Y.; Sasaki, S. Tribological Properties of Self-Assembled Monolayers Covalently Bonded to Si. *Appl. Surf. Sci.* **2008**, *255*, 3040–3045. https://doi.org/10.1016/j.apsusc.2008.08.073.

(3) Behpour, M.; Mohammadi, N. Investigation of Inhibition Properties of Aromatic Thiol Self-Assembled Monolayer for Corrosion Protection. *Corros. Sci.* **2012**, *65*, 331–339. https://doi.org/10.1016/j.corsci.2012.08.036.

(4) Appa Rao, B. V.; Yakub Iqbal, M.; Sreedhar, B. Self-Assembled Monolayer of 2-(Octadecylthio)Benzothiazole for Corrosion Protection of Copper. *Corros. Sci.* **2009**, *51*, 1441–1452. https://doi.org/10.1016/j.corsci.2009.03.034.

(5) Wink, T.; van Zuile, S. J.; Bult, A.; van Bennekom, W. P. Self-Assembled Monolayers for Biosensors. *Analyst* **1997**, *122*, 43–50.

(6) Lee, H.; Lee, W.; Lee, J. H.; Yoon, D. S. Surface Potential Analysis of Nanoscale Biomaterials and Devices Using Kelvin Probe Force Microscopy. *J. Nanomater.* **2016**, *2016*, 1–21. https://doi.org/10.1155/2016/4209130.

(7) Vilan, A.; Cahen, D. Chemical Modification of Semiconductor Surfaces for Molecular Electronics. *Chem. Rev.* **2017**, *117* (5), 4624–4666. https://doi.org/10.1021/acs.chemrev.6b00746.

(8) Aswal, D. K.; Lenfant, S.; Guerin, D.; Yakhmi, J. V.; Vuillaume, D. Self Assembled Monolayers on Silicon for Molecular Electronics. *Anal. Chim. Acta* **2006**, *568*, 84–108. https://doi.org/10.1016/j.aca.2005.10.027.

(9) Casalini, S.; Bortolotti, C. A.; Leonardi, F.; Biscarini, F. Self-Assembled Monolayers in Organic Electronics. *Chem. Soc. Rev.* **2017**, *46*, 40–71. https://doi.org/10.1039/c6cs00509h.

(10) Rampi, M. A.; Schueller, O. J. A.; Whitesides, G. M. Alkanethiol Self-Assembled Monolayers as the Dielectric of Capacitors with Nanoscale Thickness. *Appl. Phys. Lett.* **1998**, *72*, 1781–1783.

(11) Heimel, G.; Romaner, L.; Zojer, E.; Bredas, J. The Interface Energetics of Self-Assembled Monolayers on Metals. *Acc. Chem. Res.* **2008**, *41* (6), 721–729.

(12) Ishii, H.; Sugiyama, K.; Ito, E.; Seki, K. Energy Level Alignment and Interfacial Electronic Structures at Organic/Metal and Organic/Organic Interfaces. *Adv. Mater.* **1999**, *11* (8), 605–625.

(13) Campbell, I.; Rubin, S.; Zawodzinski, T.; Kress, J.; Martin, R.; Smith, D.; Barashkov, N.; Ferraris, J. Controlling Schottky Energy Barriers in Organic Electronic Devices Using Self-Assembled Monolayers. *Phys. Rev. B - Condens. Matter Mater. Phys.* **1996**, *54* (20), 14321–14324. https://doi.org/10.1103/PhysRevB.54.R14321.

(14) Evans, S. D.; Ulman, A. Surface Potential Studies of Alkyl-Thiol Monolayers Adsorbed on Gold. *Chem. Phys. Lett.* **1990**, *170*, 462–466. https://doi.org/10.1016/S0009-2614(90)87085-6.

(15) Campbell, I. H.; Kress, J. D.; Martin, R. L.; Smith, D. L.; Barashkov, N. N.; Ferraris, J. P. Controlling Charge Injection in Organic Electronic Devices Using Self-Assembled Monolayers. *Appl. Phys. Lett.* **1997**, *71* (24), 3528–3530. https://doi.org/10.1063/1.120381.

(16) Porter, M. D.; Bright, T. B.; Allara, D. L.; Chidsey, C. E. Spontaneously Organized Molecular Assemblies. 4. Structural Characterization of n-Alkyl Thiol Monolayers on Gold by Optical Ellipsometry, Infrared Spectroscopy, and Electrochemistry. *J. Am. Chem. Soc.* **1987**, *109* (12), 3559–3568. https://doi.org/10.1021/ja00246a011.

(17) Lu, J.; Delamarche, E.; Eng, L.; Bennewitz, R.; Meyer, E.; Gu, H. Kelvin Probe Force Microscopy on Surfaces : Investigation of the Surface Potential of Self-Assembled Monolayers On. *Langmuir* **1999**, *15*, 8184–8188. https://doi.org/10.1021/la9904861.

(18) Ichii, T.; Fukuma, T.; Kobayashi, K.; Yamada, H.; Matsushige, K. Phase-Separated Alkanethiol Self-Assembled Monolayers Investigated by Non-Contact AFM. *Appl. Surf. Sci.* **2003**, *210*, 99–104. https://doi.org/10.1016/S0169-4332(02)01487-3.

(19) Szwajca, A.; Wei, J.; Schukfeh, M. I.; Tornow, M. Self-Assembled Monolayers of Alkyl-Thiols on InAs: A Kelvin Probe Force Microscopy Study. *Surf. Sci.* **2015**, *633*, 53–59. https://doi.org/10.1016/j.susc.2014.11.023.

(20) Saito, N.; Hayashi, K.; Sugimura, H.; Takai, O.; Nakagiri, N. Surface Potentials of Patterned Organosilane Self-Assembled Monolayers Acquired by Kelvin Probe Force Microscopy and Ab Initio Molecular Calculation. *Chem. Phys. Lett.* **2001**, *349*, 172–177. https://doi.org/10.1016/S0009-2614(01)01097-1.

(21) Cohen, R.; Bastide, S.; Cahen, D.; Libman, J.; Shanzer, A.; Rosenwaks, Y. Controlling Surfaces and Interfaces of Semiconductors Using Organic Molecules. *Opt.*

Mater. (Amst). **1998**, *9* (1–4), 394–400. https://doi.org/10.1016/S0925-3467(97)00065-7.

(22) Veerbeek, J.; Huskens, J. Applications of Monolayer-Functionalized H-Terminated Silicon Surfaces: A Review. *Small Methods* **2017**, *1* (4), 1700072. https://doi.org/10.1002/smtd.201700072.

(23) Sugimura, H.; Sano, H.; Lee, K.-H.; Murase, K. Organic Monolayers Covalently Bonded to Si as Ultra Thin Photoresist Films in Vacuum UV Lithography. *Jpn. J. Appl. Phys.* **2006**, *45* (6B), 5456–5460. https://doi.org/10.1143/JJAP.45.5456.

(24) Magid, I.; Burstein, L.; Seitz, O.; Segev, L.; Kronik, L.; Rosenwaks, Y. Electronic Characterization of Si(100)-Bound Alkyl Monolayers Using Kelvin Probe Force Microscopy. *J. Phys. Chem. C* **2008**, *112* (18), 7145–7150. https://doi.org/10.1021/jp709973d.

(25) Faber, E. J.; De Smet, L. C. P. M.; Olthuis, W.; Zuilhof, H.; Sudhölter, E. J. R.; Bergveld, P.; Van Den Berg, A. Si-C Linked Organic Monolayers on Crystalline Silicon Surfaces as Alternative Gate Insulators. *ChemPhysChem* **2005**, *6* (10), 2153–2166. https://doi.org/10.1002/cphc.200500120.

(26) Toledano, T.; Garrick, R.; Sinai, O.; Bendikov, T.; Haj-Yahia, A. E.; Lerman, K.; Alon, H.; Sukenik, C. N.; Vilan, A.; Kronik, L.; et al. Effect of Binding Group on Hybridization across the Silicon/Aromatic-Monolayer Interface. *J. Electron Spectros. Relat. Phenomena* **2015**, *204*, 149–158. https://doi.org/10.1016/j.elspec.2015.05.019.

(27) Hu, M.; Liu, F.; Buriak, J. M. Expanding the Repertoire of Molecular Linkages to Silicon: Si-S, Si-Se, and Si-Te Bonds. *ACS Appl. Mater. Interfaces* **2016**, *8* (17), 11091–11099. https://doi.org/10.1021/acsami.6b00784.

(28) Arefi, H. H.; Fagas, G. Chemical Trends in the Work Function of Modified Si(111) Surfaces: A DFT Study. *J. Phys. Chem. C* **2014**, *118* (26), 14346–14354. https://doi.org/10.1021/jp502464r.

(29) Sugimura, H.; Hayashi, K.; Saito, N. Kelvin Probe Force Microscopy Images of Microstructured Organosilane Self-Assembled Monolayers. *Jpn. J. Appl. Phys.* **2001**, *40*, 4373.

(30) Sugimura, H.; Hayashi, K.; Saito, N.; Nakagiri, N.; Takai, O. Surface Potential Microscopy for Organized Molecular Systems. *Appl. Surf. Sci.* **2002**, *188* (3–4), 403–410. https://doi.org/10.1016/S0169-4332(01)00958-8.

(31) Hayashi, K.; Saito, N.; Sugimura, H.; Takai, O.; Nakagiri, N. Regulation of the Surface Potential of Silicon Substrates in Micrometer Scale with Organosilane Self-Assembled Monolayers. *Langmuir* **2002**, *18* (20), 7469–7472. https://doi.org/10.1021/la011707h.

(32) Sugimura, H.; Saito, N.; Maeda, N.; Ikeda, I.; Ishida, Y.; Hayashi, K.; Hong, L.; Takai, O. Surface Potential Microscopy for Chemistry of Organic Self-Assembled Monolayers in Small Domains. *Nanotechnology* **2004**, *15*, S69–S75. https://doi.org/10.1088/0957-4484/15/2/015.

(33) Vatel, O.; Tanimoto, M. Kelvin Probe Force Microscopy for Potential Distribution Measurement of Semiconductor Devices. *J. Appl. Phys.* **1995**, *77* (6), 2358–2362. https://doi.org/10.1063/1.358758.

(34) Nonnenmacher, M.; O'Boyle, M. P.; Wickramasinghe, H. K. Kelvin Probe Force Microscopy. *Appl. Phys. Lett.* **1991**, *58* (25), 2921–2923. https://doi.org/10.1063/1.105227.

(35) Jacobs, H. O.; Knapp, H. F.; Stemmer, A. Practical Aspects of Kelvin Probe Force Microscopy. *Rev. Sci. Instrum.* **1999**, *70* (3), 1756–1760. https://doi.org/10.1063/1.1149664.

(36) Saito, N.; Kadoya, Y.; Hayashi, K.; Sugimura, H.; Takai, O. Micropatterned 1-Alkene Self-Assembled Monolayer on Hydrogen-Terminated Silicon by Vacuum Ultraviolet

Lithography. *Japanese J. Appl. Physics, Part 1 Regul. Pap. Short Notes Rev. Pap.* **2003**, *42* (4 B), 2534–2537. https://doi.org/10.1143/JJAP.42.2534.

(37) Khatri, O. P.; Sano, H.; Murase, K.; Sugimura, H. Regulation of Pattern Dimension as a Function of Vacuum Pressure: Alkyl Monolayer Lithography. *Langmuir* **2008**, *24* (20), 12077–12084. https://doi.org/10.1021/la8021613.

(38) Saito, N.; Youda, S.; Hayashi, K.; Sugimura, H.; Takai, O. Alkyl Self-Assembled Monolayer Prepared on Hydrogen-Terminated Si(111) through Reduced Pressure Chemical Vapor Deposition : Chemical Resistivities in HF and NH 4 F Solutions . *Chem. Lett.* **2002**, *31* (12), 1194–1195. https://doi.org/10.1246/cl.2002.1194.

(39) Saito, N.; Youda, S.; Hayashi, K.; Sugimura, H.; Takai, O. Chemical Resistivity of Self-Assembled Monolayer Covalently Attached to Silicon Substrate to Hydrofluoric Acid and Ammonium Fluoride. *Surf. Sci.* **2003**, *532–535*, 970–975. https://doi.org/10.1016/S0039-6028(03)00158-4.

(40) Saito, N.; Hayashi, K.; Sugimura, H.; Takai, O.; Nakagiri, N. Surface Potential Images of Self-Assembled Monolayers Patterned by Organosilanes: Ab Initio Molecular Orbital Calculations. *Surf. Interface Anal.* **2002**, *34* (1), 601–605. https://doi.org/10.1002/sia.1369.

(41) Hayashi, K.; Saito, N.; Sugimura, H.; Takai, O.; Nakagiri, N. Surface Potential Contrasts between Silicon Surfaces Covered and Uncovered with an Organosilane Self-Assembled Monolayer. *Ultramicroscopy* **2002**, *91* (1–4), 151–156. https://doi.org/10.1016/S0304-3991(02)00094-3.

(42) Sano, H.; Ohno, K.; Ichii, T.; Murase, K.; Sugimura, H. Alkanethiol Self-Assembled Monolayers Formed on Silicon Substrates. *Jpn. J. Appl. Phys.* **2010**. https://doi.org/10.1143/JJAP.49.01AE09.

(43) Melitz, W.; Shen, J.; Kummel, A. C.; Lee, S. Kelvin Probe Force Microscopy and Its Application. *Surf. Sci. Rep.* **2011**, *66*, 1–27. https://doi.org/10.1016/j.surfrep.2010.10.001.

(44) Taylor, D. M.; Bayes, G. F. Calculating the Surface Potential of Unionized Monolayers. *Phys. Rev. E* **1994**, *49* (2), 1439–1449.

(45) Taylor, D. M.; Bayes, G. F. The Surface Potential of Langmuir Monolayers. *Mater. Sci. Eng. C* **1999**, *8–9*, 65–71. https://doi.org/10.1016/S0928-4931(99)00064-8.

(46) Zehner, R. W.; Parsons, B. F.; Hsung, R. P.; Sita, L. R. Tuning the Work Function of Gold with Self-Assembled Monolayers Derived from X−[C 6 H 4 −C⁝C−] n C 6 H 4 −SH (n = 0, 1, 2; X = H, F, CH 3 , CF 3 , and OCH 3) . *Langmuir* **2002**, *15* (4), 1121–1127. https://doi.org/10.1021/la981114f.

(47) Sun, Y.; Wu, D.; Liu, K.; Zheng, F. Colossal Permittivity and Low Dielectric Loss of Thermal Oxidation Single-Crystalline Si Wafers. *Materials (Basel).* **2019**, *12* (7), 1102. https://doi.org/10.3390/ma12071102.

(48) Zheng, X. H.; Chen, X. M.; Wang, T. Aging Effects on Dielectric Properties of Barium Neodymium Titanium Tantalate Ceramics. *J. Mater. Sci. Mater. Electron.* **2006**, *17* (7), 543–547. https://doi.org/10.1007/s10854-006-8241-1.

(49) Liang, H.; Zeng, Y.; Zuo, K.; Xia, X.; Yao, D.; Yin, J. The Effect of Oxidation on the Mechanical Properties and Dielectric Properties of Porous Si3N4 Ceramics. *Ceram. Int.* **2017**, *43* (7), 5517–5523. https://doi.org/10.1016/j.ceramint.2017.01.074.

(50) Linford, M. R.; Chidsey, C. E. D.; Fenter, P.; Eisenberger, P. M. Alkyl Monolayers on Silicon Prepared from 1-Alkenes and Hydrogen-Terminated Silicon. *J. Am. Chem. Soc.* **1995**, *117* (11), 3145–3155. https://doi.org/10.1021/ja00116a019.

Chapter 4: Effects of Chain Length on the Surface Potentials of 1-Alkene Self-Assembled Monolayers on n-Si (111)

4.1 Introduction

In organic electronics, the interface between surfaces is an important parameter to consider since it is often responsible for the behavior and function of the material or device[1–5]. Understanding the mechanics at device interfaces is crucial in the study of charge injection and transport behavior of charge carriers, a parameter that often determines the performance of electronic devices. In the recent years, the topic of energy level alignment at surface interfaces and how it can be controlled by the material's work function has attracted a lot of interest.[4–8]

One method of modifying the properties of solid surfaces to optimize them for specific applications is through the use of self-assembled monolayers (SAMs). SAMs have the advantage of having a reproducible spontaneous assembly and studies have shown that they are capable of forming very thin homogenous films on a substrate[9,10]. Understanding how certain molecules which form SAMs can be used to modify surface potentials is significant because it plays a fundamental role in the optimization of surfaces and can allow a more efficient charge injection at the interface. Studies have identified several factors that affect the surface potential changes caused by a SAM to a material surface, such as the packing density of the monolayer[11,12], strength and orientation of the molecular dipole[13–15], and degree of order of the monolayer[16].

In the past years, much research has been done on the study of surface modifications of metal using organic molecules[3–5,17–23], however the study of molecular interfaces with semiconductors have recently been gaining interest[8,24–26]. Nowadays, silicon is one of the most widely used semiconductor in the field of electronics, therefore understanding how it can be modified using SAMs can significantly improve the current technology[27].

Previous studies have investigated the effects of the molecular length of SAM molecules on the resulting surface potential of metals[19,28], but similar research on semiconductors are not as well-studied. A Kelvin Probe study by Evans and Ulman found that increasing the length of alkyl thiol SAMs on gold increased surface potential by about 9.3 mV per methylene unit[19]. A related study by Lu et al. found a similar trend of increasing surface potential for increasing chain length for alkylthiols on gold[28]. Tailoring the work function or surface potential of substrates is a promising topic in material science, and understanding if a similar relationship exists between chain length and SAMs on silicon will be beneficial to the advancement of molecular electronics.

In this chapter, we compare the surface potential changes brought about by 1-alkene SAMs on n-type Si (111). The precursor molecules chosen for this study have chain lengths of 10 carbon atoms and above because past studies have established that longer chains result to more organized SAMs[29–32]. Longer chain lengths increase the Van der Waals interaction between precursor molecules and lead to more well-ordered structures. (Author name) conducted computation simulations and found that shorter chains ($n <= 7$) resulted to larger fluctuations in tilt and orientation angles which translated to less-ordered SAMs[29]. Aside from limiting our choice of precursor molecules to those with 10 carbon atoms and above, we also chose to work with even-chained molecules to avoid any odd-even effect that have been known occur due to the geometry of the molecules and the way they are grafted on to the substrate[29,33].

To map the local potential changes on our sample, we used Kelvin Probe Force Microscopy (KPFM). This method can simultaneously map the topography of the surface while detecting changes in the surface potential of the material by measuring changes in contact potential difference between the surface and the cantilever tip[34–36]. The SAMs we used in this study were made from 1-alkene precursors with hydrocarbon chain lengths of n = 10, 12, 14, 16, 18 and 20. Using KPFM we observed the changes in surface potential due to the chain

length variations. To account for variations in surface potential that may arise due to different cantilever tips used during analysis, micropatterned SAMs were used during KPFM analysis while hexadecyl SAM (n = 16) served as reference for all the other SAMs. 1-alkene SAMs have shown to have good potential to be used as a photoresist in micropatterning due to ease of removal via VUV photolithography[37–39], and their stability against HF etching due to the strong Si-C bond[40,41].

Past KPFM studies have been conducted using a similar method where the surface potential differences were measured and analyzed in relation to the terminal function groups of SAMs grafted to silicon[13,15,25,26,42,43]. In **Chapter 3** we focused on the surface potential changes when the terminal functional groups were the same but the interfacial bonds were varied. In this work we aim to observe the surface potential changes due to the different lengths of 1-alkene SAMs covalently-bonded to silicon. Since silicon is widely used in present-day technology, this information will be useful in understanding and developing devices with increased charge injection efficiency.

4.2. Methodology

4.2.1 Materials

Polished (111)-oriented silicon wafers used in this study were from Electronics and Materials Corp. The wafers were phosphorus-doped (n-type) and have a resistivity of 1-10 Ω cm. The SAM precursors were 1-decene (>95%), 1-dodecene (>95%), 1-tetradecene (>90%), 1-hexadecene (>99%), 1-octadecene (>90%), and 1-eicosene (>97%), and were all purchased from Tokyo Chemical Industry. Ethanol (99.5%), and mesitylene (98%) used for washing and solvent were purchased from Nacalai Tesque. Hydrofluoric acid (HF) and ammonium fluoride (NH_4F) from Morita Chemical was used for chemical etching. All the chemicals were used without further purification.

4.2.2 Sample preparation

Silicon wafers cut into 1 × 1 cm^2 pieces and were ultrasonically cleaned for 20 minutes using ethanol followed by 20 minutes in ultrapure water. The wafers underwent photochemical cleaning in ambient conditions using vacuum ultraviolet (VUV) light with a Xe-excimer source (UER 20-172V, Ushio) for 20 minutes. To remove the native silicon oxide on the wafer, the wafers were etched in 5% HF solution for 5 minutes in the dark, followed immediately by etching in a 40% NH_4F solution (heated to 80°C to remove any dissolved oxygen) for 1 minute. This process terminates the surface with hydrogen and forms hydrogen-terminated silicon (H-Si). The H-Si substrate was then placed in in a custom-made quartz vessel which consisted of a rectangular cell of 5 mm thickness attached to one end of a cylindrical tube with a volume of about 100 cm^3.

The reference SAM to be used in this study is formed from a 1-alkene molecule with a chain length equal to 16 and will be referred to as C16 SAM on this chapter (Figure 4.1a). To form this reference SAM, 20 mL of neat 1-hexadecene was used as the precursor solution. This was placed in the vessel together with the H-Si substrate and was irradiated with UV light (REX-250, Asahi spectra) for 1 hour to initiate the SAM formation. To remove any dissolved oxygen in the precursor solution, it was purged with N_2 gas for at least 30 minutes prior to immersion of the H-Si substrate. Additional degassing was also done for 30 minutes after placing the silicon wafer in the solution, before starting the irradiation process. The setup was continuously purged with N_2 gas during the irradiation process. After irradiation, the substrate was ultrasonically cleaned in ethanol and ultrapure water for 10 minutes each to remove any physisorbed molecules on the surface. This reference C16 SAM will be the basis for all the other KPFM measurements of the other SAMs in this study.

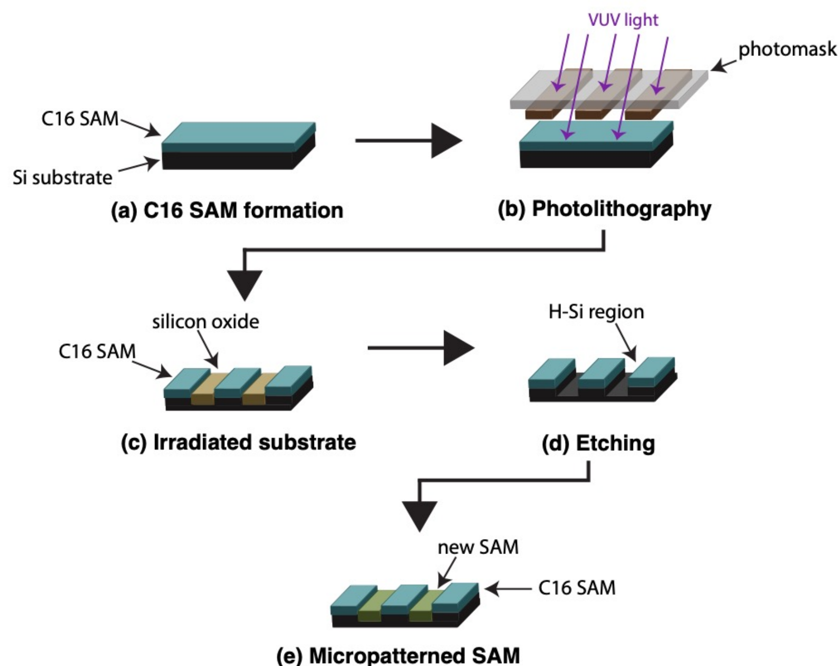

Figure 4.1. Formation of micropatterned SAMs using VUV photolithography

Micropatterned SAMs were prepared via VUV photolithography with a Xe-excimer lamp (UER20-172V, Ushio) having a wavelength of 172 nm and intensity of 10 mW cm^{-2} (Figure 4.1b). The sample was placed at a distance of 5 mm from the lamp window. The pressure was regulated to 1000 Pa inside the chamber, as optimized in Chapter 2. To form the micropatterns on the SAM, a photomask consisting of 100 nm thick chromium pattern attached to a 2 mm thick quartz plate, whose transparency at λ=172 nm is 93%, was placed on top of the C16 SAM during VUV irradiation. To remove the silicon oxide that formed during irradiation, the substrate was once again etched in 5% HF and 40% NH_4F solution. This step converts the irradiated regions into H-Si where a new SAM can once again be grafted using the same method described earlier (Figure 4.1d). Precursor molecules of varying lengths were used to form C10, C12, C14, C16, C18 and C20 SAM. Neat precursors were used in the formation of all SAMs except for the C20 SAM. The precursor for the C20 SAM (1-eicosene) is solid at room temperature and thus it was first heated to 40 ℃ a 0.5 M solution with

mesitylene as the solvent was used as the precursor solution of the C20 SAM.

4.2.3 Characterization

A commercial KPFM based on amplitude modulation (MFP-3D Oxford Instruments) was used to measure the surface potential difference and topography contrast of between the reference C16 SAM and the new SAM. The system uses a two-pass procedure where a topography is measured first via tapping mode and the surface potential measurement is done in lift mode. The scan areas used in this study was 90 μm × 90 μm. KPFM measurements were performed in ambient environment using Rh-coated silicon cantilever tips (SI-DF-3R, Hitachi Hitech) with a resonance frequency of about 27 kHz. The modulation frequency oscillated at around the same frequency as the cantilever, with an amplitude of 1.0 V. KPFM probe scan rates between 0.5 to 0.8 Hz was used during measurements.

Each of the SAMs used in this study was also individually characterized via static contact angle meter (DM 500, Kyowa Interface Science CA-X Co.), X-ray photoelectron spectroscopy (ESCA-3400 Kratos Analytical), ellipsometry (FE-5000, Otsuka Electronics) and atomic force microscopy to ensure that it is uniformly formed and densely-packed.

4.3. Results and Discussion

KPFM was used to compare the surface potentials of 6 different 1-alkene SAMs on Si (111). All measurements were done in reference to the C16 SAM to offset the differences in surface potential brought about by the different cantilever tips used in this study. Figure 4.2 shows the surface potential (Figure 4.2a - 4.2f) and topographic (Figure 4.2g – 4.2l) images of the micropatterned SAMs. Regions with higher surface potentials are shown as brighter areas in the images while lower surface potentials appear darker. Table 4.1 summarizes the measurements obtained from our KPFM analysis. SAMs with a lower surface potential than

the reference C16 SAM appear as negative while those with a higher surface potential are listed as positive. For the C16-C16 sample (Figure 4.2d), a small surface potential contrast of -15.3 ± 1.8 mV was observed, with the new C16 SAM having a lower surface potential compared to the reference. This difference is due to the slight damage on the reference C16 region that is a result of the etching during the photolithography process. Figure 4.3 shows a closer look at the surfaces of the SAMs in this study. All SAMs displayed a uniform monolayer with clear terrace steps, however small etch pits can be observed for all the reference C16 regions. Comparison of the two C16 regions in the C16-C16 sample (Figures 4.3d and 4.3j) shows the slight difference in quality between the two. The reference C16 SAM is slightly damaged, thus the underlying silicon substrate is exposed to the environment and is possibly more prone to oxidation. In **Chapter 3** we demonstrated that oxidation of H-Si leads to a large increase in its surface potential[44]. For the C16-C16 sample, although most of the silicon surface under the reference C16 SAM is still protected from oxidation, we believe that damaged regions have allowed certain regions to oxidize more quickly which would result to a slight increase in surface potential. Multiple C16-C16 samples were prepared and analyzed and we have confirmed that this slight increase in surface potential is reproducible and thus reliable.

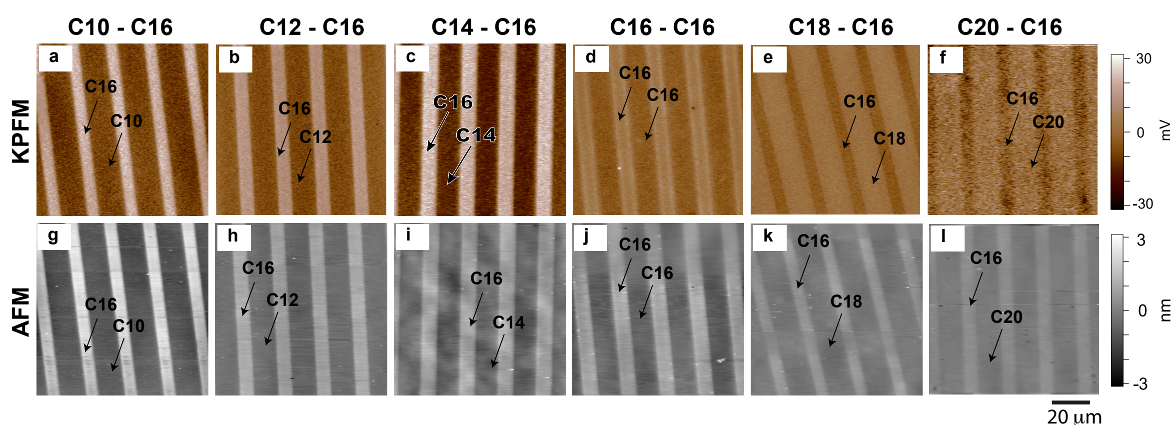

Figure 4.2. Simultaneously obtained (a-f) surface potential and (g-l) AFM height images of the micropatterned samples, corresponding to (a,g) C10-C16, (b,h) C12-C16, (c,i) C14-C16, (d,j) C16-C16, (e,k) C18-C16, and (f,l) C20-C16.

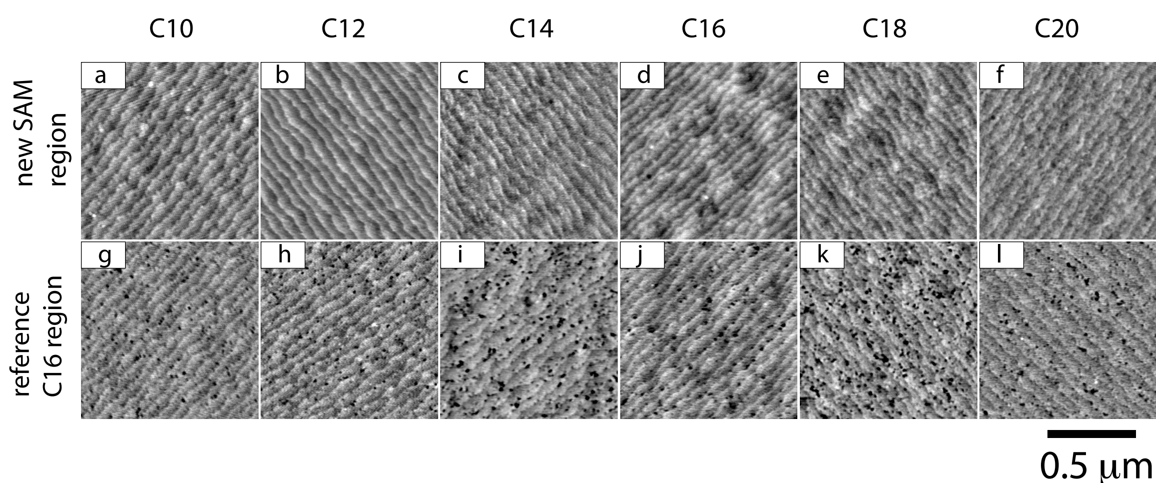

Figure 4.3. AFM topography focusing on new SAMs (a-f) and reference C16 (g-l) regions of the micropatterned surfaces, corresponding to (a,g) C10-C16, (b,h) C12-C16, (c,i) C14-C16, (d,j) C16-C16, (e,k) C18-C16, and (f,l) C20-C16. All the new SAM regions show clear terrace and steps. The corresponding C16 reference regions (g-l) exhibit damage in the form of etch pits.

Table 4.1. Summary of surface potential and topography contrast using KPFM scans for micropatterned samples.

Samples	Surface Potential Contrast (mV)	Topography Contrast (nm)
C10-C16	-28.93 ± 5.14	-2.08 ± 0.16
C12-C16	-26.83 ± 2.99	-1.89 ± 0.10
C14-C16	-52.82 ± 3.13	-1.56 ± 0.20
C16-C16	-15.27 ± 1.79	-1.38 ± 0.09
C18-C16	+18.22 ± 1.23	-0.92 ± 0.07
C20-C16	+15.28 ± 1.83	-0.74 ± 0.09

The topographic contrasts of the micropatterns SAMs are shown in Figure 4.2g – 4.2l. Table 4.1 summarizes the topographic contrast between the new SAMs and the reference C16 SAM. Negative values indicate that the region being measured has a lower topography than the reference C16 SAM. In the AFM images, higher topography regions appear brighter while lower topography are darker. For all samples, the reference C16 SAM displayed a higher topography than the new SAM region, even for SAMs prepared with molecules having a longer chain length (C18 and C20). This is explained by the diagram in Figure 4.1. In the VUV photolithography process, the reference C16 SAM not covered by the photomask is removed and replaced by a silicon oxide layer which extends below the original surface of the silicon substrate. When this silicon oxide layer is removed via etching in HF and NH_4F, grooves or indentations are left in the original silicon substrate[39,45]. Thus, when the new SAM is formed, the precursor molecules are grafted at a lower level than the reference C16 SAM. Comparison of the C16-C16 sample shows that the photolithography and etching process lowers the surface of the silicon substrate by about 1.38 nm (Table 4.1), which is the measured topographic

difference between the new and reference C16 SAM. This value is much greater than the difference in length brought about by the addition of 2 (for C18) or 4 (for C20) methylene units, thus both these SAMs appear at a lower topography in the AFM scans (Figure 4.2k and 4.2l).

Figure 4.4 shows a linear correlation between the difference in topography and the chain length of the precursor molecules used to form the new SAM. Our measurements show that as the molecular chain length of the precursor increases there is an estimated increase of 0.14 nm per methylene unit. We compared this with thickness measurements on individual SAMs using ellipsometry (Figure 4.5). Results from our ellipsometry tests show a thickness increase of about 0.11 nm per methylene unit. It should be noted that thickness estimated by ellipsometry often have some uncertainty due to the undefined refractive index of SAMs, resulting in the difference of slope between the AFM and ellipsometry. However, these values provide several points of comparison between each SAM sample. The results we obtain from AFM and ellipsometry measurements are close to the values reported by Evans and Ulman[19] (an increase of 0.1 nm per methylene unit) and Porter et al.[31] (increase of 0.15 nm per methylene unit) on their studies on alkylthiol SAMs on gold.

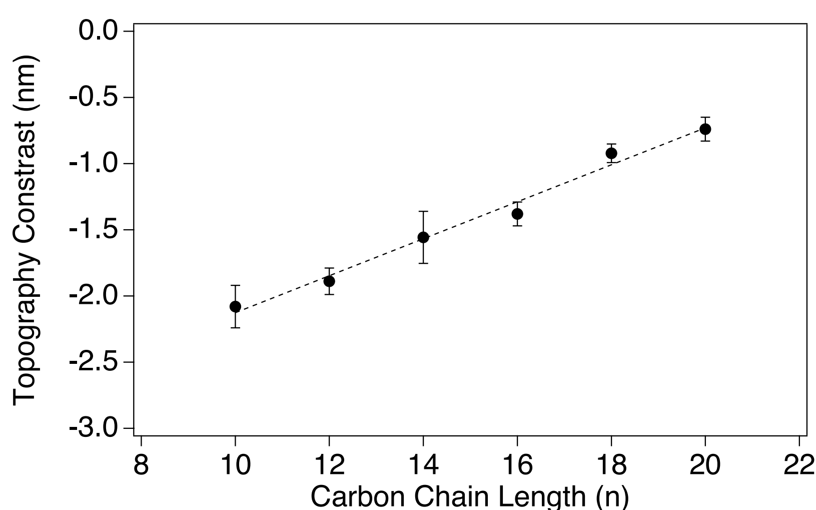

Figure 4.4. Topographic contrast between newly formed SAM and the reference C16 SAM regions

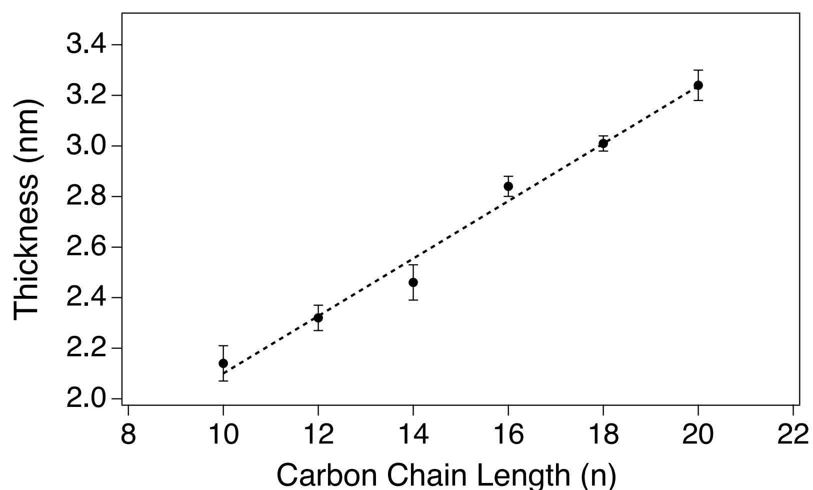

Figure 4.5. Ellipsometric thicknesses of SAMs formed from various 1-alkene precursors with different carbon chain lengths

Table 4.2. Summary of characterization results for individual SAMs and the H-Si substrate. The dipole moment of each precursor was computed using PM7 simulation in MOPAC.

Sample	Dipole moment (D)	Atomic concentration			WCA (°)
		C (%)	O (%)	Si (%)	
H-Si	-	5.6 ± 0.6	2.2 ± 1.0	92.2 ± 1.1	85.8 ± 1.8
C10	0.537	23.5 ± 1.3	5.5 ± 0.6	71.0 ± 1.7	104.5 ± 1.5
C12	0.539	26.3 ± 2.2	8.9 ± 1.0	64.7 ± 2.4	103.7 ± 0.5
C14	0.542	31.9 ± 3.2	3.2 ± 0.9	64.9 ± 3.2	106.0 ± 1.2
C16	0.543	33.1 ± 2.0	5.8 ± 1.1	61.1 ± 2.7	106.0 ± 0.8
C18	0.543	35.1 ± 3.3	6.8 ± 0.9	58.1 ± 3.0	105.8 ± 1.6
C20	0.543	36.2 1.9	3.8 ± 0.9	60.0 ± 2.6	106.1 ± 1.0

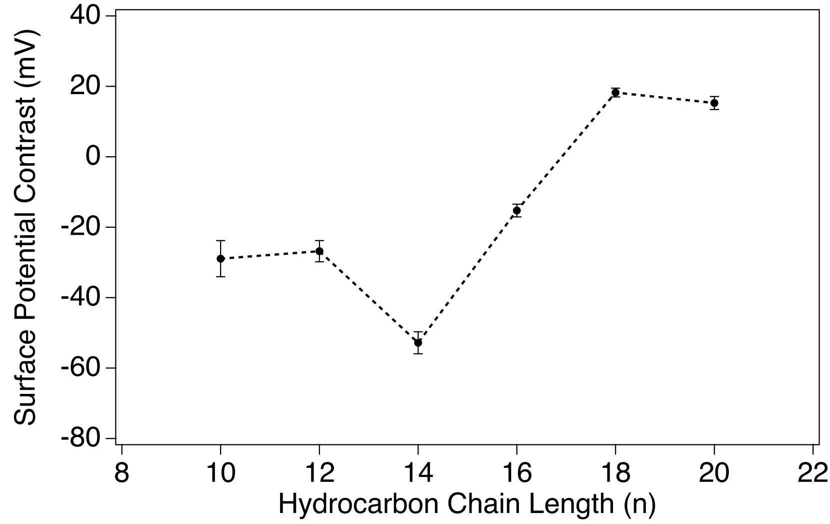

Figure 4.6. Surface potential contrasts between each new SAM and reference C16 region

Ellipsometry and AFM topographic results both demonstrate that there is a linear dependence of the SAM thickness to the length of the precursor molecule, as shown in Figures 4.4 and 4.5, however no clear correlation between surface potential and chain length was observed via KPFM (Figure 4.6). The SAM's surface potential can be computed for using Equation 4.1. In this model, terms ϕ_{Si} and ϕ_{tip} correspond to the work functions of the silicon substrate and the tip, while e is equal to the electric charge[25,26,43]. The net dipole perpendicular to the substrate surface is denoted by μ while A corresponds to the area occupied by the molecule, ϵ_0 is the permittivity of free space and ϵ_{SAM} is the relative permittivity or dielectric constant of the SAM. This second term is often used in the computation of surface potential and is derived from the Helmholtz equation[10,17,18]. Since the two SAMs to be compared in our study are grafted to the same substrate and measured simultaneously using the same KPFM tip, the first terms will cancel out and Equation 4.1 can be simplified to Equation 4.2, where V_{SAM1} and V_{SAM2} correspond to the surface potentials of the new SAM and reference C16 SAM respectively.

$$V_{SAM} = -\frac{\phi_{Si} - \phi_{tip}}{e} + \frac{\mu}{A\epsilon_0\epsilon_{SAM}}$$ Equation 4.1

$$V_{SAM1} - V_{SAM2} = \frac{\mu_{SAM1}}{A_{SAM1}\epsilon_0\epsilon_{SAM1}} - \frac{\mu_{SAM2}}{A_{SAM2}\epsilon_0\epsilon_{SAM2}}$$ Equation 4.2

When comparing the changes in surface potential due to the different lengths of the precursor molecules, we can assume that these changes in surface potential are a result of changes brought about by the SAM being measured (V_{SAM1}), since the surface potential of the reference C16 SAM (V_{SAM2}) is constant for all the samples in our study. These changes in surface potential between the SAMs of different lengths may be attributed to differences in dipole moment, area occupied by the molecule and dielectric constants of the SAMs, as modeled by Equation 4.2.

The dipole moment of the precursor molecules of our SAMs were computed for using Molecular Orbital Package (MOPAC) with the PM7 set and are summarized in Table 4.2. Our computation show that there is a slight increase in molecular dipole with increasing hydrocarbon chain length up to n = 16. Beyond this, the molecular dipole remains the same. A study by Cornil et al.[46] observed similar results in their computation study, where they demonstrated that increasing the length of alkylthiol molecules increased the molecular dipole minimally and eventually comes to a fixed constant. Their study showed that these molecules are composed of two local dipoles located around the chain ends, rather than the traditional idea of the molecule having a positive pole on one end and a negative pole on another. Their computations suggested that the net dipole moment of the molecule would simply be a sum of these two dipoles located at the ends of the molecule, which explains why the dipoles are not significantly affected by the length of the spacer chain. A different study by Szwajca et al. used parameterized model 5 (PM5) computations to calculate the dipole moments of alkylthiol

molecules having a chain lengths ranging from n = 6 to n = 18[47]. Their results showed that the dipole moments varied very little as chain lengths increased, which agreed with the previous study. Similary, Sushko and Shluger performed density functional theory (DFT) calculations on the gas phase dipole moments of alkylthiols with various chain length and found that there is very little change in the dipole moment of the molecule beyond 8 carbon atoms[48]. Their paper also utilized the concept that the molecules are composed of two-dipole system with a head group dipole and a tail group dipole. In their study, the tail group dipole is due to the binding of the carbon atom to 3 hydrogen atoms and one carbon atom, rather than 2 hydrogen atoms and 2 carbon atoms found in the backbone region. On the other hand, the head group was due to the carbon-sulfur bond of the thiol group.

Using the values obtained in our computations, an initial increase in dipole moment was found for C10 to C16. Equation 4.2 would suggest that surface potential should increase as the chain length is elongated due to this, however our experimental results did not agree, suggesting that other factors also need to be considered in interpreting the surface potential of our SAM systems. However it should also be noted that the dipole moments in our study were obtained using semi-empirical computations for a single molecule, as opposed to the dipole moment of the SAM itself. Previous studies have found that the net dipole moment of the SAM is often different from that of the precursor molecule due to interactions between individual dipoles, resulting in a possible depolarization of the SAM[46,49].

Other factors that may affect the surface potential of the SAM aside from dipole moment is the molecular packing and the dielectric behavior. Past studies on the surface potential of alkylthiol SAMs on Au have found a linear dependence on the precursor molecule chain length, which was attributed to the changing dielectric behavior of the SAM[19,23]. However, a more recent study on the effects of alkylthiol chain length on these SAMs on an InAs substrate found no correlation between work function and chain length[47]. The researchers'

computations suggested that the molecular packing of the SAMs varied as the lengths of the precursors changed. Generally, SAMs formed using shorter alkyl chains are more disordered and have a looser packing than those formed using longer alkyl chains[29,31]. Previous studies have found some correlation between the SAM molecular packing to its dielectric behavior. Romaner et al.[11] found that denser molecular packing of SAMs resulted to a greater effective dielectric constant. They explain their findings using the idea of depolarization, which has also been observed by several researchers[11,12,46,50,51]. In SAMs, each molecule generates its own electric field due to its intrinsic dipole. The electric field produced by the molecules induces a second dipole moment in the opposite direction, which would result in the reduction of the dipole effects of the neighboring molecules. Increasing the packing of the molecules in the SAM would result in a more prominent depolarization effect, which would affect the dielectric constant of the SAM. The idea that the dielectric constant of the monolayer is affected by the molecular packing has been further confirmed by other researchers[46,50,52]. According to Equation 4.2, a greater dielectric constant would reduce the surface potential of the SAM. In our study, assuming that the SAMs using precursors of shorter molecular lengths would have a less-dense packing, it would also result to a lower dielectric constant, thereby having a higher surface potential. This might explain why our C10 and C12 SAMs have higher surface potential than that of C14, despite its lower dipole moment.

Although it is not directly part of Equation 4.2, the SAM quality is another important factor to consider when conducting studies on surface potential since these measurements are very sensitive. To determine the quality of our SAMs, each one was tested individually.

XPS analysis was done to check if the molecules were successfully grafted on the silicon substrate (Figure 4.7). The binding energies and peak intensities were referenced and normalized to the Si 2p peak of bulk silicon at 99.5 eV. The atomic percent concentrations of oxygen, carbon and silicon were obtained and are listed in Table 4.2. Looking at the XPS data

for the H-Si sample, a large increase in the carbon concentration was observed after the substrate underwent UV irradiation while immersed in the SAM precursor solution. This is true for all (C10 to C20) SAMs. This suggests that the hydrocarbon chains were successfully grafted onto the H-Si substrate. Furthermore, the C 1s peak intensity increased as the length of the precursor molecule was increased, due to the presence of more carbon atoms in the thicker SAMs. For all SAM samples, the Si 2p scan showed a single peak centered at 99.5 eV and no peak was present at 103 eV, which indicates that there is no detectable interfacial oxide between the substrate and the SAM. However, looking at the atomic concentration of oxygen in the SAMs, large variations can be observed which suggests that some SAMs contained more oxygen on the surface compared to others. Several samples were tested for each type of SAM and the amount of oxygen present in each SAM was consistent, indicating that these variations were not simply due to exposure to ambient environment or random contaminants on the surface but is a property of the SAM itself. The samples with the lowest oxygen concentration are the C14 and C20 samples, having an atomic concentration of 3.2% and 3.8% respectively. This is much lower than the oxygen concentration of the other SAMs which ranged between 5.5% to 8.9%. Relating this low oxygen concentration of C14 and C20 to the surface potential measurements in Figure 4.7, we can observe that the surface potential value increases from C10 to C12 but drops suddenly for C14. Similarly, for C16 an C18 the surface potential increases as the chain length is increased, but drops suddenly for C20. Although there is no linear correlation between the atomic concentration of oxygen and the surface potential, it is possible that drastic changes in oxygen content of the SAM can result to great variations on our KPFM measurements. Not much study has been dedicated to the relationship between oxidation and surface potentials of SAMs, however in Chapter 3 we showed that silicon oxide significantly increases the surface potential of H-Si by almost 200 mV, suggesting that if silicon oxide is present on the sample, the surface potential might increase. In the formation of SAMs,

only about 50-55% of the silicon surface would actually be grafted to a molecule[45,53], leaving the rest of the surface exposed and prone to oxidation. In most cases, the dense monolayer would still be able to passivate the silicon surface and protect the ungrafted silicon atoms from oxidation[54,55]. This is particularly true for dense alkyl SAMs which are extremely hydrophobic. In Table 4.2 the static water contact angles (WCA) of our SAMs and the H-Si substrate are listed. H-Si itself is hydrophobic and has a WCA of about 86 degrees. After SAM formation, WCA increased to 104 to 106 degrees due to the hydrophobic nature of methyl groups[56]. This high value of the WCA suggests that the molecules were successfully grafted onto the H-Si substrate with methyl side facing up. Surface potential measurements using the KPFM method are affected by the screening of adsorbed water on the material[57,58] thus it is better to check if this might be the cause of the KPFM variations in our study. However, the WCA of our SAM samples did not exhibit much difference, especially for chain lengths greater than 14. Thus, we can assume that variations in the surface potential is most likely not a result of adsorbed water.

Although no interfacial oxide layer was detected at 103 eV in the XPS scan, it is possible that trace amounts of oxidation were formed on the silicon surface of the different SAMs during sample preparation, leading to the detection by our KPFM measurements.

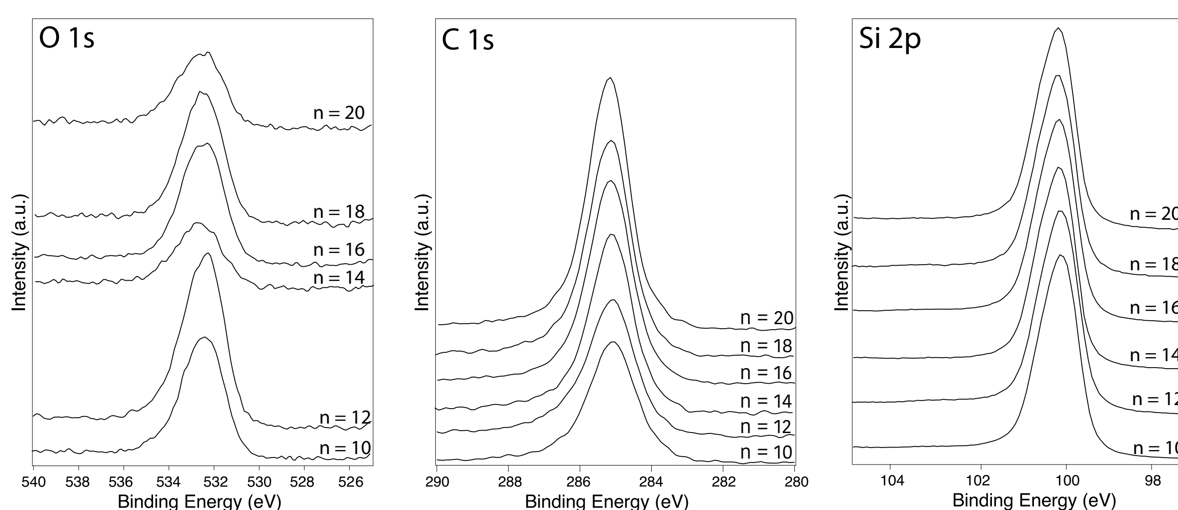

Figure 4.7. XPS spectra of the SAMs on H-Si obtained from the 1-alkene precursors with different carbon chain lengths

At the moment the reason for the variation in the oxygen content during SAM formation is difficult to identify. Further study is advised to truly understand the source of the varying oxygen content in the SAM. A previous research, for example, studied the possible sources of oxygen in amine-terminated alkylthiol SAMs on gold using a variety of characterization methods such as X-ray photoelectron spectroscopy (XPS), time-of-flight secondary ion mass spectroscopy (ToF-SIMS), sum frequency generation (SFG) and near edge x-ray absorption fine structure (NEXAFS) spectroscopy[59]. Unfortunately, no similar study has been conducted on alkyl SAMs on silicon.

Our results on this chapter demonstrate that aside from dipole moment, the surface potential of the SAM may be affected by other factors such as SAM molecular packing, and trace oxidation present on the silicon substrate. Although computations show that the dipole moment of the precursor molecules are higher for those with a longer hydrocarbon backbone, the results in our experiment show that these other factors must also be considered, especially for SAMs formed on a silicon substrate. While previous studies on thiol SAMs grafted to metals have shown that they are able to linearly modify the substrate work function with respect to precursor chain length, our results suggest that the situation is not simple for SAMs on silicon due to its sensitivity to various factors. However, our KPFM measurement results demonstrate that changing the molecular chain length of the SAM precursor may be one way to modify or optimize the surface potential of silicon. Our results show that factors such as molecular packing and SAM quality should be considered when predicting the surface potential of the material.

4.4. Conclusions

KPFM was used to measure the surface potential contrasts between SAMs of varying chain lengths on n-type Si (111) substrate. Micropatterned SAMs were formed using VUV

photolithography using C16 SAM as a photoresist. The C16 SAM was also used as a reference during KPFM measurements to remove possible variations that may occur due to differences in the KPFM probe tip and underlying substrate. Other tests measured the SAMs other properties such as ellipsometric thickness, atomic compositions, water contact angles and morphologies to determine the qualities of the individual SAMs. The measurements obtained using KPFM, combined with the data obtained from the other tests, provided us with insight of how various factors affect the surface potential of the material. Our findings suggest that the differences in the surface potential between the SAMs (C10 to C20) were a result of differences in the dipole moment of the precursor molecules, changes in SAM dielectric properties due to differences in molecular packing, and varying oxygen content at the surface.

We recommend that more in depth studies on the oxygen content in alkyl SAMs on silicon be conducted as this may provide a meaningful insight on how this parameter can affect the surface potential of the system. Furthermore, additional studies on other SAM systems (such as different molecules on Si (111), or using different substrates such as silicon with a different doping type and/or density, or perhaps even other semiconductors), may give us a clearer understanding of how various factors can be optimized to tailor the surface potential of SAM covered substrates, which is crucial in the improvement of charge carrier injection for molecular electronics.

References

(1) Miozzo, L.; Yassar, A.; Horowitz, G. Surface Engineering for High Performance Organic Electronic Devices: The Chemical Approach. *J. Mater. Chem.* **2010**, *20*, 2513–2538. https://doi.org/10.1039/b922385a.

(2) Gao, Y. Surface Analytical Studies of Interfaces in Organic Semiconductor Devices.

Mater. Sci. Eng. R Reports **2010**, *68* (3), 39–87. https://doi.org/10.1016/j.mser.2010.01.001.

(3) Kanai, K.; Honda, M.; Ishii, H.; Ouchi, Y.; Seki, K. Interface Electronic Structure between Organic Semiconductor Film and Electrode Metal Probed by Photoelectron Yield Spectroscopy. *Org. Electron. physics, Mater. Appl.* **2012**, *13* (2), 309–319. https://doi.org/10.1016/j.orgel.2011.11.024.

(4) Hill, I. G.; Rajagopal, A.; Kahn, A.; Hu, Y. Molecular Level Alignment at Organic Semiconductor-Metal Interfaces. *Appl. Phys. Lett.* **1998**, *73* (5), 662–664. https://doi.org/10.1063/1.121940.

(5) Demirkan, K.; Mathew, A.; Weiland, C.; Yao, Y.; Rawlett, A. M.; Tour, J. M.; Opila, R. L. Energy Level Alignment at Organic Semiconductor/Metal Interfaces: Effect of Polar Self-Assembled Monolayers at the Interface. *J. Chem. Phys.* **2008**, *128*, 074705. https://doi.org/10.1063/1.2832306.

(6) Ishii, H.; Sugiyama, K.; Ito, E.; Seki, K. Energy Level Alignment and Interfacial Electronic Structures at Organic/Metal and Organic/Organic Interfaces. *Adv. Mater.* **1999**, *11* (8), 605–625.

(7) Leung, C.; Kao, L.; Su, S.; Feng, J.; Chan, T. Relationship between Surface Dipole, Work Function and Charge Transfer: Some Exceptions to an Established Rule. *Phys. Rev. B - Condens. Matter Mater. Phys.* **2003**, *68* (19), 1–6. https://doi.org/10.1103/PhysRevB.68.195408.

(8) He, T.; Ding, H.; Peor, N.; Lu, M.; Corley, D. A.; Chen, B.; Ofir, Y.; Gao, Y.; Yitzchaik, S.; Tour, J. M. Silicon/Molecule Interfacial Electronic Modifications. *J. Am. Chem. Soc.* **2008**, *130* (5), 1699–1710. https://doi.org/10.1021/ja0768789.

(9) Ulman, A. Formation and Structure of Self-Assembled Monolayers. *Chem. Rev.* **1996**, *96*, 1533–1554.

(10) Aswal, D. K.; Lenfant, S.; Guerin, D.; Yakhmi, J. V.; Vuillaume, D. Self Assembled Monolayers on Silicon for Molecular Electronics. *Anal. Chim. Acta* **2006**, *568*, 84–108. https://doi.org/10.1016/j.aca.2005.10.027.

(11) Romaner, L.; Heimel, G.; Ambrosch-Draxl, C.; Zojer, E. The Dielectric Constant of Self-Assembled Monolayers. *Adv. Funct. Mater.* **2008**, *18* (24), 3999–4006. https://doi.org/10.1002/adfm.200800876.

(12) Romaner, L.; Heimel, G.; Zojer, E. Electronic Structure of Thiol-Bonded Self-Assembled Monolayers: Impact of Coverage. *Phys. Rev. B - Condens. Matter Mater. Phys.* **2008**, *77* (4), 1–9. https://doi.org/10.1103/PhysRevB.77.045113.

(13) Saito, N.; Hayashi, K.; Sugimura, H.; Takai, O.; Nakagiri, N. Surface Potentials of Patterned Organosilane Self-Assembled Monolayers Acquired by Kelvin Probe Force Microscopy and Ab Initio Molecular Calculation. *Chem. Phys. Lett.* **2001**, *349*, 172–177. https://doi.org/10.1016/S0009-2614(01)01097-1.

(14) Campbell, I. H.; Kress, J. D.; Martin, R. L.; Smith, D. L.; Barashkov, N. N.; Ferraris, J. P. Controlling Charge Injection in Organic Electronic Devices Using Self-Assembled Monolayers. *Appl. Phys. Lett.* **1997**, *71* (24), 3528–3530. https://doi.org/10.1063/1.120381.

(15) Saito, N.; Hayashi, K.; Sugimura, H.; Takai, O.; Nakagiri, N. Surface Potential Images of Self-Assembled Monolayers Patterned by Organosilanes: Ab Initio Molecular Orbital Calculations. *Surf. Interface Anal.* **2002**, *34* (1), 601–605. https://doi.org/10.1002/sia.1369.

(16) Milde, P.; Zerweck, U.; Eng, L. M.; Abel, M.; Giovanelli, L.; Nony, L.; Mossoyan, M.; Porte, L.; Loppacher, C. Interface Dipole Formation of Different ZnPcCl8 Phases on Ag(111) Observed by Kelvin Probe Force Microscopy. *Nanotechnology* **2008**, *19*, 1–6. https://doi.org/10.1088/0957-4484/19/30/305501.

(17) Miura, Y.; Kimura, S.; Kobayashi, S.; Iwamoto, M.; Imanishi, Y.; Umemura, J. Negative Surface Potential Produced by Self-Assembled Monolayers of Helix Peptides Oriented Vertically to a Surface. *Chem. Phys. Lett.* **1999**, *315* (1–2), 1–6. https://doi.org/10.1016/S0009-2614(99)01191-4.

(18) Howell, S.; Kuila, D.; Kasibhatla, B.; Kubiak, C. P.; Janes, D.; Reifenberger, R. Molecular Electrostatics of Conjugated Self-Assembled Monolayers on Au(111) Using Electrostatic Force Microscopy. *Langmuir* **2002**, *18* (13), 5120–5125. https://doi.org/10.1021/la0157014.

(19) Evans, S. D.; Ulman, A. Surface Potential Studies of Alkyl-Thiol Monolayers Adsorbed on Gold. *Chem. Phys. Lett.* **1990**, *170*, 462–466. https://doi.org/10.1016/S0009-2614(90)87085-6.

(20) Zehner, R. W.; Parsons, B. F.; Hsung, R. P.; Sita, L. R. Tuning the Work Function of Gold with Self-Assembled Monolayers Derived from X−[C 6 H 4 −C⁝C−] n C 6 H 4 −SH (n = 0, 1, 2; X = H, F, CH 3 , CF 3 , and OCH 3) . *Langmuir* **2002**, *15* (4), 1121–1127. https://doi.org/10.1021/la981114f.

(21) Lee, C. S.; Tang, J. X.; Zhou, Y. C.; Lee, S. T. Interface Dipole at Metal-Organic Interfaces: Contribution of Metal Induced Interface States. *Appl. Phys. Lett.* **2009**, *94* (11), 11–13. https://doi.org/10.1063/1.3099836.

(22) Rousseau, R.; De Renzi, V.; Mazzarello, R.; Marchetto, D.; Biagi, R.; Scandolo, S.; Del Pennino, U. Interfacial Electrostatics of Self-Assembled Monolayers of Alkane Thiolates on Au(111): Work Function Modification and Molecular Level Alignments. *J. Phys. Chem. B* **2006**, *110* (22), 10862–10872. https://doi.org/10.1021/jp061720g.

(23) Lu, J.; Delamarche, E.; Eng, L.; Bennewitz, R.; Meyer, E.; Gu, H. Kelvin Probe Force Microscopy on Surfaces : Investigation of the Surface Potential of Self-Assembled Monolayers On. *Langmuir* **1999**, *15*, 8184–8188. https://doi.org/10.1021/la9904861.

(24) Kuo, C. H.; Liu, C. P.; Lee, S. H.; Chang, H. Y.; Lin, W. C.; You, Y. W.; Liao, H. Y.; Shyue, J. J. Effect of Surface Chemical Composition on the Work Function of Silicon Substrates Modified by Binary Self-Assembled Monolayers. *Phys. Chem. Chem. Phys.* **2011**, *13* (33), 15122–15126. https://doi.org/10.1039/c1cp20590k.

(25) Sugimura, H.; Hayashi, K.; Saito, N. Kelvin Probe Force Microscopy Images of Microstructured Organosilane Self-Assembled Monolayers. *Jpn. J. Appl. Phys.* **2001**, *40*, 4373.

(26) Hayashi, K.; Saito, N.; Sugimura, H.; Takai, O.; Nakagiri, N. Regulation of the Surface Potential of Silicon Substrates in Micrometer Scale with Organosilane Self-Assembled Monolayers. *Langmuir* **2002**, *18* (20), 7469–7472. https://doi.org/10.1021/la011707h.

(27) Vilan, A.; Cahen, D. Chemical Modification of Semiconductor Surfaces for Molecular Electronics. *Chem. Rev.* **2017**, *117* (5), 4624–4666. https://doi.org/10.1021/acs.chemrev.6b00746.

(28) Lü, J.; Eng, L.; Bennewitz, R.; Meyer, E.; Güntherodt, H. J.; Delamarche, E.; Scandella, L. Surface Potential Studies of Self-Assembling Monolayers Using Kelvin Probe Force Microscopy. *Surf. Interface Anal.* **1999**. https://doi.org/10.1002/(SICI)1096-9918(199905/06)27:5/6<368::AID-SIA530>3.0.CO;2-W.

(29) Ramin, L.; Jabbarzadeh, A. Odd À Even Effects on the Structure , Stability , and Phase Transition of Alkanethiol Self-Assembled Monolayers. *Langmuir* **2011**, No. 27, 9748–9759. https://doi.org/10.1021/la201467b.

(30) Gooding, J. J.; Mearns, F.; Yang, W.; Liu, J. Self-Assembled Monolayers into the 21st Century: Recent Advances and Applications. *Electroanalysis* **2003**, *15* (2), 81–96. https://doi.org/10.1002/elan.200390017.

(31) Porter, M. D.; Bright, T. B.; Allara, D. L.; Chidsey, C. E. Spontaneously Organized Molecular Assemblies. 4. Structural Characterization of n-Alkyl Thiol Monolayers on

Gold by Optical Ellipsometry, Infrared Spectroscopy, and Electrochemistry. *J. Am. Chem. Soc.* **1987**, *109* (12), 3559–3568. https://doi.org/10.1021/ja00246a011.

(32) Soliman, A. I. A.; Utsunomiya, T.; Ichii, T.; Sugimura, H. 1,2-Epoxyalkane: Another Precursor for Fabricating Alkoxy Self-Assembled Monolayers on Hydrogen-Terminated Si(111). *Langmuir* **2018**, *34* (44), 13162–13170. https://doi.org/10.1021/acs.langmuir.8b02717.

(33) Tao, F.; Bernasek, S. L. Understanding Odd − Even Effects in Organic Self-Assembled Monolayers. *Chem. Rev.* **2007**, *107*, 1408–1453. https://doi.org/10.1021/cr050258d.

(34) Melitz, W.; Shen, J.; Kummel, A. C.; Lee, S. Kelvin Probe Force Microscopy and Its Application. *Surf. Sci. Rep.* **2011**, *66*, 1–27. https://doi.org/10.1016/j.surfrep.2010.10.001.

(35) Nonnenmacher, M.; O'Boyle, M. P.; Wickramasinghe, H. K. Kelvin Probe Force Microscopy. *Appl. Phys. Lett.* **1991**, *58* (25), 2921–2923. https://doi.org/10.1063/1.105227.

(36) Palermo, V.; Palma, M.; Samori, P. Electronic Characterization of Organic Thin Films by Kelvin Probe Force Microscopy. *Advanced Materials*. January 19, 2006, pp 145–164. https://doi.org/10.1002/adma.200501394.

(37) Saito, N.; Kadoya, Y.; Hayashi, K.; Sugimura, H.; Takai, O. Micropatterned 1-Alkene Self-Assembled Monolayer on Hydrogen-Terminated Silicon by Vacuum Ultraviolet Lithography. *Japanese J. Appl. Physics, Part 1 Regul. Pap. Short Notes Rev. Pap.* **2003**, *42* (4 B), 2534–2537. https://doi.org/10.1143/JJAP.42.2534.

(38) Khatri, O. P.; Sano, H.; Murase, K.; Sugimura, H. Regulation of Pattern Dimension as a Function of Vacuum Pressure: Alkyl Monolayer Lithography. *Langmuir* **2008**, *24* (20), 12077–12084. https://doi.org/10.1021/la8021613.

(39) Sugimura, H.; Sano, H.; Lee, K.-H.; Murase, K. Organic Monolayers Covalently

Bonded to Si as Ultra Thin Photoresist Films in Vacuum UV Lithography. *Jpn. J. Appl. Phys.* **2006**, *45* (6B), 5456–5460. https://doi.org/10.1143/JJAP.45.5456.

(40) Saito, N.; Youda, S.; Hayashi, K.; Sugimura, H.; Takai, O. Alkyl Self-Assembled Monolayer Prepared on Hydrogen-Terminated Si(111) through Reduced Pressure Chemical Vapor Deposition : Chemical Resistivities in HF and NH 4 F Solutions . *Chem. Lett.* **2002**, *31* (12), 1194–1195. https://doi.org/10.1246/cl.2002.1194.

(41) Saito, N.; Youda, S.; Hayashi, K.; Sugimura, H.; Takai, O. Chemical Resistivity of Self-Assembled Monolayer Covalently Attached to Silicon Substrate to Hydrofluoric Acid and Ammonium Fluoride. *Surf. Sci.* **2003**, *532–535*, 970–975. https://doi.org/10.1016/S0039-6028(03)00158-4.

(42) Hayashi, K.; Saito, N.; Sugimura, H.; Takai, O.; Nakagiri, N. Surface Potential Contrasts between Silicon Surfaces Covered and Uncovered with an Organosilane Self-Assembled Monolayer. *Ultramicroscopy* **2002**, *91* (1–4), 151–156. https://doi.org/10.1016/S0304-3991(02)00094-3.

(43) Sugimura, H.; Hayashi, K.; Saito, N.; Nakagiri, N.; Takai, O. Surface Potential Microscopy for Organized Molecular Systems. *Appl. Surf. Sci.* **2002**, *188* (3–4), 403–410. https://doi.org/10.1016/S0169-4332(01)00958-8.

(44) Garcia, M. C. T.; Utsunomiya, T.; Ichii, T.; Sugimura, H. Surface Potential Contrasts between 1-Alkene, 1-Thiol and 1-Alcohol Self-Assembled Monolayers on Silicon (111) Substrate. *Jpn. J. Appl. Phys.* **2020**, *59* (SD), SDDC06. https://doi.org/10.7567/1347-4065/ab5925.

(45) Sugimura, H. Self-Assembled Monolayer on Silicon. In *Nanocrystalline Materials*; 2006. https://doi.org/10.1016/B978-008044697-4/50016-8.

(46) Cornil, D.; Olivier, Y.; Geskin, V.; Cornil, J. Depolarization Effects in Self-Assembled Monolayers: A Quantum-Chemical Insight. *Adv. Funct. Mater.* **2007**, *17* (7), 1143–1148.

https://doi.org/10.1002/adfm.200601116.

(47) Szwajca, A.; Wei, J.; Schukfeh, M. I.; Tornow, M. Self-Assembled Monolayers of Alkyl-Thiols on InAs: A Kelvin Probe Force Microscopy Study. *Surf. Sci.* **2015**, *633*, 53–59. https://doi.org/10.1016/j.susc.2014.11.023.

(48) Sushko, M. L.; Shluger, A. L. Dipole-Dipole Interactions and the Structure of Self-Assembled Monolayers. *J. Phys. Chem. B* **2007**, *111*, 4019–4025. https://doi.org/10.1021/jp0688557.

(49) Sushko, B. M. L.; Shluger, A. L. Intramolecular Dipole Coupling and Depolarization in Self-Assembled Monolayers **. *Adv. Funct. Mater.* **2008**, *18*, 2228–2236. https://doi.org/10.1002/adfm.200701305.

(50) Cahen, D.; Naaman, R.; Vager, Z. The Cooperative Molecular Field Effect. *Adv. Funct. Mater.* **2005**, *15* (10), 1571–1578. https://doi.org/10.1002/adfm.200500187.

(51) Whitesides, G. M.; Kriebel, J. K.; Love, J. C. Molecular Engineering of Surfaces Using Self-Assembled Monolayers. *Sci. Prog.* **2005**, *88* (Pt 1), 17–48. https://doi.org/10.3184/003685005783238462.

(52) Peor, N.; Sfez, R.; Yitzchaik, S. Variable Density Effect of Self-Assembled Polarizable Monolayers on the Electronic Properties of Silicon. *J. Am. Chem. Soc.* **2008**, *130* (12), 4158–4165. https://doi.org/10.1021/ja077933g.

(53) Scheres, L.; Giesbers, M.; Zuilhof, H. Organic Monolayers onto Oxide-Free Silicon with Improved Surface Coverage: Alkynes versus Alkenes. *Langmuir* **2010**, *26* (7), 4790–4795. https://doi.org/10.1021/la9035503.

(54) Alderman, N.; Danos, L.; Grossel, M. C.; Markvart, T. Kelvin Probe Studies of Alkyl Monolayers on Silicon (111) for Surface Passivation. *RSC Adv.* **2013**, *3* (43), 20125–20131. https://doi.org/10.1039/c3ra42526f.

(55) Linford, M. R.; Chidsey, C. E. D.; Fenter, P.; Eisenberger, P. M. Alkyl Monolayers on

Silicon Prepared from 1-Alkenes and Hydrogen-Terminated Silicon. *J. Am. Chem. Soc.* **1995**, *117* (11), 3145–3155. https://doi.org/10.1021/ja00116a019.

(56) Sano, H.; Maeda, H.; Matsuoka, S.; Lee, K. H.; Murase, K.; Sugimura, H. Self-Assembled Monolayers Directly Attached to Silicon Substrates Formed from 1-Hexadecene by Thermal, Ultraviolet, and Visible Light Activation Methods. *Jpn. J. Appl. Phys.* **2008**, *47*, 5659–5664. https://doi.org/10.1143/JJAP.47.5659.

(57) Sugimura, H.; Ishida, Y.; Hayashi, K.; Takai, O.; Nakagiri, N. Potential Shielding by the Surface Water Layer in Kelvin Probe Force Microscopy. *Appl. Phys. Lett.* **2002**, *80* (8), 1459–1461. https://doi.org/10.1063/1.1455145.

(58) Nakagiri, N.; Sugimura, H.; Ishida, Y.; Hayashi, K.; Takai, O. Effects of an Adsorbed Water Layer and Self-Assembled Organosilane Monolayers on Scanning Probe Microscopy of Silicon Pn Structures. *Surf. Sci.* **2003**, *532–535*, 999–1003. https://doi.org/10.1016/S0039-6028(03)00456-4.

(59) Baio, J. E.; Weidner, T.; Brison, J.; Graham, D. J.; Gamble, L. J.; Castner, D. G. Amine Terminated SAMs: Investigating Why Oxygen Is Present in These Films. *J. Electron Spectros. Relat. Phenomena* **2009**, *172* (1–3), 2–8. https://doi.org/10.1016/j.elspec.2009.02.008.

Chapter 5: Investigation on the effects of Si-C and Si-O interface bonds on the surface potential and conductivity of aromatic SAMs on n-Si (111)

5.1. Introduction

SAMs have been used in several surface applications including friction control[1,2], corrosion prevention[3,4] and biosensing[5,6], and recent studies have also probed its applications in molecular electronics[7–11] where they have been found to be helpful in improving charge injection between material interfaces. Charge injection efficiency can be enhanced by SAMs through the introduction of a dipole moment to the surface[10,12,13]. This dipole layer shifts the potential at the surface and modifies the substrate work function[14,15]. The orientation and strength of this dipole moment can be easily adjusted through the use of different functional groups[16–18].

In **Chapter 3** we demonstrated how alkene SAMs are able to modify the surface potential of n-Si (111) through the use of interfacial bonds. SAM precursor molecules have an intrinsic dipole moment which can modify the surface potential of silicon when grafted. Aside from this intrinsic dipole moment, the surface potential may also be affected by the docking chemistry of the SAM[16], as we have shown in Chapter 3. While the intrinsic dipole moment of the precursor molecule can provide initial insight on the resulting surface potential, the chemical bonding of the adsorbate to the substrate often results in charge rearrangements at the interface, which can lead to differences between the dipole of the precursor molecule and the dipole of the SAM itself[16]. In this case, the contributions to the net dipole moment of the SAM depend on the strength of the interaction between the molecule and substrate[16] and the polarizability of the molecule backbone[19].

There are several ways in which a molecule can be grafted to a silicon surface to form a SAM. Several studies have focused on silanes, where the molecule is grafted through an Si-O-Si bond and an interfacial oxide is present between the silicon and molecule[1,20,21]. In molecular electronics, these types of SAMs are often used as electrical insulators or dielectrics[22,23], where the thickness can easily be controlled through the molecular length of the precursor molecule. Other researchers have demonstrated that direct attachment of the molecule to the silicon substrate is also possible through covalent bonds such as Si-C[24–27], Si-O[24,25,28], Si-S[24,29], Si-N[24,28] and Si-Te[29]. By altering the covalent bond between the SAM molecule and the silicon substrate, the energy levels at the interface is modified which can affect the surface potential of the substrate, as well as the conduction through the molecule[16,28,30–32]. By grafting the molecules directly to the silicon substrate, a good electrical connection can be established[33]. In **Chapters 3 and 4** we focused on SAMs formed from are long-chained molecules having saturated σ bonds. These saturated bonds in the molecule have been known to result in SAMs having low conductivity, and thus capable of sustaining high electric fields before breakdown[34]. In this chapter we will incorporate molecules with unsaturated bonds into our SAMs. When unsaturated bonds are present in the precursor molecules, such as in the case of aromatic molecules, other electrical properties of silicon may be achieved[31,35,36]. Similar to surface potential, the electronic properties, such as conductivity, of the surface may be affected by SAM parameters including the molecule-substrate bond[31].

In this chapter we investigate the effects of Si-C and Si-O bonding of aromatic SAMs attached directly to silicon on the surface potential and conductive properties. Previous chapters have focused on long-chained molecules with saturated bonds. This time we discuss the effects of using short-chained molecules with an aromatic headgroup bonded to silicon using different covalent bonds. We have chosen to use styrene ($C_6H_5CH{=}CH_2$), 4-phenyl-1-butene ($C_6H_5(CH_2)_2CH{=}CH_2$), benzyl alcohol ($C_6H_5CH_2$-OH), and 3-phenyl-1-propanol

($C_6H_5(CH_2)_3$-OH) as our aromatic precursors. These molecules have a phenyl headgroup attached to a short methylene chain. We believe that the conjugation in the phenyl group as well as the short methylene spacer can help with introducing conductive properties to our SAMs.

Measurement of the surface potential of SAMs were conducted using micropatterned SAMs formed via VUV photolithography, as discussed in **Chapter 2**. This is to account for any variations that may occur during our measurements. The reference SAM used is formed from a 1-alkene molecule to create an alkyl SAM. Alkyl-SAMs grafted directly to the silicon substrate with Si-C bonds display high chemical resistivity[25,37,38] and thus are good photoresist materials in photolithograpy. The precursor for the reference SAM is 1-hexadecene ($CH_3(CH_2)_{13}CH{=}CH_2$). This forms a strong Si-C bond with the silicon substrate and has demonstrated resistivity to HF etching[25], which is important during the micropatterning process.

Surface potential measurements of SAMs were conducted using Kelvin Probe Force Microscopy (KPFM) while conductive AFM (CAFM) was used to measure the current passing through the SAMs. These methods allow us to map the local surface potential distribution and local conductivities of the sample surface simultaneously with its topography.

5.2. Experimental Methods

5.2.1. Materials

Phosphorus low-doped n-type Silicon (111) wafer with resistivity range of 1-10 Ω cm from Electronics and Materials Corp were used as the SAM substrates in these experiments. The SAM precursors were styrene (>99%, stabilized with TBC), benzyl alcohol (>99%), 4-phenyl-1-butene (>98%), and 3-phenyl-1-propanol (>98%). All precursors were purchased from Tokyo Chemical Industry. Ethanol (99.5%), and mesitylene (98%) that were used during

the experiments were purchased from Nacalai Tesque. Hydrofluoric acid (HF) and ammonium fluoride (NH_4F) used during H-Si preparation were purchased from Morita Chemical. All chemicals were used as received and without further purification.

5.2.2. Sample Preparation

The procedure for preparation of the micropatterned SAMs are shown in Figure 5.1. The Si (111) wafers were cut into 1×1 cm^2 pieces and ultrasonically cleaned in ethanol and ultrapure water (UPW) for 20 minutes each. This was followed by photochemical cleaning in ambient environment using vacuum ultraviolet (VUV) light from a Xe-excimer lamp source (UER 20-172V, Ushio) to remove organic contaminants on the surface of the wafer. Hydrogen-terminated silicon (H-Si, Figure 5.a) was prepared by etching the substrate in 5% hydrofluoric acid (HF) solution for 5 minutes in the dark to remove the native silicon oxide. This was followed by immersion in a 40% ammonium fluoride (NH_4F) solution for 60 seconds to terminate the surface with hydrogen. The NH_4F solution was heated to 80°C prior to the substrate immersion to eliminate any dissolved oxygen which may result in the etch pits on the substrate. The H-Si substrate was washed thoroughly in UPW after the etching process.

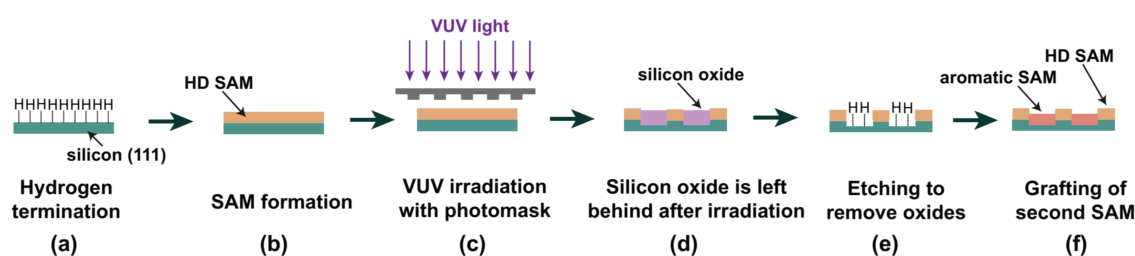

Figure 5.1. Formation of micropatterned SAMs

The reference SAM used in this study was formed using neat 1-hexadecene (HD) as a precursor and will be referred to as HD SAM in this chapter (Figure 1b). The H-Si substrate was first placed in a custom-made quartz vessel which consisted of a rectangular quartz cell of 5 mm thickness which is attached to a cylindrical tube with a volume of about 100 cm^3. The H-Si substrate and about 20 mL of the 1-hexadecene precursor were placed inside the vessel and irradiated with UV light (REX-250, Asahi spectra) for 1 hour. To prevent the oxidation of the silicon substrate during the grafting process, the system was purged with N_2 gas for at least 30 minutes prior to irradiation. The N_2 gas flow was kept on during the entire irradiation process. After irradiation, the sample was removed from the vessel and ultrasonically cleaned using ethanol and UPW for 10 minutes each to remove any physisorbed molecules on the surface. The resulting HD SAM formed on the silicon substrate was used as the photoresist and reference material for the following experiments.

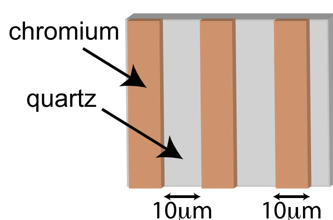

Figure. 5.2. Schematic illustration of photomask used during VUV irradiation

The schematic of the photolithography process is shown in Figure 5.1c. The HD SAM was irradiated through a photomask with VUV light using a Xe-excimer lamp (UER20-172V, Ushio) having a wavelength of 172 nm and intensity of 10 mW cm^{-2}. The photomask used consisted of 100 nm thick chromium pattern attached to a 2 mm thick quartz plate, whose transparency at λ=172 nm was 93% (Figure 5.2). Irradiation through this photomask allowed us to cover regions of the HD SAM while permitting VUV light to irradiate the uncovered regions. During VUV irradiation, the pressure inside the chamber was kept at ~10^3 Pa and the

sample was placed at a distance of 5mm away from the lamp window. The sample was irradiated for 30 minutes. These conditions used in the photolithography process was optimized in Chapter 2. The VUV light cause oxygen excitation which converts the oxygen inside the chamber to a more reactive singlet and triplet states (O(1D) and O(3P)). The excited oxygen degraded the exposed monolayer and converted the region to silicon oxide (Figure. 1d). To form a micropatterned sample which contains two SAMs on the same substrate, the sample must once again undergo etching to remove the silicon oxide and terminate the irradiated region with hydrogen (H-Si), allowing a new SAM to be grafted in its place.

The etching process after VUV photolithography is very similar to the one described above, however the etching time in HF was shortened from 5 minutes to 3 minutes, and etching time in NH_4F was shortened from 60 seconds to 45 seconds (as discussed in Chapter 2). This was done to minimize the damage experienced by the HD SAM that is still grafted onto some regions of the irradiated sample (Figure 5.1e). After the removal of the silicon oxide and formation of H-Si on the irradiated regions, a new SAM was grafted in its place using the same UV irradiation method described earlier (Figure 5.1f) using the aromatic precursors. The following were used for the formation of the aromatic SAMs : styrene (1 M solution), benzyl alcohol (neat), 4-phenyl-1-butene (1 M solution), and 3-phenyl-1-propanol (2 M solution). Mesitylene was used as a solvent for all the precursor solutions. The resulting SAMs will be referred to as Styrene SAM (styrene), BA SAM (benzyl alcohol), 4P1B SAM (4-phenyl-1-butene), and 3P1P SAM (3-phenyl-1-propanol). The diagram of the SAMs grafted to silicon is shown in Figure 5.3. Two of the aromatic SAMs (styrene SAM and 4P1B SAM) are grafted to silicon via a Si-C bond while the other two (BA SAM and 3P1P SAM) are grafted via a Si-O bond.

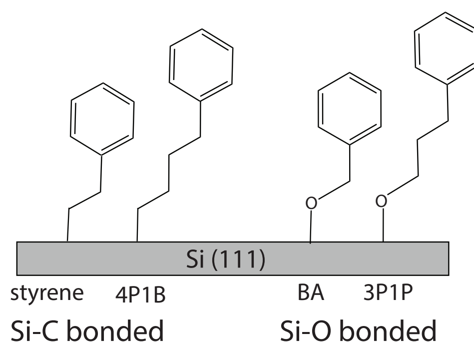

Figure 5.3. Diagram of the molecules grafted on Si substrate via Si-C and Si-O bonds

5.2.3. Characterization

All the SAMs were investigated individually to determine its quality using X-ray photoelectron spectroscopy (XPS, ESCA-3400 Kratos Analytical), static contact angle meter (DM 500, Kyowa Interface Science CA-X Co.), atomic force microscopy (AFM, MFP-3D, Oxford Instruments), and ellipsometry (FE-5000, Otsuka Electronics).

For the micropatterned SAMs, Kelvin Probe Force Microscopy (KPFM) based on amplitude modulation (AM) AFM was used to map the topography and surface potential contrasts of the micropatterned SAMs using a two-pass procedure. This process scans the topographic line first using AM mode and is followed by surface potential measurements using lift mode. All measurements were conducted in an ambient environment using a Rh-coated silicon cantilever tip (SI-DF-3R, Hitachi Hitech). The cantilever resonance frequency was approximately 27 kHz. The modulation frequency oscillated at around the same frequency as the cantilever, with an amplitude of 1.0 V. The scanning probe rate used ranged from 0.5 to 0.8 Hz.

Conductive atomic force microscopy (CAFM) based on contact-mode AFM was performed to measure the electrical conductivity of the SAMs. Measurements were done in contact mode using a Rh-coated silicon cantilever tip (SI-DF-3R, Hitachi Hitech) with a spring constant of 1.6 Nm^{-1}. A transimpedance amplifier with an 82 MΩ feedback resistor was used

to convert the current signal to the voltage. The tip load was kept at 4.35 nN. A -1.0 V bias was applied to the tip relative to the grounded silicon substrate.

5.3. Results and Discussion

5.3.1. Formation of aromatic SAMs

The surface potential and conductivity measurements of SAMs may be affected by its quality, thus it is important to first determine the SAM formed well before conducting any KPFM or CAFM measurements. In this section we measure the water contact angle (WCA), and film thicknesses of the single component SAMs. We also analyze its composition and surface topography via XPS and AFM. The properties of the aromatic SAMs along with the H-Si substrate and HD SAM to be used as photoresist during micropatterning are listed in Table 5.1

The WCA of the H-Si substrate and HD SAM were measured to be about 85.5 degrees and 106.0 degrees respectively. This is in good agreement with past literature where the H-Si substrate displayed good hydrophobicity upon preparation. The much higher WCA of HD SAM is due to the presence of a dense methyl-terminated surface, indicating that the SAM was well formed. For the aromatic SAMs, the WCA were much lower than that of HD SAM's, ranging from about 82 to 86 degrees. These are in agreement with a previous study on phenyl terminated SAM formed on oxide-free silicon which resulted in values between 80 to 81 degrees[39]. Measurements that the Si-C bonded SAMs (styrene and 4P1B) exhibited higher WCA than the Si-O bonded SAMs (BA and 3P1P). Si-C bonded SAMs showed a WCA of about 85 degrees as opposed to the Si-O bonded SAMs which had about 82 to 83 degrees. The lower WCA of the aromatic SAMs compared to the HD SAM is expected due to the phenyl headgroup being much less hydrophobic than the methyl headgroup[40]. However, since the

WCA of the aromatic SAMs were very close to that of H-Si, it is difficult to conclude if the molecule was grafted based on this test alone, thus XPS analysis was conducted.

Figure 5.4 shows the C 1s, O 1s and Si 2p peaks obtained from XPS analysis and the atomic percent concentrations are listed in Table 5.1 All binding energies and intensities of the scans were referenced and normalized to the Si 2p peak of bulk silicon at 99.5 eV. The increase of the C 1s atomic percent concentration from 5.4% (H-Si) to about 20-24% (for Si-C bonded SAMs) and 17-19% (for Si-O bonded SAMs) suggest that the precursor molecules were successfully grafted to the substrate and that the SAMs were formed with good order with 1 hour of UV irradiation. Compared to HD SAM, the C 1s atomic percent concentrations of the aromatic SAMs were much lower. This is most likely due to the fact that the precursor molecules for the aromatic SAMs consist of less carbon atoms, and not significantly affected by the molecule packing of the SAMs. A study by Harada found that despite the difference in molecular structure, long alkyl SAMs and aromatic SAMs experience similar limitations when it comes to surface coverage[31]. SAMs formed from long hydrocarbons are known to be able to pack densely to due the strong intermolecular force is present between chains. For the aromatic SAMs, it is thought that the primary intermolecular force between molecules is the $\pi-\pi$ stacking of the phenyl rings which allow them to have good order and molecular packing as well.

The Si 2p spectra shows a single peak centered at 99.5 eV for all the aromatic SAMs. No visible peak was present at 103 eV which suggests that the underlying Si substrates were well passivated with the precursor molecules (Figure 5.4). The O 1s concentration for the Si-O bonded SAMs was higher than the Si-C bonded SAMs, which is expected due to the -OH group present in the head group of the SAM precursor. The small amount of O 1s concentration detected suggests that although the Si 2p scan did not show a peak at 103 eV, trace amounts of silicon oxide might be present on the surface. Previous researchers conducted a spectroscopic

study on aromatic SAMs on Si(111) and found that the trace oxidation detected by XPS originated from oxidation of the silicon surface during the SAM growth and not from contamination or oxidation of the sample as it was loaded to the UHV XPS chamber[31]. The complete inhibition of the passivation and oxidation of the silicon substrate is not achievable for aromatic SAMs due to its 50% molecular packing[28,31,35]. However, this amount of coverage for aromatic SAMs is considered already densely packed due to steric hindrances.

Table 5.1. Water contact angle (WCA), ellipsometric thickness and XPS atomic % concentration of formed SAMs

Sample	WCA (°)	Ellipsometric thickness (nm)	XPS Atomic % Concentration		
			C 1s (%)	O 1s (%)	Si 2p (%)
H-Si	85.5 ± 1.8	1.49 ± 0.1	5.4 ± 0.8	3.2 ± 0.3	91.4 ± 1.1
HD SAM	106.0 ± 1.8	2.53 ± 0.24	33.5 ± 2.4	6.3 ± 1.2	60.2 ± 3.0
Si-C bonded SAM					
Styrene SAM	85.4 ± 0.8	2.05 ± 0.02	20.8 ± 1.3	3.6 ± 1.3	75.5 ± 0.3
4P1B SAM	84.7 ± 0.7	2.10 ± 0.18	23.9 ± 1.0	5.0 ± 1.2	71.1 ± 2.1
Si-O bonded SAM					
BA SAM	82.0 ± 0.6	1.92 ± 0.11	17.5 ± 2.1	5.0 ± 2.1	77.5 ± 2.7
3P1P SAM	82.5 ± 2.1	1.99 ± 0.04	18.3 ± 0.4	7.5 ± 0.5	74.2 ± 0.9

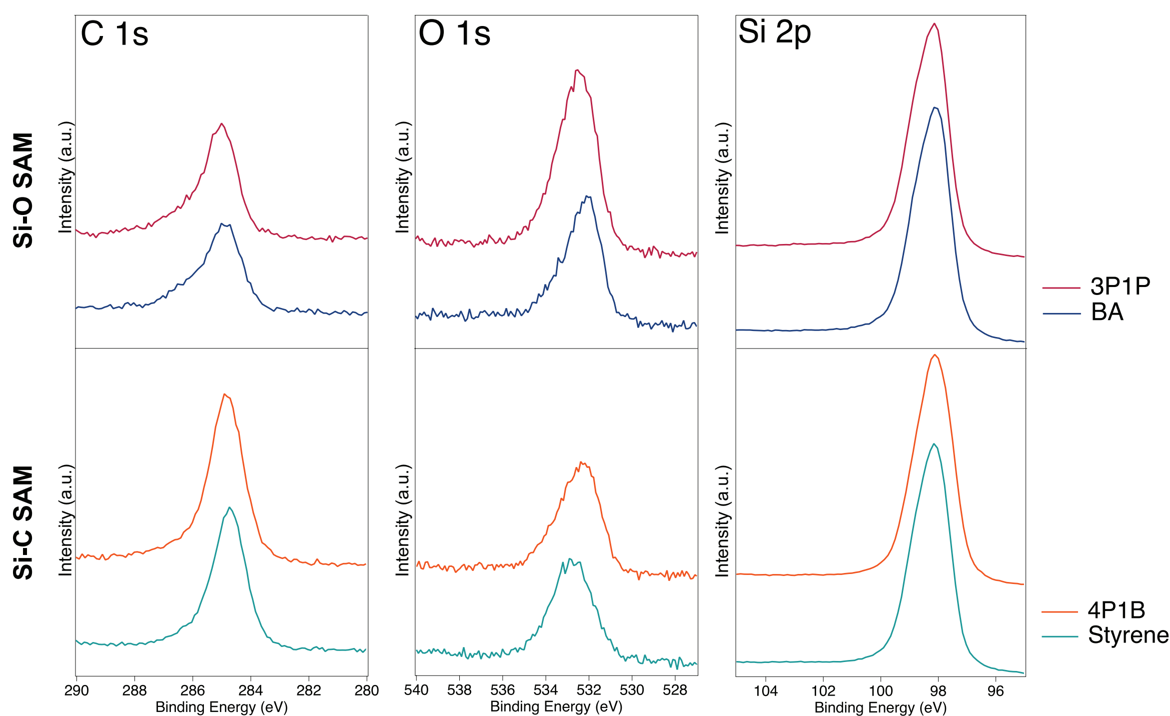

Figure 5.4. XPS spectra of the Si-O and Si-C bonded SAMs

The thickness of the SAMs was measured using ellipsometry. Although obtaining an accurate measurement of the SAM thickness using this method is difficult due to the unknown refractive index of the SAM, it provides a good basis for comparison between our aromatic SAM samples. Measurements showed that the thickness of HD SAM is 2.53 nm. Aromatic SAMs were found to have lower thicknesses between 2.05 to 2.10 nm for the Si-C bonded SAMs, and 1.92 to 1.99 nm for the Si-O bonded SAMs. In comparison to the long hydrocarbon chain of the HD molecule, the precursor molecules for the aromatic SAMs consisted of a benzene ring and a short methyl chain (about 1-2 units long), which resulted to a lower film thickness. However, the thickness of the aromatic SAMs were significantly greater than that of H-Si which suggests that the SAMs were successfully grafted to the substrate

Measurements during ellipsometry also showed that Si-C bonded SAMs were slightly thicker than the Si-O bonded SAMs. Our MOPAC computations estimated the molecular length of styrene at about 6.821 Å, and benzyl alcohol at 6.629 Å. Additionally, the reported

bond length of Si-C (1.90 Å) is also slightly longer than that of Si-O (1.64 Å)[41]. These agree with the results of our ellipsometry measurements. Another possibility is that the molecules in the Si-O SAMs were oriented with a greater tilt angle than the Si-C SAMs. The difference in their molecular length is very small and the ellipsometry measurements gave a more noticeable difference. This result, combined with the lower WCA of the Si-O SAMs might suggest that the molecules for Si-O SAMs were slightly more tilted than the Si-C SAM, possibly due to lower molecular density. Previous studies on Si-C bonded alkyl-phenyl molecules suggested that the more tilted molecules resulted to a lower WCA[28,35] This is due to the increased exposure of the hydrophobic C-H bonds when the molecules are more vertically oriented, as opposed to when they are more tilted.

The surface features of the aromatic SAMs were studied under AM-AFM and are shown in Figure 5.5. The images show that clear terraces and atomic steps were present for all the aromatic SAM samples. This suggests that they were uniformly formed on the H-Si substrate.

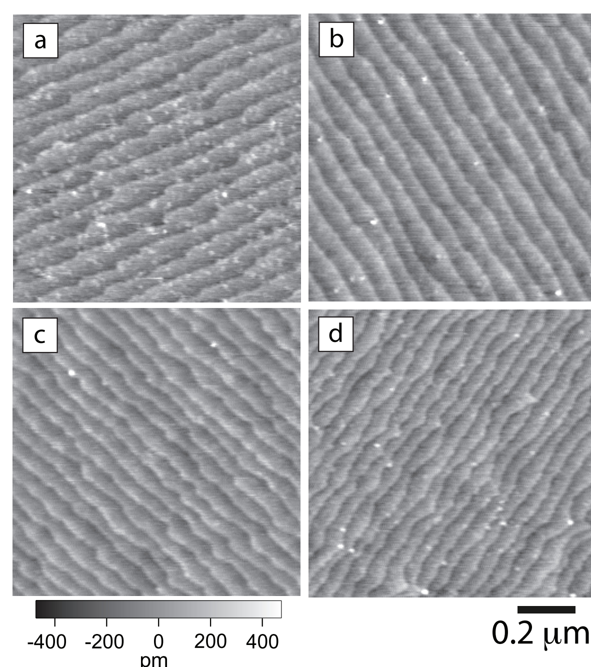

Figure 5.5. AFM images of the terrace step structure of (a) styrene SAM, (b) 4P1B SAM, (c) BA SAM and (d) 3P1P SAM

The results of our individual investigations of the single component aromatic SAMs suggests that these molecules formed highly-ordered monolayers on n-Si(111) despite the short alkyl chain length and the bulky phenyl group. Although the Van der Waals interaction between the chains were not as high as those of molecules with longer chains, dense monolayers were able to form possibly due to the π–π stacking of the aromatic rings[35]. XPS results show that there was minimal oxidation present on the silicon substrate after aromatic SAM formation. This information is important because in Chapter 4 we have already demonstrated how even slight oxidation of the underlying silicon substrate can heavily affect the KPFM measurements. Oxidation is also known to affect conduction through the monolayer[31,42], thus we needed to make sure our SAMs were of acceptable quality before proceeding with using them to form the micropatterned SAMs to be used for KPFM and CAFM analysis. The findings in our investigation show that these SAMs are suitable for the surface potential and conductivity measurements.

5.3.2. KPFM Measurements for Surface Potential

The previous section showed that the aromatic SAMs were able to form well on H-Si, and thus are suitable to be used for preparation of micropatterned SAMs to be used in KPFM measurements. Surface potentials of the aromatic SAMs were measured against the HD SAM reference. Figure 5.6 presents the AFM and KPFM images of the samples, and the results are summarized in Table 5.2. In the AFM scans, the brighter regions correspond to the reference HD SAM which has higher topography, while the darker regions correspond to the aromatic SAMs. This is in agreement with the findings in our previous section (Table 5.1) where we established that the aromatic SAMs have a lower thickness than the HD SAM. Additionally, the aromatic SAMs which were grafted after the VUV photolithography and etching were attached to regions of the substrate which had been lowered due to etching (Figure 5.1f). In

Chapter 4 we showed that the VUV photolithography process and the etching lowers the topography of the irradiated silicon substrate by about 1.38 nm. Thus, the reference HD SAM has a higher topography than any of the aromatic SAMs we used here.

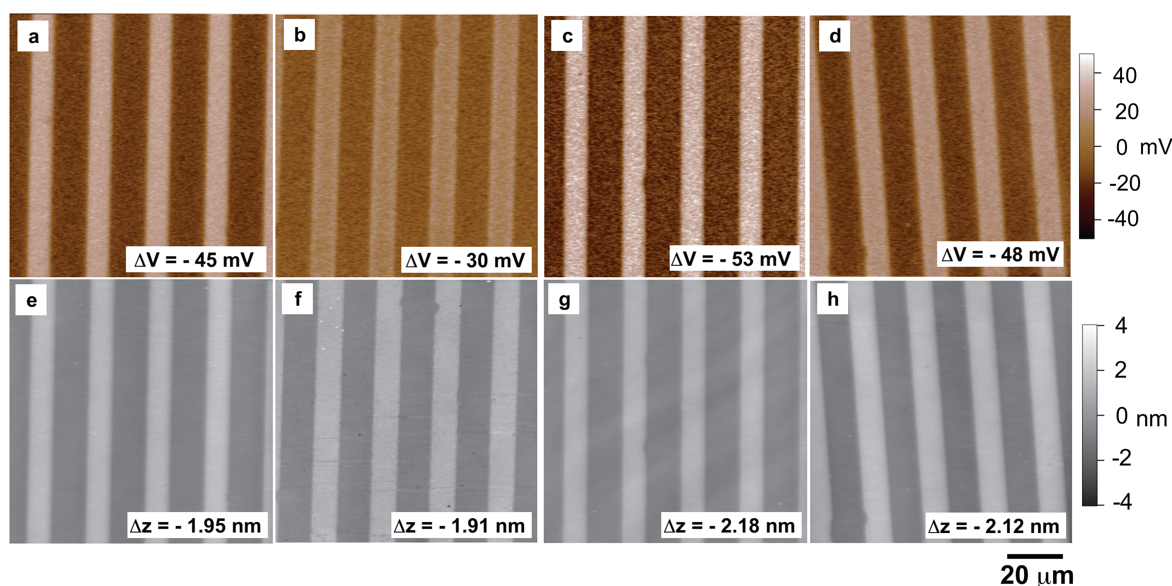

Figure 5.6. Simultaneously obtained (a-d) surface potential and (e-h) AFM height images of the micropatterned samples, corresponding to (a,e) styrene SAM, (b,f) 4P1B SAM, (c,g) BA SAM, and (d,h) 3P1P SAM. We used HD SAM as reference at all samples

In Chapter 4 we also demonstrated how the surface potential of a newly-deposited HD SAM was lower than that of the reference HD SAM by 15.3 mV despite being formed from the same HD molecule. We explained that this was possibly due to the damage that occurs on the reference HD region during the etching process. We can confirm that the reference HD region undergoes damage in the form of etch pits in Figure 5.7, which shows the topographic images obtained on the newly-deposited aromatic SAM region and the reference HD SAM region. We found that this increase in the surface potential due to this damage of the HD SAM was reproducible during our experiments thus the region can still act as a reliable reference for KPFM measurements as long as this difference is considered.

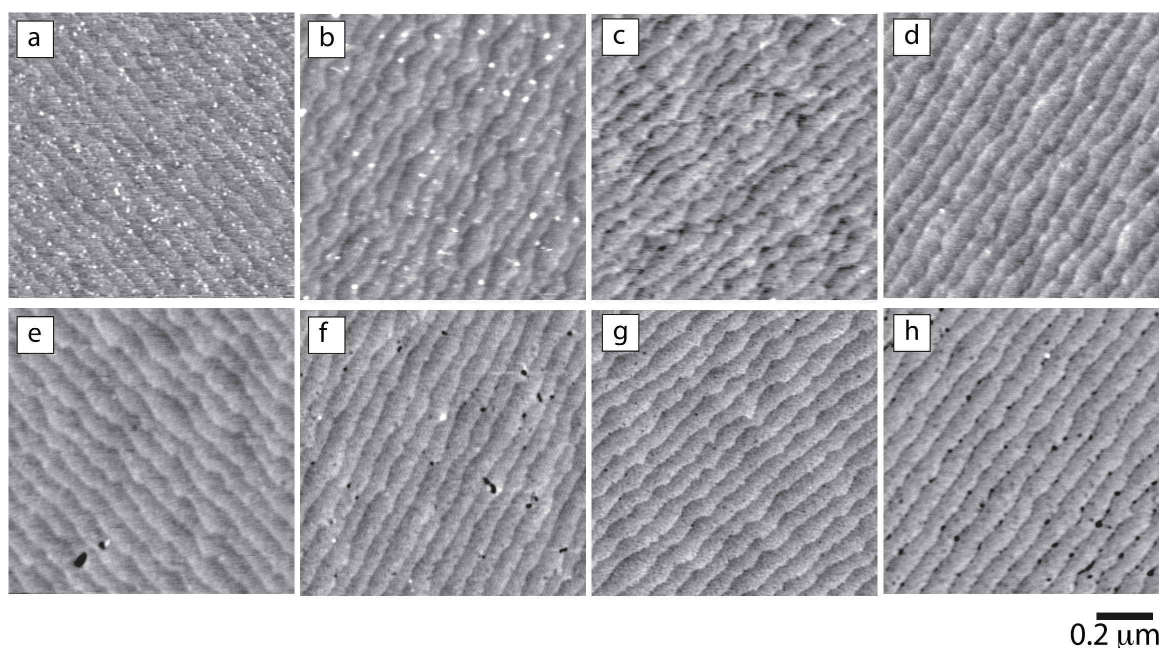

Figure 5.7. AFM images of aromatic SAMs (a-d) and reference HD SAM (e-h) regions of the micropatterned surfaces, corresponding to (a,e) HD-styrene, (b,f) HD-4P1B, (c,g) HD-BA, and (d,h) HD-3P1P. The corresponding HD SAM reference regions (e-h) exhibit damage in the form of etch pits.

Table 5.2. Surface potential and topography contrast of micropatterned SAMs

	Surface potential contrast (mV)	Topography contrast (nm)
HD-HD	-15.3 ± 1.8	-1.38 ± 0.09
Si-C bonded		
HD-Styrene	-45.2 ± 7.1	-1.95 ± 0.10
HD-4P1B	-30.3 ± 1.0	-1.91 ± 0.07
Si-O bonded		
HD-BA	-52.5 ± 6.6	-2.18 ± 0.30
HD-3P1P	-47.5 ± 3.3	-2.12 ± 0.25

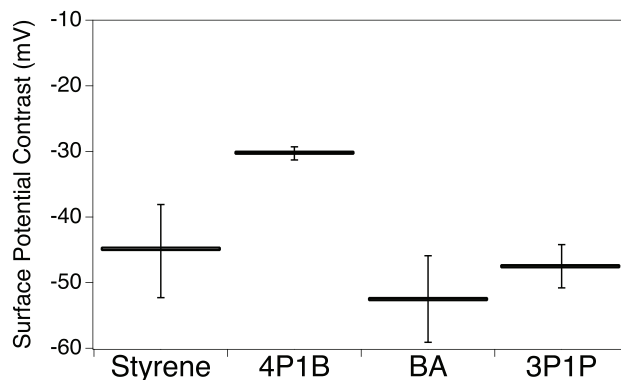

Figure 5.8. Surface potential contrasts of the SAM with respect to reference HD SAM

KPFM measurements of our HD-aromatic SAMs yielded a contrast of -45.2 mV, -30.3 mV, –52.5 mV and -47.5 mV for styrene SAM, 4P1B SAM, BA SAM and 3P1P SAM respectively. This is summarized in Figure 5.8. When the change in surface potential of HD SAM due to the etching damage is considered, the actual contrasts are computed to be -29.9 mV, -15.0 mV, -37.2 mV and -32.2 mV for styrene SAM, 4P1B SAM, BA SAM and 3P1P SAM respectively.

Surface potentials of SAMs are affected by the dipole moment of the molecules grafted on the surface, the molecular packing and the dielectric constant of the SAM. Equation 5.1 shows the surface potential of the SAM during KPFM, where ϕ_{Si} and ϕ_{tip} correspond to the work functions of the silicon substrate and the tip, and e is the electric charge[18,43,44]. The second term in Equation 5.1 denotes the net dipole perpendicular to the surface as μ, the area occupied by the molecule as A, the permittivity of free space as ϵ_0, and the relative permittivity or dielectric constant of the SAM as ϵ_{SAM}. In the case of our experiments, the HD SAM and aromatic SAMs are deposited on the same silicon substrate, thus the surface potential contrast between them can be obtained using Equation 5.2 where V_{SAM} and $V_{\mathrm{SAM(HD)}}$ are the surface potentials of the aromatic SAM and reference HD SAM respectively.

$$V_{SAM} = -\frac{\phi_{Si}-\phi_{tip}}{e} + \frac{\mu}{A\epsilon_0\epsilon_{SAM}} \quad \text{Equation 5.1}$$

$$V_{SAM} - V_{SAM(HD)} = \frac{\mu_{SAM}}{A_{SAM}\epsilon_0\epsilon_{SAM}} - \frac{\mu_{SAM(HD)}}{A_{SAM(HD)}\epsilon_0\epsilon_{SAM(HD)}} \quad \text{Equation 5.2}$$

In both Equations 5.1 and 5.2, the net dipole moment of the SAM (μ) is the component of the dipole moment perpendicular to the substrate surface[44]. This can be affected by the gas phase dipole of the molecule as well as the interface dipole between molecule and substrate, which is what we are investigating in this study. Previous studies have been conducted where molecules were attached to the substrate via the same interfacial bond. In those cases the researchers used simplified molecule computations to obtain μ, without considering the interfacial dipole moment since the interfacial dipole moment was assumed to be constant for all SAMs due to the identical binding group[17,44,45]. In such a scenario, any difference in surface potential would be a result of the remaining part of the molecule. However, in our experiments the interfacial bond between molecule and substrate is different, thus the interfacial dipole is something that needs to be considered.

The dipole moment of the aromatic SAMs were computed for using MOPAC semi-empirical computations (Figures 5.9 and 5.10). In Figure 5.9, we computed only for the dipole moments of the precursor molecules, before they attach to the silicon substrate, while in Figure 5.10 we attached the molecule to a single silicon atom. We assumed that this is what the molecule whole look like once they are grafted to the silicon substrate. It is important to note that these are semi-empirical computations using only one silicon atom instead of a silicon slab consisting of several layers, which is usually used in papers doing computational analysis[16,28,46] and thus might not be entirely accurate in computing for the dipole moment of the SAM. However, our computations provide a good estimate of the dipole moments which can be used

for comparison with one another. The differences in the dipole moments of the molecules before and after attaching to the silicon substrate shows that some charge rearrangement in the molecular backbone takes place, which alter its dipole moment upon grafting. It is clear that the interfacial bond is quite significant in the final dipole moment of the SAM when it is grafted to the substrate. Comparing our computations with our KPFM experimental results, we find that they agree qualitatively.

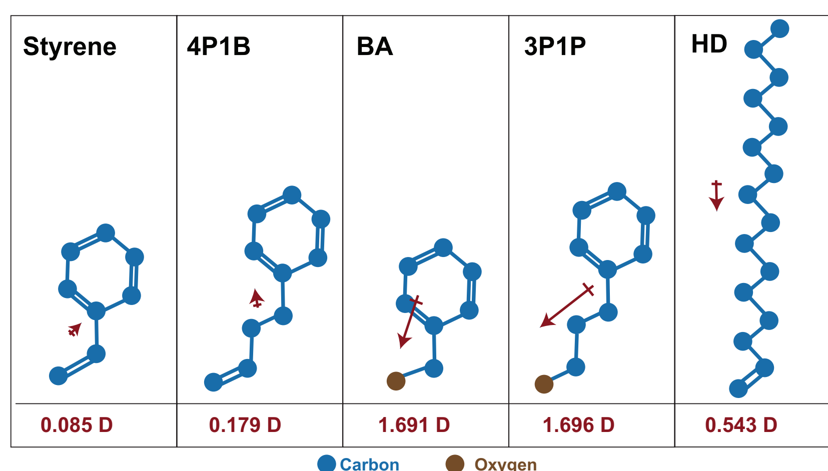

Figure 5.9. Dipole moments of precursor molecules computed via MOPAC

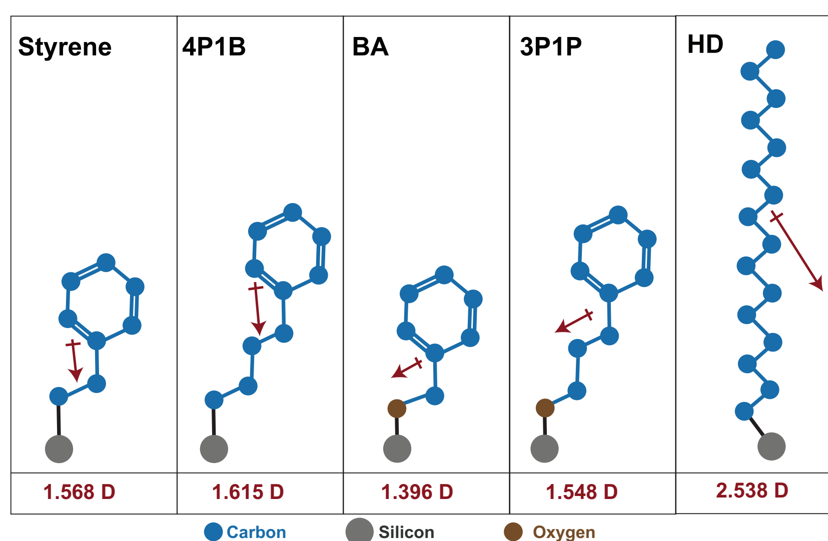

Figure 5.10. Dipole moments of molecules on Si computed via MOPAC

For the interfacial dipole, an alkyl chain bound to silicon results to a positive pole at the silicon side and a negative pole on the carbon side, due to the higher electronegativity of carbon[47]. In the case of Si-O bonded SAM, there electronegativity difference between the oxygen and Si is increased, resulting to a greater interface dipole. The interfacial dipole is usually quite small compared to the dipole moment due to the SAM backbone, however it is enough to lead to differences in the final net dipole moment of the SAM. In our computations for the net dipole moment of the SAMs after grafting to the silicon substrate, the positive pole points away from the surface (Figure 5.10). In this situation, the potential at the surface is increased. This results to a decrease in the electron affinity and the work function of the surface. We can visualize this decrease in work function as an electron from the conduction band of the surface being accelerated by the positive pole of the dipole to the local vacuum, making it easier for the electron to break free[48]. A dipole oriented in the opposite direction (with the negative pole away from the surface), will decrease the surface potential while increasing the electron affinity and work function due to the additional barrier the electron has to cross to escape from the surface.

Looking at the KPFM results for our aromatic SAMs, we found that these SAMs have a lower surface potential than the reference HD SAM. This agrees with our MOPAC computations which show that the dipole moments of the aromatic SAMs were lower than the HD molecule (Figure 5.10). The lower surface potentials of aromatic SAMs can also be due to the difference in the dielectric constants of the HD and aromatic SAMs. Aromatic SAMs typically have a greater dielectric constant compared to alkyl SAMs which would result to a lower surface potential[35].

Our KPFM results also show that Si-O bonded SAMs have a lower surface potential than the Si-C SAMs. MOPAC computations confirm that the dipole moments of the Si-O bonded SAMs are lower than that of the Si-C bonded ones. Additionally, under the assumption

that the molecules are slightly more tilted as suggested by the WCA and ellipsometry results in the previous section, the dipole moment would be reduced even more since only the component normal to the surface will be considered. If the Si-O bonded SAMs have a lower packing density compared to the Si-C bonded SAMs as suggested by the individual investigation of the SAMs, which would result in a larger A_{SAM}, which further lowers the surface potential, consistent with Equation 5.1 All of these are in agreement with our KPFM measurements.

5.3.4. CAFM Measurements for conductivity

In **Chapters 3** and **4** we formed SAMs using molecules having saturated carbon bonds, in this chapter the conjugation in the phenyl rings of the precursor molecules can possibly provide the SAMs with some degree of conductivity. Several studies have reported the good electrical conductivity of aromatic SAMs[31,35,36]. To determine if the SAMs in our study is able to conduct current, we used CAFM to observe its conductive properties. The CAFM scans and the measured current passing through the SAMs are shown in Figure 5.11 and Table 5.3. The difference in the current passing through the reference HD SAM and aromatic SAMs in the CAFM scans were summarized using histogram plots rather than line profiles due to the large variations we observed during the measurements.

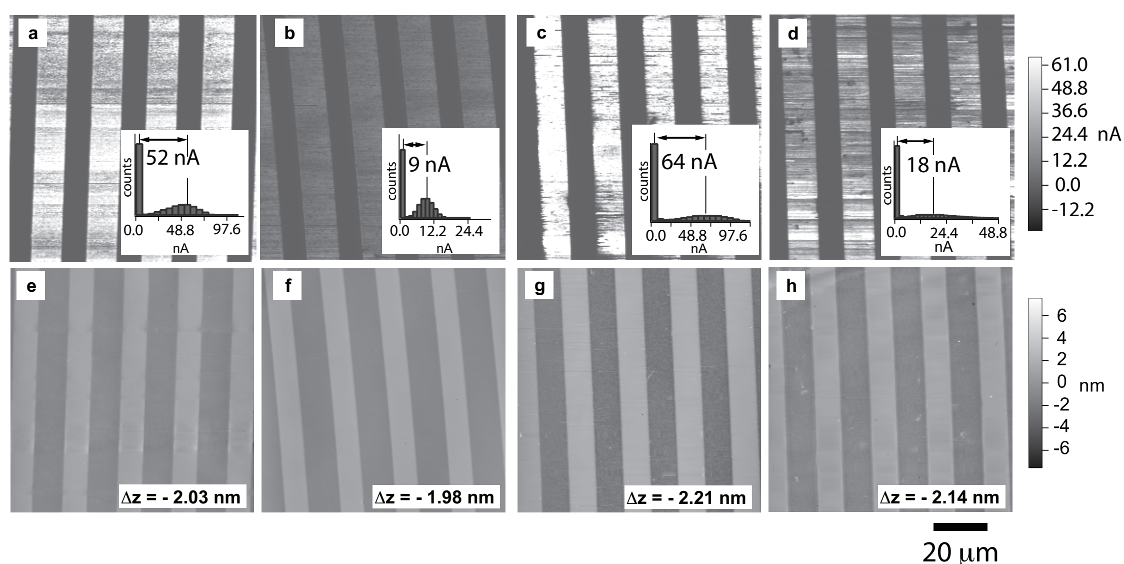

Figure 5.11. Simultaneously obtained (a-d) CAFM and (e-h) AFM height) images of the micropatterned samples, corresponding to (a,e) styrene SAM, (b,f) 4P1B SAM, (c,g) BA SAM, and (d,h) 3P1P SAM. All samples used HD SAM as reference

Table 5.3. CAFM and topography contrast of micropatterned SAMs

	Current (nA)	Topography Contrast (nm)
Si-C Bonded		
HD – Styrene	52.3	-2.03 ± 0.11
HD – 4P1B	8.9	-1.98 ± 0.07
Si-O Bonded		
HD – BA	63.5	2.21 ± 0.26
HD – 3P1P	17.7	2.14 ± 1.88

The topography of the micropatterned SAMs in the AFM images are in agreement with our KPFM scans where the aromatic SAMs have lower topography than the reference HD SAM. Measurement of the accompanying AFM scans during CAFM resulted to greater topographic contrast between the aromatic and reference HD SAM compared to that those measured during KPFM, however the trend is consistent with each other and the values are within the boundaries of standard deviation.

The CAFM scans show that the HD SAM regions have very little conductivity with practically no current passing through it (Figure 5.11). However, due to the short lengths of the methyl spacer and the conjugation of the phenyl headgroup, the aromatic SAMs exhibited much a higher current in the CAFM scans, ranging from 9 nA to 64 nA. The conjugated system of the aromatic SAMs result in overlapping π orbitals with delocalized electrons which can increase conductivity of the SAMs because the electrons can move freely around this region. Studies have shown that romatic monolayers are known to have superior electrical conductance compared to aliphatic ones[49]. The conduction mechanism for short, conjugated molecules is believed to be off-resonance tunnelling[50]. In the case of saturated molecules, the dominant mechanism of charge transport is believed to be through-bond tunelling[51]. In this situation, current flows along the backbone of the molecule through the overlapping sigma bonds. A previous study on the conductivity of alkanethiol SAMs found that conductance decreased exponentially as molecule length increases[50–52]. This is due to the rapid decrease in tunnelling rate as the distance increases, thus leading to a very low conductance for longer alkane chains. In the case of our experiments, this explains why the HD SAM regions exhibited almost no current in the CAFM scans. This also explains why the aromatic molecules having a longer methyl chain spacer (4P1B and 3P1P) had lower conductivity compared to those with a shorter methyl spacer (styrene and BA).

Comparing the results of the conductivity of the aromatic SAMS, our findings show that the Si-O bonded SAMs exhibited higher current than the Si-C bonded SAMs. One possible explanation is due to the thinner layer of the Si-O SAMs compared to the Si-C SAMs. In our investigation on the single component SAMs, the ellipsometry results showed that Si-O SAMs had a lower thickness compared to Si-C SAMs. The thinner layer would allow electrons to pass through with more ease, resulting to a higher current[31]. Another possible explanation is that the difference in the binding of the SAMs to the silicon substrate played a part in the difference

in their conductivity. A previous study on the transport properties of Si-C and Si-O bonds on alkyl/alkyloxy SAMs on Si (100) investigated the effects of the Si-C and Si-O bonds[47]. The researchers found that that Si-O bonded SAMs experienced less length-related damping of the current passing through the monolayers, as well as having a lower electron effective mass than Si-C bonded ones. In semiconductor physics, the mobility of free carriers in a material and conductivity are inversely proportional to the carrier effective mass[53], which might explain why our Si-O SAMs exhibited higher currents. However, further studies will be needed to confirm if this same results are true for aromatic SAMs on n-Si(111).

5.4. Conclusions

The results of our investigation on the quality of the single component aromatic SAMs show that the molecules formed organized and dense monolayers on the H-Si substrate despite the short length of the molecules. The XPS peaks and atomic percent concentrations suggest that the molecules grafted well to the substrate and passivated the underlying silicon from oxidation. The WCA and ellipsometry measurements suggest that the Si-O bonded SAMs resulted in molecules which are more tilted compared to the Si-C bonded SAMs, leading to lower water angles and thicknesses.

In the KPFM analysis, Si-O bonded SAMs were found to have a lower surface potential compared to Si-C bonded SAMs. This is in agreement with dipole moments estimated via MOPAC semi-empirical computations. The MOPAC computations suggest that the precursor molecules undergo charge rearrangement upon grafting to the silicon substrate leading to large differences in the intrinsic dipole moment of the molecule and its dipole moment upon SAM formation.

The CAFM findings show that the aromatic SAM regions exhibited conductive properties while the reference HD SAM region allowed very little current to pass through. The

Si-O bonded SAMs exhibited larger currents compared to the Si-C bonded SAMs, possibly due to the thickness difference and the difference in the interfacial bonds.

The results of our study suggests that the Si-C and Si-O binding of the SAMs resulted to differences in their molecular packing, net dipole moments, surface potential, and conductivity. Further studies on the band alignment at interfaces and the electronic transport behavior of these SAMs can give us a clearer understanding of how the interface dipole can affect the surface potential/work function and conductivity of these materials.

References

(1) Booth, B. D.; Vilt, S. G.; Lewis, J. Ben; Rivera, J. L.; Buehler, E. A.; McCabe, C.; Jennings, G. K. Tribological Durability of Silane Monolayers on Silicon. *Langmuir* **2011**, *27*, 5909–5917.

(2) Nakano, M.; Ishida, T.; Sano, H.; Sugimura, H.; Miyake, K.; Ando, Y.; Sasaki, S. Tribological Properties of Self-Assembled Monolayers Covalently Bonded to Si. *Appl. Surf. Sci.* **2008**, *255*, 3040–3045. https://doi.org/10.1016/j.apsusc.2008.08.073.

(3) Behpour, M.; Mohammadi, N. Investigation of Inhibition Properties of Aromatic Thiol Self-Assembled Monolayer for Corrosion Protection. *Corros. Sci.* **2012**, *65*, 331–339. https://doi.org/10.1016/j.corsci.2012.08.036.

(4) Appa Rao, B. V.; Yakub Iqbal, M.; Sreedhar, B. Self-Assembled Monolayer of 2-(Octadecylthio)Benzothiazole for Corrosion Protection of Copper. *Corros. Sci.* **2009**, *51*, 1441–1452. https://doi.org/10.1016/j.corsci.2009.03.034.

(5) Wink, T.; van Zuile, S. J.; Bult, A.; van Bennekom, W. P. Self-Assembled Monolayers for Biosensors. *Analyst* **1997**, *122*, 43–50.

(6) Lee, H.; Lee, W.; Lee, J. H.; Yoon, D. S. Surface Potential Analysis of Nanoscale

Biomaterials and Devices Using Kelvin Probe Force Microscopy. *J. Nanomater.* **2016**, *2016*, 1–21. https://doi.org/10.1155/2016/4209130.

(7) Vilan, A.; Cahen, D. Chemical Modification of Semiconductor Surfaces for Molecular Electronics. *Chem. Rev.* **2017**, *117* (5), 4624–4666. https://doi.org/10.1021/acs.chemrev.6b00746.

(8) Aswal, D. K.; Lenfant, S.; Guerin, D.; Yakhmi, J. V.; Vuillaume, D. Self Assembled Monolayers on Silicon for Molecular Electronics. *Anal. Chim. Acta* **2006**, *568*, 84–108. https://doi.org/10.1016/j.aca.2005.10.027.

(9) Casalini, S.; Bortolotti, C. A.; Leonardi, F.; Biscarini, F. Self-Assembled Monolayers in Organic Electronics. *Chem. Soc. Rev.* **2017**, *46*, 40–71. https://doi.org/10.1039/c6cs00509h.

(10) Campbell, I. H.; Kress, J. D.; Martin, R. L.; Smith, D. L.; Barashkov, N. N.; Ferraris, J. P. Controlling Charge Injection in Organic Electronic Devices Using Self-Assembled Monolayers. *Appl. Phys. Lett.* **1997**, *71* (24), 3528–3530. https://doi.org/10.1063/1.120381.

(11) Zojer, E.; Taucher, T. C.; Hofmann, O. T. The Impact of Dipolar Layers on the Electronic Properties of Organic/Inorganic Hybrid Interfaces. *Adv. Mater. Interfaces* **2019**, *6* (14), 1900581. https://doi.org/10.1002/admi.201900581.

(12) Egger, D. A.; Rissner, F.; Gerold, R. M.; Hofmann, O. T.; Wittwer, L.; Heimel, G.; Zojer, E. Self-Assembled Monolayers of Polar Molecules on Au(111) Surfaces: Distributing the Dipoles. *Phys. Chem. Chem. Phys.* **2010**, *12* (17), 4291–4294. https://doi.org/10.1039/c004746p.

(13) Campbell, I.; Rubin, S.; Zawodzinski, T.; Kress, J.; Martin, R.; Smith, D.; Barashkov, N.; Ferraris, J. Controlling Schottky Energy Barriers in Organic Electronic Devices Using Self-Assembled Monolayers. *Phys. Rev. B - Condens. Matter Mater. Phys.* **1996**,

54 (20), 14321–14324. https://doi.org/10.1103/PhysRevB.54.R14321.

(14) Zehner, R. W.; Parsons, B. F.; Hsung, R. P.; Sita, L. R. Tuning the Work Function of Gold with Self-Assembled Monolayers Derived from X-[C6H4-C=C-]NC6H4-SH (n = 0 , 1 , 2 ; X = H , F , CH3 , CF3 , and OCH3). **1999**, No. 10, 1121–1127.

(15) Tantitarntong, P.; Zalar, P.; Matsuhisa, N.; Nakano, K.; Lee, S.; Yokota, T.; Tajima, K.; Someya, T. High Sensitivity Tuning of Work Function of Self-Assembled Monolayers Modified Electrodes Using Vacuum Ultraviolet Treatment. *ACS Appl. Mater. Interfaces* **2017**, *9* (34), 28151–28156. https://doi.org/10.1021/acsami.7b09756.

(16) Arefi, H. H.; Fagas, G. Chemical Trends in the Work Function of Modified Si(111) Surfaces: A DFT Study. *J. Phys. Chem. C* **2014**, *118* (26), 14346–14354. https://doi.org/10.1021/jp502464r.

(17) Saito, N.; Hayashi, K.; Sugimura, H.; Takai, O.; Nakagiri, N. Surface Potentials of Patterned Organosilane Self-Assembled Monolayers Acquired by Kelvin Probe Force Microscopy and Ab Initio Molecular Calculation. *Chem. Phys. Lett.* **2001**, *349*, 172–177. https://doi.org/10.1016/S0009-2614(01)01097-1.

(18) Sugimura, H.; Hayashi, K.; Saito, N.; Nakagiri, N.; Takai, O. Surface Potential Microscopy for Organized Molecular Systems. *Appl. Surf. Sci.* **2002**, *188* (3–4), 403–410. https://doi.org/10.1016/S0169-4332(01)00958-8.

(19) Aqua, T.; Cohen, H.; Sinai, O.; Frydman, V.; Bendikov, T.; Krepel, D.; Hod, O.; Kronik, L.; Naaman, R. Role of Backbone Charge Rearrangement in the Bond-Dipole and Work Function of Molecular Monolayers. *J. Phys. Chem. C* **2011**, *115* (50), 24888–24892. https://doi.org/10.1021/jp208411f.

(20) Haensch, C.; Hoeppener, S.; Schubert, U. S. Chemical Modification of Self-Assembled Silane Based Monolayers by Surface Reactions. *Chem. Soc. Rev.* **2010**, *39* (6), 2323. https://doi.org/10.1039/b920491a.

(21) Sugimura, H.; Hozumi, A.; Kameyama, T.; Takai, O. Organosilane Self-Assembled Monolayers Formed at the Vapour/Solid Interface. In *Surface and Interface Analysis*; 2002. https://doi.org/10.1002/sia.1358.

(22) Hill, I. G.; Weinert, C. M.; Kreplak, L.; van Zyl, B. P. Influence of Self-Assembled Monolayer Chain Length on Modified Gate Dielectric Pentacene Thin-Film Transistors. *Appl. Phys. A* **2009**, *95* (1), 81–87. https://doi.org/10.1007/s00339-008-4992-2.

(23) Gala, F.; Zollo, G. Dielectric Properties of Self-Assembled Monolayer Coatings on a (111) Silicon Surface. *J. Phys. Chem. C* **2015**, *119* (13), 7264–7274. https://doi.org/10.1021/acs.jpcc.5b00193.

(24) Veerbeek, J.; Huskens, J. Applications of Monolayer-Functionalized H-Terminated Silicon Surfaces: A Review. *Small Methods* **2017**, *1* (4), 1700072. https://doi.org/10.1002/smtd.201700072.

(25) Sugimura, H.; Sano, H.; Lee, K.-H.; Murase, K. Organic Monolayers Covalently Bonded to Si as Ultra Thin Photoresist Films in Vacuum UV Lithography. *Jpn. J. Appl. Phys.* **2006**, *45* (6B), 5456–5460. https://doi.org/10.1143/JJAP.45.5456.

(26) Magid, I.; Burstein, L.; Seitz, O.; Segev, L.; Kronik, L.; Rosenwaks, Y. Electronic Characterization of Si(100)-Bound Alkyl Monolayers Using Kelvin Probe Force Microscopy. *J. Phys. Chem. C* **2008**, *112* (18), 7145–7150. https://doi.org/10.1021/jp709973d.

(27) Faber, E. J.; De Smet, L. C. P. M.; Olthuis, W.; Zuilhof, H.; Sudhölter, E. J. R.; Bergveld, P.; Van Den Berg, A. Si-C Linked Organic Monolayers on Crystalline Silicon Surfaces as Alternative Gate Insulators. *ChemPhysChem* **2005**, *6* (10), 2153–2166. https://doi.org/10.1002/cphc.200500120.

(28) Toledano, T.; Garrick, R.; Sinai, O.; Bendikov, T.; Haj-Yahia, A. E.; Lerman, K.; Alon, H.; Sukenik, C. N.; Vilan, A.; Kronik, L.; et al. Effect of Binding Group on

Hybridization across the Silicon/Aromatic-Monolayer Interface. *J. Electron Spectros. Relat. Phenomena* **2015**, *204*, 149–158. https://doi.org/10.1016/j.elspec.2015.05.019.

(29) Hu, M.; Liu, F.; Buriak, J. M. Expanding the Repertoire of Molecular Linkages to Silicon: Si-S, Si-Se, and Si-Te Bonds. *ACS Appl. Mater. Interfaces* **2016**, *8* (17), 11091–11099. https://doi.org/10.1021/acsami.6b00784.

(30) Garcia, M. C. T.; Utsunomiya, T.; Ichii, T.; Sugimura, H. Surface Potential Contrasts between 1-Alkene, 1-Thiol and 1-Alcohol Self-Assembled Monolayers on Silicon (111) Substrate. *Jpn. J. Appl. Phys.* **2020**, *59* (SD), SDDC06. https://doi.org/10.7567/1347-4065/ab5925.

(31) Harada, Y.; Koitaya, T.; Mukai, K.; Yoshimoto, S.; Yoshinobu, J. Spectroscopic Characterization and Transport Properties of Aromatic Monolayers Covalently Attached to Si(111) Surfaces. *J. Phys. Chem. C* **2013**, *117* (15), 7497–7505. https://doi.org/10.1021/jp309918p.

(32) Ishii, H.; Sugiyama, K.; Ito, E.; Seki, K. Energy Level Alignment and Interfacial Electronic Structures at Organic/Metal and Organic/Organic Interfaces. *Adv. Mater.* **1999**, *11* (8), 605–625.

(33) Zhao, J.; Uosaki, K. Electron Transfer through Organic Monolayers Directly Bonded to Silicon Probed by Current Sensing Atomic Force Microscopy: Effect of Chain Length and Applied Force. *J. Phys. Chem. B* **2004**, *108* (44), 17129–17135. https://doi.org/10.1021/jp049719+.

(34) Rampi, M. A.; Schueller, O. J. A.; Whitesides, G. M. Alkanethiol Self-Assembled Monolayers as the Dielectric of Capacitors with Nanoscale Thickness. *Appl. Phys. Lett.* **1998**, *72*, 1781–1783.

(35) Toledano, T.; Sazan, H.; Mukhopadhyay, S.; Alon, H.; Lerman, K.; Bendikov, T.; Major, D. T.; Sukenik, C. N.; Vilan, A.; Cahen, D. Odd-Even Effect in Molecular Electronic

Transport via an Aromatic Ring. *Langmuir* **2014**, *30* (45), 13596–13605. https://doi.org/10.1021/la503536f.

(36) Ishida, T.; Mizutani, W.; Aya, Y.; Ogiso, H.; Sasaki, S.; Tokumoto, H. Electrical Conduction of Conjugated Molecular SAMs Studied by Conductive Atomic Force Microscopy. *J. Phys. Chem. B* **2002**, *106* (23), 5886–5892. https://doi.org/10.1021/jp0134749.

(37) Saito, N.; Youda, S.; Hayashi, K.; Sugimura, H.; Takai, O. Alkyl Self-Assembled Monolayer Prepared on Hydrogen-Terminated Si(111) through Reduced Pressure Chemical Vapor Deposition : Chemical Resistivities in HF and NH 4 F Solutions . *Chem. Lett.* **2002**, *31* (12), 1194–1195. https://doi.org/10.1246/cl.2002.1194.

(38) Sano, H.; Maeda, H.; Ichii, T.; Murase, K.; Noda, K.; Matsushige, K.; Sugimura, H. Alkyl and Alkoxyl Monolayers Directly Attached to Silicon: Chemical Durability in Aqueous Solutions. *Langmuir* **2009**, *25* (10), 5516–5525.

(39) Popoff, R. T. W.; Zavareh, A. A.; Kavanagh, K. L.; Yu, H. Z. Reduction of Gold Penetration through Phenyl-Terminated Alkyl Monolayers on Silicon. *J. Phys. Chem. C* **2012**, *116* (32), 17040–17047. https://doi.org/10.1021/jp304351b.

(40) Kim, S.-J.; Ryu, K.; Chang, S. W. Solution-Processed Organic Field-Effect Transistors Patterned by Self-Assembled Monolayers of Octadecyltrichlorosilane and Phenyltrichlorosilane. *J. Mater. Sci.* **2010**, *45* (2), 566–569. https://doi.org/10.1007/s10853-009-4047-x.

(41) Stevens, M. J. Thoughts on the Structure of Alkylsilane Monolayers. *Langmuir* **1999**, *15* (8), 2773–2778. https://doi.org/10.1021/la981064e.

(42) Seitz, O.; Böcking, T.; Salomon, A.; Gooding, J. J.; Cahen, D. Importance of Monolayer Quality for Interpreting Current Transport through Organic Molecules: Alkyls on Oxide-Free Si. *Langmuir* **2006**, *22* (16), 6915–6922. https://doi.org/10.1021/la060718d.

(43) Sugimura, H.; Hayashi, K.; Saito, N. Kelvin Probe Force Microscopy Images of Microstructured Organosilane Self-Assembled Monolayers. *Jpn. J. Appl. Phys.* **2001**, *40*, 4373.

(44) Hayashi, K.; Saito, N.; Sugimura, H.; Takai, O.; Nakagiri, N. Regulation of the Surface Potential of Silicon Substrates in Micrometer Scale with Organosilane Self-Assembled Monolayers. *Langmuir* **2002**, *18* (20), 7469–7472. https://doi.org/10.1021/la011707h.

(45) Hayashi, K.; Saito, N.; Sugimura, H.; Takai, O.; Nakagiri, N. Surface Potential Contrasts between Silicon Surfaces Covered and Uncovered with an Organosilane Self-Assembled Monolayer. *Ultramicroscopy* **2002**, *91* (1–4), 151–156. https://doi.org/10.1016/S0304-3991(02)00094-3.

(46) Natan, A.; Zidon, Y.; Shapira, Y.; Kronik, L. Cooperative Effects and Dipole Formation at Semiconductor and Self-Assembled-Monolayer Interfaces. *Phys. Rev. B* **2006**, *73* (193310), 1–4. https://doi.org/10.1103/PhysRevB.73.193310.

(47) Thieblemont, F.; Seitz, O.; Vilan, A.; Cohen, H.; Salomon, E.; Kahn, A.; Cahen, D. Electronic Current Transport through Molecular Monolayers: Comparison between Hg/Alkoxy and Alkyl Monolayer/Si(100) Junctions. *Adv. Mater.* **2008**, *20* (20), 3931–3936. https://doi.org/10.1002/adma.200800659.

(48) He, T.; Ding, H.; Peor, N.; Lu, M.; Corley, D. A.; Chen, B.; Ofir, Y.; Gao, Y.; Yitzchaik, S.; Tour, J. M. Silicon/Molecule Interfacial Electronic Modifications. *J. Am. Chem. Soc.* **2008**, *130* (5), 1699–1710. https://doi.org/10.1021/ja0768789.

(49) Abu-Husein, T.; Schuster, S.; Egger, D. A.; Kind, M.; Santowski, T.; Wiesner, A.; Chiechi, R.; Zojer, E.; Terfort, A.; Zharnikov, M. The Effects of Embedded Dipoles in Aromatic Self-Assembled Monolayers. *Adv. Funct. Mater.* **2015**, *25* (25), 3943–3957. https://doi.org/10.1002/adfm.201500899.

(50) Tao, N. J. Electron Transport in Molecular Junctions. *Nanosci. Technol. A Collect. Rev.*

from Nat. Journals **2009**, *1*, 173–181. https://doi.org/10.1142/9789814287005_0019.

(51) Wang, W.; Lee, T.; Reed, A. Mechanism of Electron Conduction in Self-Assembled Alkanethiol Monolayer Devices. *Phys. Rev. B - Condens. Matter Mater. Phys.* **2003**, *68* (12), 1–7. https://doi.org/10.1103/PhysRevB.68.035416.

(52) Wang, W.; Lee, T.; Reed, M. A. Electron Tunnelling in Self-Assembled Monolayers. *Reports Prog. Phys.* **2005**, *68* (3), 523–544. https://doi.org/10.1088/0034-4885/68/3/R01.

(53) Edwards, P. P.; Porch, A.; Jones, M. O.; Morgan, D. V.; Perks, R. M. Basic Materials Physics of Transparent Conducting Oxides. *Dalt. Trans.* **2004**, No. 19, 2995–3002. https://doi.org/10.1039/b408864f.

Chapter 6 : Summary and Conclusions

In this thesis we investigated the effects of the interface dipole and molecular length of self-assembled monolayers (SAMs) on the surface potential of n-Si(111). The presence of SAMs on a surface yields a dipole layer which is capable of shifting the vacuum level at material interfaces. The shift in the vacuum level results in a change in surface potential or work function of the substrate which is useful in improving the charge injection of carriers at interfaces. By understanding how different molecules can modify the surface potential or work function of silicon, we can improve its performance in the field of electronics.

Our surface potential measurements were conducted via Kelvin Probe Force Microscopy (KPFM). To account for any possible variations that may occur due to the different cantilever tips used during measurements, micropatterned SAMs formed via vacuum ultraviolet (VUV) photolithography was used during measurements, with one SAM acting as a reference. SAM formed from 1-hexadecene (HD SAM) was formed on the silicon substrate and irradiated with VUV light through a photomask to obtain the micropatterns. We determined the optimum VUV irradiation time and chamber pressure required to degrade the HD SAM and form clear micropatterns. A series of etching tests were also conducted to determine the ideal etching time in HF and NH_4F to remove the silicon oxide formed during VUV photolithography while doing minimal damage to the reference HD SAM. Despite slight changes in surface potential due to damage during the etching step of the VUV photolithography process, the HD SAM proved to be a stable reference in our measurements.

By using molecules with similar structures but different binding groups with silicon, we investigated the effects of the interface dipole to the net dipole moment of the SAM. We formed HD, HDT and HDO SAMs from 1-hexadecene, 1-hexadecanethiol and 1-hexadecanol precursors. The differences in their binding to silicon (Si-C, Si-S and Si-O) resulted in different interface dipoles which affected the net dipole moment and final surface potential of the SAMs.

We also measured the difference in surface potentials of aromatic SAMs bound to silicon via Si-C and Si-O bonds. For both straight-chain and aromatic molecules, the interfacial bond with the substrate resulted to differences in net dipole moment and surface potentials of the SAMs. We computed for the dipole moments of the molecules using using Molecular Package (MOPAC) semi-empirical computations and the results agreed qualitatively with the KPFM results. Using conductive AFM (CAFM) we were also able to compare the electrical current passing through the aromatic SAMs and the reference HD SAM. Our results showed that the difference in the binding group also resulted to differences in the electrical conductivity of the aromatic SAMs.

We also looked at the effect of molecular length of the SAM precursor molecules on the surface potential of the n-Si(111) substrate. Using 1-alkene precursors we formed SAMs with a molecular length of n = 10, 12, 14, 16, 18 and 20. We limited our precursor molecules to even-numbered chains to avoid any odd-even effect that might occur. Although there was a linear increase in topography with increasing chain length, surface potentials did not exhibit a clear correlation with chain length. Our findings suggest that the surface potentials of the SAMs were affected by the dipole moment of the precursor molecules, changes in SAM dielectric properties due to differences in molecular packing, and varying oxygen content at the surface.

This information is useful in the field of molecular electronics for surface modification. Increasing our understanding of how surface potential can be controlled or affected by different parameters can lead to further improvement of the charge carrier efficiency of electronic devices.

Acknowledgements

First, I would like to express my utmost appreciation to my supervisor Prof. Dr. Hiroyuki Sugimura for giving me the opportunity to do my PhD work in the Nanoscopic Surface Architecture (NSA) Laboratory here in Kyoto University. With him being an expert in the field of self-assembled monolayers, it was an honor to study under his guidance. I was very blessed to have found a supervisor who not only encouraged me to do my best in research, but to also experience Japanese culture. I want to thank him for his advice, guidance and encouragement that allowed me to finish my PhD.

I also want to express my gratitude to Prof. Dr. Kuniaki Murase (Department of Material Science and Engineering, Kyoto University) and Prof. Dr. Hirofumi Yamada (Department of Electronic Science and Engineering, Kyoto University) for dedicating time and attention to understand my research and offering constructive advice to improve my dissertation. Their suggestions and feedback helped shaped my dissertation to what it is today.

I would like to thank Prof. Dr. Takashi Ichii (Associate Professor, NSA Lab, Kyoto University) and Prof. Dr. Toru Utsunomiya (Assistant Professor, NSA Lab, Kyoto University) for all the guidance they have given me in my 4 years in the lab. They have provided me with constant direction in my research work and have motivated me to work hard in my experiments and manuscript writing. Their instruction and feedback were crucial to my growth as a PhD student.

I want to thank our laboratory secretary Ms. Setsuko Yoshikubo for her assistance in handling important documents that I needed during my stay in Japan, and for always making sure that I am adjusting well when I first arrived here. I also want to express my gratitude to Ms. Sari Nakano for her assistance in handling my university documents while Ms. Yoshikubo was away.

I want to express my appreciation to the Japanese Government, specifically to the Ministry of Education, Culture, Sports, Science and Technology (MEXT) for their financial support during my student life in Japan. Without the scholarship, studying in Japan would not have been possible for me.

I want to say thank you to my senior PhD students in the lab - Dr. Cheng-Tse Wu and Dr. Ahmed Soliman. Dr. Wu gave me constant encouragement during my time as a PhD student and has shared many of what he has learned in the lab with me, as well as many interesting facts about his life in Taiwan and Japan. Dr. Soliman taught me many things about self-assembled monolayers and also shared his Egyptian culture with me. I will treasure the things I have learned from them.

I want to express my sincere appreciation to my friends in the NSA laboratory for making my stay very pleasant and memorable. Thank you to Ms. Lihting Lin who gladly accepted the position of my tutor when I first arrived and helped me adjust to my new life in Japan. Thank you to my friends Ms. Licen Lin and Mr. Yifan Bao for the many talks we shared, especially about our experiences as foreign students in Japan. Thank you to Mr. Wataru Kubota for his patience and kindness in teaching me to use AFM, KPFM and CAFM, as well as many other things in the lab. Thank you to Mr. Mitsuhiro Gonda for all his help as we finished our PhD together. I also want to thank Mr. Kazuyuki Itakura, Mr. Makoto Murata, Mr. Kosuke Imura, Mr. Hiroshi Shimakawa, Mr. Yuya Yamada, Mr. Kunhua Yu and Mr. Noboru Hiwasa for taking the time to teach me how to handle the different equipment and other matters related to the laboratory. I also want to express my gratitude to other lab members who were not specifically mentioned here.

I want to thank the University of the Philippines Los Banos for allowing me to grab this opportunity to study abroad. I want to express my appreciation especially to my colleagues in the Institute of Mathematical Sciences and Physics for all their encouragement and support.

Thank you to Dr. Alvin Karlo Tapia and Dr. Marvin U. Herrera for sharing what they learned about being a foreign student in Japan. Thank you to my friends Ms. Armida Gillado, Mr. Dustin Loren Almanza, Mr. Jason Albia, Dr. Alexandra Santos, Ms. Destiny Lutero and Mr. Allen Nazareno for the encouragement and prayers.

I also want to thank my good friends Ms. Sabrina Alo and Dr. Camille Ramos-Sangalang for their prayers and emotional support.

Thank you to the Kyoto Association of Pinoy Scholars (KAPS) for allowing me to find fellow Filipinos students who are on a similar journey as me. Thank you especially to Ms. Anna Obispo and Dr. Armand Rola who arrived in Japan the same time I did and became my first friends here in Kyoto.

I want to express my deepest gratitude to my Grace International Christian Church (GICC) Family. Thank you to Ninong Pastor Joseph Ricohermoso and Ninang Jo Ann Ricohermoso for their prayers. Thank you to my bible study leaders Dr. Cerrone Cabanos and Dr. Heidie Frisco-Cabanos for their spiritual guidance. Thank you as well to all my brothers and sisters in Christ who prayed for me and listened to all my struggles while I was a student.

I want to thank my family for their endless support while I was on this PhD journey. Thank you to my parents, Dr. Arnulfo G. Garcia and Dr. Yolanda T. Garcia, for the many pep-talks, prayers and encouragement when I struggled during my studies. Thank you for being such amazing role models and showering me with so much love. Thank you to my sister, Ms. Ezra Garcia-Del Rosario and her husband, Mr. Steve Kurt Del-Rosario for bearing with me through many phone calls when I needed emotional support.

I want to express my utmost gratitude to my husband, Mr. Ray Gabriel Diva for his unwavering support. His optimism and never-ending encouragement pushed me and gave me strength when I was ready to give up.

Most importantly, I want to thank God for His endless blessings, wisdom, encouragement and strength. I thank Him for leading me through all the trials and guiding me day by day during this PhD journey. To God be the glory.

Maria Carmela T. Garcia

Achievements

Journal Articles

(1) **Garcia, M. C. T.;** Utsunomiya, T.; Ichii, T.; Sugimura, H. Surface Potential Contrasts between 1-Alkene, 1-Thiol and 1-Alcohol Self-Assembled Monolayers on Silicon (111) Substrate. *Jpn. J. Appl. Phys*. 2020, 59 (SDDC06), 1–9.

(2) **Garcia, M. C. T**.; Utsunomiya, T.; Ichii, T.; Sugimura, H. Kelvin Probe Force Microscopy Studies on the Influence of Hydrocarbon Chain Length on 1-Alkene Self-Assembled Monolayers on Si (111). *Jpn. J. Appl. Phys*. 2021, No. 111.

Submitted Articles

(1) **Garcia, M. C. T.;** Utsunomiya, T.; Ichii, T.; Sugimura, H. Surface Potential and Local Conductivity Measurements of Micropatterned Aromatic Monolayers Covalently Attached to n-Si(111) via Si-C and Si-O bonds. *Submitted to Jpn. J. Appl. Phys. 2022*

List of Presentation at Conferences

(1) **Garcia, M. C. T**.; Utsunomiya, T.; Ichii, T.; Sugimura, H. "Surface Potential Contrasts between 1-Alkene, 1-Thiol and 1-Alcohol Self-Assembled Monolayers on Silicon (111) Substrate". 10th International Conference on Molecular Electronics and BioElectronics (M&BE 10). Nara Kasugano International Forum, Nara, Japan. (June 25-27, 2019)

(2) **Garcia, M. C. T**.; Utsunomiya, T.; Ichii, T.; Sugimura, H. "Kelvin Probe Force Microscopy Studies on the Influence of Hydrocarbon Chain Length on 1-Alkene Self-Assembled Monolayers on Si (111)". 28th International Colloquium on Scanning Probe Microscopy (ICSPM 28). Held online. (December 10, 2020)

(3) **Garcia, M. C. T**.; Utsunomiya, T.; Ichii, T.; Sugimura, H. "Surface Potential Measurements of Micropatterned Aromatic Monolayers Covalently Attached to n-Si(111) via Si-C and Si-O bonds". 29th International Colloquium on Scanning Probe Microscopy (ICSPM 28). Held online. (December 9-10, 2021)

Curriculum Vitae

GARCIA, Maria Carmela Tan
mtgarcia2@up.edu.ph

EDUCATION

June 2002 – April 2006	Bachelor of Science in Applied Physics, University of the Philippines Los Banos
June 2009 – April 2012	Master of Science in Material Science and Engineering, University of the Philippines Diliman
April 2018 – September 2018	Research Student, Kyoto University
October 2018 – March 2022	Doctor of Philosophy in Material Science and Engineering, Kyoto University

APPOINTMENTS & POSITIONS

June 2006 – May 2009	Instructor at the Institute of Mathematical Sciences and Physics, University of the Philippines Los Banos
June 2012 – March 2022	Assistant Professor at the Institute of Mathematical Sciences and Physics, University of the Philippines Los Banos

SCHOLARSHIPS AWARDED

April 2018 – September 2021	Japanese Government (Monbukagakusho : MEXT) Scholarship